

*aus dem*  
Deutschen Krebsforschungszentrum Heidelberg  
(Vorstandsvorsitzender: Prof. Dr. Michael Baumann)

Abteilung Medizinische Physik in der Strahlentherapie  
(Leiter: Prof. Dr. Oliver Jäkel)

in Zusammenarbeit mit  
Hochschule Heilbronn Medizinische Informatik  
(Dekan: Prof. Dr. Rolf Bendl)

---

# **Implementation of safe human robot collaboration for ultrasound guided radiation therapy**

---

Inauguraldissertation  
zur Erlangung des Doctor scientiarum humanarum (Dr. sc. hum.)  
*an der*  
Medizinischen Fakultät Heidelberg  
*der*  
Ruprecht-Karls-Universität

*vorgelegt von*  
Peter Karl Seitz

*aus*  
Heilbronn

2022



Dekan: Prof. Dr. med. Dr. h. c. Hans-Georg Kräusslich  
Doktorvater: Prof. Dr. Christian P. Karger



für Bea



# Contents

<b>Contents</b>	<b>1</b>
<b>Acronyms</b>	<b>5</b>
<b>List of Figures</b>	<b>7</b>
<b>List of Tables</b>	<b>9</b>
<b>1 Introduction</b>	<b>11</b>
1.1 Motivation . . . . .	11
1.2 Open Challenges . . . . .	13
1.3 Objectives . . . . .	14
<b>2 Material and Methods</b>	<b>15</b>
2.1 Fundamentals . . . . .	15
2.1.1 State of the art . . . . .	15
2.1.2 US Systems . . . . .	17
2.1.3 Tracking . . . . .	17
2.1.4 Robot motion planning . . . . .	17
2.1.5 Safe Human Robot Collaboration (HRC) . . . . .	20
2.1.6 Medical Imaging Interaction Toolkit (MITK) . . . . .	21
2.1.7 Preliminary work . . . . .	21
2.2 Clinical scenario . . . . .	22
2.2.1 Experimental Setup . . . . .	22
2.2.2 Clinical Workflow . . . . .	24
2.2.3 Coordination systems . . . . .	25
2.3 Implementation . . . . .	28
2.3.1 Architecture . . . . .	28
2.3.2 Integration of modalities into MITK . . . . .	28
2.3.3 Combined Modality . . . . .	28
2.3.4 Interaction with MITK . . . . .	30
2.3.5 Robot Motion . . . . .	31
2.4 Breathing and Motion Compensation . . . . .	34
2.4.1 Requirements . . . . .	34
2.4.2 Implementation . . . . .	35

2.4.3	Volume scan . . . . .	36
2.4.4	Breathing and motion compensation (BaMC) Tests . . . . .	36
2.5	Autonomous Positioning . . . . .	37
2.5.1	Implementation . . . . .	37
2.5.2	Reference frames . . . . .	37
2.5.3	Positioning strategies . . . . .	37
2.5.4	Experiments . . . . .	39
2.6	Safety . . . . .	41
2.6.1	Force Sensor . . . . .	41
2.6.2	Collision types . . . . .	41
2.6.3	Collision detection . . . . .	42
2.6.4	Reactions . . . . .	44
2.6.5	Validation tests . . . . .	44
<b>3</b>	<b>Results</b>	<b>47</b>
3.1	Clinical workflow and user interaction . . . . .	47
3.1.1	Visualization widget . . . . .	49
3.1.2	US probe positioning . . . . .	49
3.2	Breathing and Motion Compensation . . . . .	49
3.2.1	Stable contact and deformation less . . . . .	49
3.2.2	Steady image plane . . . . .	50
3.2.3	Mutable position and scanning motions . . . . .	50
3.3	Autonomous positioning . . . . .	53
3.3.1	Comparison between different positioning strategies . . . . .	53
3.3.2	Precision and accuracy of the autonomous method . . . . .	53
3.3.3	Force acting on phantom . . . . .	54
3.4	Safety . . . . .	54
3.4.1	Calibration force sensor . . . . .	56
3.4.2	Collision detection during setup motions . . . . .	58
3.4.3	Collision detection during BaMC . . . . .	58
3.4.4	Safety reactions . . . . .	62
<b>4</b>	<b>Discussion</b>	<b>65</b>
4.1	Experimental setup . . . . .	65
4.2	User interaction . . . . .	66
4.3	Breathing and Motion compensation . . . . .	67
4.4	Autonomous positioning . . . . .	69
4.5	Safety . . . . .	70
4.6	Conclusion . . . . .	71
<b>5</b>	<b>Conclusion</b>	<b>73</b>
<b>6</b>	<b>Zusammenfassung</b>	<b>75</b>
<b>7</b>	<b>Bibliography</b>	<b>77</b>



<i>CONTENTS</i>	3
<b>8 Own contribution</b>	<b>83</b>
8.1 Implementation and validation . . . . .	83
8.2 Own publications . . . . .	83
<b>Appendix</b>	<b>85</b>
<b>Lebenslauf</b>	<b>91</b>
<b>Danksagung</b>	<b>93</b>



# Acronyms

**AS** assisted.

**BaMC** Breathing and motion compensation.

**CS** coordination system.

**CT** computer tomography.

**DOF** Degrees of Freedom.

**FA** fully autonomous.

**GUI** Graphical User Interface.

**HRC** Human Robot Collaboration.

**HRI** human-robot-interaction.

**IGRT** Image Guided Radiation Therapy.

**LIN** linear.

**LINAC** Linear Accelerator.

**M** manual.

**MITK** Medical Imaging Interaction Toolkit.

**MJ** manual and joystick.

**MLC** multi-leaf collimator.

**MRT** magnetic resonance tomography.

**MTA** Medical Technical Assistant.

**MVS** manual and visual servoing.

**PTP** point-to-point.

**TCP** Tool Center Point.

**TCS** Tool coordination system.

**US** Ultrasound.

**USgRT** Ultrasound guided radiation therapy.

# List of Figures

2.1	Experimental setup in the Ultrasound guided radiation therapy (USgRT) Lab at the DKFZ . . . . .	24
2.2	Concept of the underlying Workflow . . . . .	26
2.3	US probe mount and the different coordination systems coordination system (CS). . . . .	27
2.4	Software architecture . . . . .	29
2.5	Robot motions based on clinical workflow . . . . .	33
2.6	Motion path for autonomous positioning . . . . .	38
2.7	Collision position . . . . .	43
3.1	Visualization of treatment scenario . . . . .	48
3.2	Force visualization . . . . .	48
3.3	US probe positioning widget . . . . .	49
3.4	BaMC: Force on TCP . . . . .	51
3.5	BaMC: Deviation of image plane . . . . .	52
3.6	Distance between planned and achieved surface contact point . . . . .	54
3.7	Force during autonomous positioning approach . . . . .	55
3.8	Acceleration effect on the force sensor . . . . .	56
3.9	Force sensor calibration . . . . .	57
3.10	Collision during BaMC . . . . .	60
3.11	Collision during BaMC . . . . .	61
3.12	Comparison of the different detection methods for navel $a3_3$ collisions . . . . .	62
3.13	Force reduction after emergency motion . . . . .	63



# List of Tables

- 2.1 Collision points per robot limb. . . . . 42
- 2.2 Collision detection mechanisms. . . . . 44
- 2.3 Test Positions for collisions during BaMC. . . . . 45
  
- 3.1 Comparison of different positioning strategies . . . . . 53
  
- 8.1 Collision detection for each detection method for Axilliar 45 US position. . . . . 86
- 8.2 Collision detection for each detection method for Axilliar 90 US position. . . . . 87
- 8.3 Collision detection for each detection method for Navel US position. . . . . 88
- 8.4 Collision detection for each detection method for Subcostal US position. . . . . 89





# 1

# Introduction

## 1.1 Motivation

Over the last decade image guided systems have improved radiation therapy [Verellen et al., 2008]. Image Guided Radiation Therapy (IGRT) is state of the art in daily clinical routine. The aim of IGRT is to identify deviations of the patient's anatomy of the day from the planning situation. These deviations are distinguished between interfractional (deviations between fractions, due to weight loss or tumor shrinkage) and intrafractional (deviations during a fraction due to e.g. breathing motion or different filling levels of organs) [Schwahofer und Jäkel, 2018]. Through IGRT, more precise and therefore safer radiation therapy can be delivered with tighter safety measures [Sterzing et al., 2011].

Towards this purpose, various image modalities are employed. Currently, X-ray imaging is the most ubiquitously utilized modality, but in some institutions, Ultrasound (US) has been introduced already for several reasons [Fontanarosa et al., 2015, Kuban et al., 2005, Langen et al., Western et al., 2015, Harris et al., 2021]: US is a real time imaging modality, providing high quality soft tissue contrast while also being free of radiation exposure. The approach to Ultrasound guided radiation therapy (USgRT), therefore, dates back several years. First attempts have shown that a control loop between image acquisition and treatment can be closed [Martin. F. Fase, 2016]. As a result, a multi-leaf collimator (MLC) was able to be controlled based on US image data [Hsu et al., 2005, Ipsen et al., 2016a]. This preliminary work suggests that adaptive radiotherapy using US is achievable and could reduce existing safety margins [Chandra et al., 2003]. In addition a comparison between US guided and cone beam guided ultrasound, the accuracy of positioning using ultrasound was significantly increased [Boda-Heggemann et al., 2009], although it has some systematic differences [McNair et al., 2006].

A central concern to USgRT is the handling of the US probe during radiation therapy. Especially for untrained persons, US is a challenging modality that requires specialized knowledge and skills. In general, the US probe must be guided manually by a person in order to achieve the desired US image plane. This is impossible during radiation therapy due to radiation in the treatment room. Elekta Clarity Autoscan, as one of the already available systems avoids the

complexity of US positioning and relies on a simple static support in a transperineal US [Fontanarosa et al., 2015]. The system is specifically designed for the treatment of the prostate and is being tested for cervical cancers [Mason et al., 2017], as well, since the selected image plane is not affected by bony structures or air. However, in vivo trials have shown that this methodology is prone to poorly placed US probes or to patient movement [Grimwood et al., 2018].

Especially in the abdominal region, respiratory movements cause surface movements, which makes using static holders impossible. Therefore, the use of tactile robots were investigated, which are capable of maintaining the connection between the patient and the US probe. Although [Priester et al., 2013] have shown a general plausibility, the successful implementation of USgRT in treatment has yet to be fully developed. Hence, various different ways of USgRT utilization have been reported in the literature, ranging from self-developed robots [Salcudean et al., 1999, Tutkun Şen et al., 2013, Sen et al., 2017] to adaptations with commercial robots [Ipsen et al., 2021]. An overview is given in [Fontanarosa et al., 2015, von Haxthausen et al., 2021]. Today the highly innovative topic of robot assisted [Gerlach und Schlaefer, 2022] and image guided interventions [Unger et al., 2021] not only includes robot assisted US imaging [von Haxthausen et al., 2021, Priester et al., 2013] but also focuses in a variety of scenarios, such as long-term motion monitoring [Ipsen et al., 2021] and scanning applications [Abbas et al., 2021, Aalamifar et al., 2016, Chen et al., 2021].

Unfortunately, these approaches cannot yet be translated into clinical practice and applied to patients. A key holistic approach that links the individual components is missing. This includes the integration of the different modalities, as well as, a general description of a clinical workflow including the integration of robot control, as well as, registration of the imaging modalities in the Graphical User Interface (GUI) of the irradiation devices.

Furthermore, no safe human-robot-interaction (HRI) has yet been developed and formulated for this purpose. Existing research is lacking control possibilities to dynamically adjust the Breathing and motion compensation (BaMC) and to correct a desired US plane in the process. Furthermore, there is a lack of adequate methods to position the US probe efficiently, rapidly and precisely on the patient. Critical questions regarding the safety of such an approach remain unresolved. For example, there is no proof of the forces acting at the patient during BaMC and whether these forces can be maintained at a constant level.

However, once these challenges are solved, a robotic US application can be rolled out for most US applications. Anatomical structures already potentially demonstrated are primarily the prostate and liver [Fontanarosa et al., 2015, Schlosser, 2016, Western et al., 2015, Kuhlemann et al., 2015], but the kidney [Schlosser, 2016], cervix [Mason et al., 2017] and pancreas [Fuss et al., 2003] are also possible. In addition, other diagnostic robotic US examinations are also conceivable, as shown in [Virga et al., 2016]

## 1.2 Open Challenges

Several fundamental problems need to be resolved in order to actualize the clinical application of USgRT. The following challenges have been identified for this thesis:

### **C1: Integration of modalities**

A seamless integration of all necessary hardware and software components is vital to attain a holistic USgRT approach. Consequently, a key challenge is to establish a cross-platform communication. Interoperability covers everything from sensor data acquisition and evaluation, to the resulting outputs of robot movements.

### **C2: Clinical workflow**

USgRT has a complex interaction of different hardware and software components, controlled and managed by human collaborators. Ensuring a time efficient and proper workflow is fundamental for clinical application. This includes the development of a general user interaction concept based on a user interface as well as control concepts of the robot.

### **C3: A clinically-usable, robot-guided US acquisition:**

A core requirement for USgRT is a stable and continuous US image acquisition. It requires a permanent connection between patient surface and US probe. This connection is essential to prevent air-introduced total reflections that cause image information to be missed. For abdominally-located US probe positions, respiratory motions affect the connection and the US probe have to track the patient surface. This is commonly referred to as BaMC. In addition to clinical application, remote manipulation of the US probe during BaMC is crucial and one of the key challenges.

### **C4: Safe Human Robot Collaboration (HRC):**

In general, HRC are individually adapted and implemented for different applications. Particular care must be taken when implementing direct contact with humans. Meanwhile, it still remains undefined how such an application should be implemented and which mechanisms need to be included. Therefore, the challenge is to find a safe way of handling the robot in order to protect the patient. This includes mechanisms for collision detection and avoidance, as well as, measures to reduce emergency situations.

There has already been some progress made in addressing these challenges, and their subsequent approaches. In particular, the BaMC is frequently applied to newer technologies and in continuous development, from individual and specially-adapted proprietary robots, to commercial lightweight robots. Especially through the latter, medical robotics is experiencing a renaissance. By eliminating the need for hardware proprietary developments, interfaces can be defined and software concepts and components can be exchanged. With this development, the focus is now increasingly shifting towards programming and testing. In this work, new techniques for force estimation and measurement have been considered decisively, enabling the implementation of new algorithms with increased patient safety.

In addition, open source scientific platforms such as Medical Imaging Interaction Toolkit (MITK), provide an interface for networking medical devices that facilitate the modular integration of new features in an existing software platform. For instance, the fusion of US and tracking system enabled an application, including workflow, for an image-guided needle biopsy. This example exhibits how existing platforms make both C1 and C2 feasible. They can serve as a common thread but always require adaptation to the hardware components that are still missing.

However, it is important to emphasize that while the identified challenges can be considered individually, they are directly and indirectly related to each other. Essentially, they are inter-related and mutually dependent. The greatest challenge is, therefore, to review the individual challenges as a whole and to solve them interdependently. It is precisely this holistic approach that is neglected in current publications, but which is quintessential for the future of USgRT in clinical application.

In addition to the above challenges, additional challenges exist that are necessary to developing a holistic approach to USgRT, but are not part of this work. This includes, for example, image evaluation and calibration. This is because these challenges first require clarification of how the robot and US probe can be safely applied to the patient. The primary goal for this work is to solve the challenges of C1-C4 in correspondence with and in relation to each other.

### 1.3 Objectives

The primary objective of this thesis is to solve the challenges of C1 - C4. In order to accomplish this, fundamental approaches arise that can be formulated as the following objectives.

#### **O1: The integration of required components for a clinical implementation of USgRT into existing platforms.**

The purpose of this work in relation to O1 is to show that different modalities can be integrated and combined by means of suitable interfaces. In addition, the combination of these modalities while using a suitable user control enables a future clinical workflow.

#### **O2: A continuous US imaging by using a commercial lightweight robot with an implemented BaMC.**

The purpose of this work in relation to O2 is to exhibit, that stable imaging can be achieved using lightweight robots and associated software. This further includes remote manipulation of the US probe, both in translation and in orientation, as well as, the maintenance of a constant contact pressure.

#### **O3: Finding and implementation of safety measures that allow the robot to be used in patients.**

The purpose of this work in relation to O3 is to demonstrate that a secure application can be established in the context of HRI. This includes the safety of the staff, as well as, the patient. For the latter, in particular, occurring forces and risks for the patient due to collisions or large forces need to be detected and prevented.

# 2

## Material and Methods

### Disclosures to this work:

The core idea of this work grew out of my bachelor and master thesis [Seitz, 2018]. Some of those developed functions were used and modified. During my Ph.D., a systematic improvement of all aspects, as well as, comprehensive validations, of the preliminary work, have been performed in addition to the presented. In case functions of the master thesis have been used they were cited with [Seitz, 2018].

Parts of this work (section 2.5.1 and section 2.4) been published in:

**Peter Karl Seitz**, Beatrice Baumann, Wibke Johnen, Cord Lissek, Johana Seidel, Rolf Bendl. Development of a robot-assisted ultrasound-guided radiation therapy (USgRT) *Int J CARS* 15, 491–501, December 2020. doi: 10.1007/s11548-019-02104-y

## 2.1 Fundamentals

### 2.1.1 State of the art

[Gerlach und Schlaefer, 2022] presents an up-to-date review of robotic systems used in radiotherapy and radiosurgery, as well as research. Detached from radiotherapy, [von Haxthausen et al., 2021] presents current systems in medical robotics in the context of Ultrasound (US) imaging. Concepts based on additional imaging modalities are considered in [Unger et al., 2021]. Older reviews of robotics in US guided radiotherapy are shown in the related works of [Fontanarosa et al., 2015] and [O’Shea et al., 2016] and in [Priester et al., 2013].

From the above publications, it can be seen that especially in the beginning the use of self-

developed robot systems were focused on [Tutkun Şen et al., 2013], but meanwhile now available commercial robot systems, like the robot also used here, are increasingly used [Ipsen et al., 2021]. Previous publications show more basic evidence, such as multi-leaf collimator (MLC) tracking. More recent questions address the clinical practicality of the systems [Sen et al., 2017, Elek et al., 2017]. [Camps et al., 2018], for example, provides a workflow for application to the prostate. In particular, this work highlights that for future use of the system, US acquisition should be operator independent. Additionally, this work considers the adjustment of beam angles to avoid collisions. A systematic approach to usability for telemanipulation of an US probe was presented by [Giuliani et al., 2020].

US based robotic assisted applications apart from radiotherapy include needle insertion [Priester et al., 2013, Esteban et al., 2018]. Other applications are located in diagnostics such as abdominal aneurysm scans [Virga et al., 2016]. An overview of these robotic arm assisted sonography systems and their potential clinical applications is provided [Swerdlow et al., 2017]. A recent application resulted from the Corona-induced distancing between physician and patient. Thus, [Akbari et al., 2021] could show how such a system can be used in this scenario.

### **Placement strategies**

There are several aspects to consider for the placement of the US probe. For example, [Wu et al., 2006] shows the effect of the US probe on therapy planning, as the US probe within the irradiation beam is associated with a significant reduction in dose. An alternative US probe as presented by [Schlosser et al., 2010] is currently still under research and therefore not considered for this work. However, according to [Gerlach et al., 2017b, Gerlach et al., 2017a], the plan quality can be maintained by selecting suitable beam directions and a suitable US probe position.

Placement of the US probe in a clinical context has not yet been conclusively resolved in the literature, and only sparse information can be found on how to bring the US probe to the patient. [Lediju Bell et al., 2014] show a repeated placement of the US probe, but with different contact pressures during the trial. In [Ipsen et al., 2021] a semi-autonomous method using a game controller is described, but not further validated.

### **Scan**

There are various methods for creating three-dimensional US images. In addition to specially built 3D transducers [Huang und Zeng, 2017], three-dimensional volumes can also be reconstructed using 2D transducers and a displacement of these. Following methods involves robot guidance for this purpose.

[Graumann et al., 2016] describe in their work a scanning motion based on surface data to create a volume of interest. Other possibilities are described by [Huang et al., 2019] and [Jiang et al., 2020], which are limited to immobile body regions, such as the forearm. Newer methods use, among other things, an additional force sensor [Chen et al., 2021] to align the image plane or deal with network problems and synchronization issues [Abbas et al., 2021]. In recent publications, however, combined approaches based on a master-slave method and haptic input devices can also be found [Geng et al., 2020].

### 2.1.2 US Systems

The development of US goes back to the piezoelectric effect [Pollet, 2012] discovered by Pierre and Jaques Curi. Modern US devices use this effect to send sound waves into the body and measure the response time. Reflections from organ boundaries allow a two-dimensional image to be acquired with a typical B mode ultrasound. For more in-depth insights into US, the books [Barnett und Morley, 2012, Jürgen Debus, 2012, Hassani, 1976] are recommended. Since this work does not include any image evaluation and processing, only effects that arise during the positioning of the US and thus must be considered for the Ultrasound guided radiation therapy (USgRT) will be discussed here. Mainly, for the ultrasound image, the artefacts caused by the functional mode have to be taken into account. As shown by [Barr et al., 2013], air in particular plays a crucial role, since total reflection occurs due to the very high impedance. This means that sound cannot be generated behind air and thus represents the reason for the required contact pressure of the transducer to the patient surface and the intended use of the robot. Furthermore, it also shows limitations for USgRT. For example, the lungs cannot be examined by US. There is also a similar reduction in the quality of the image with bony structures. These reflect the sound due to their high density and thus hide posterior structures [Barr et al., 2013].

The given limitations restrict the investigation area of US, however [Noble und Boukerroui, 2006] could show in their survey, that computer-assisted segmentations of several organs: Breast, prostate, kidney, gall bladder and liver are possible.

### 2.1.3 Tracking

Tracking systems enable objects to be positioned in space with sub-millimetre accuracy. For this purpose, the Polaris Spectra used in this work is based on two infrared cameras. These are arranged at an angle to each other and take synchronously images. In this system, the tools to be tracked are equipped with a so-called rigid body. This contains three or more reflective spheres, which are detected in both camera images. The spatial assignment is done by triangulation based on the arrangement of the spheres.

Different calibration methods are used to define the transformation between rigid body and desired position on the tool. In the context of US, The transformation between US image plane and rigid body is searched and there are a few examples for calibration methods in this regard [Muratore und Galloway, 2001, Bø et al., 2015]. Based on these basic methods, there is an open source platform which allows calibration based on a tilting motion of the USimage [Moult et al., 2017]. In robotic US image calibration, automatic calibration procedures are also demonstrated [Aalamifar et al., 2016, Zhukov, 2022].

### 2.1.4 Robot motion planning

In this section, the aspects relevant to robot control are reviewed. It is important to note that the concepts and implementations defined here are specific to the KUKA lbr iiwa Med lightweight robot used and are therefore not necessarily valid for other robot systems. For example, this robot has seven axes and thus seven controllable degrees of freedom, which enable it to perform additional movements compared to other industrially used robots. The axis labeling, as well as, the arm components of the robot are numbered consecutively starting with the robot base up to the flange. The end joints 6, 7 and 8 are summarized in this context as hand, 3,4 and 5 as arm and

1 and 2 as shoulder. The robot is programmed using the Sunrise OS development environment provided by the manufacturer. In the following, subject terms required for programming are placed in their context:

**Programming Sunrise OS:** Sunrise OS is an Eclipse based development IDE for Java programs especially for the robot. The development environment offers possibilities to access for example the safety control and objects of the robot.

**SmartPad:** The SmartPad is an interaction device to control the robot. It is not necessary for the medical version of the LBR, but the SmartPad can be used to store robot positions (frames). Additionally it can be used to start or test programs. Furthermore, the robot can be controlled manually via the SmartPad, whereby manual in this case means that individual axes can be moved with the help of buttons. This is altogether called jogging.

**handguiding:** An alternative for jogging the robot is the so-called hand guiding. Here, foot or hand switches are used to adjust the compliance of the robot so that it can be guided directly by hand. If the work refers to hand guidance, then this method was used and not the jogging via the SmartPad.

**Robot pose:** The joint position of the robot at a point in time is called the robot pose.

**Frames:** Similar to the robot pose, a frame stores this information (cartesian axis information: X,Y,Z, cartesian rotation in Euler angle:  $\alpha, \beta, \gamma, r$ ). In contrast, the frame stores both the orientation and the spatial position, as well as, in the case of the KUKA LBR iiwa med the redundancy angle  $r$ . Frames can be applied to any points or objects in space and serve as a reference for the robot as to which coordinates are to be approached with which orientation. Frames can be related to each other and built up hierarchically. This means that a child frame can describe a transformation to a corresponding parent frame. The defined frames can be reached by the robot (flange coordination system (CS)) or with an connected tool frame.

**Tool:** The object mounted on the flange is called a tool in robotics. For easier manipulation of the tool, a corresponding Tool coordination system (TCS) can be defined on it.

**Motions:** An implemented robot motion in Sunrise OS is composed of five key components: 1. What is being moved? For example, the tool or the robot flange 2. How is moved? Synchronously or asynchronously. In a synchronous movement, the next line in the program follows only after the robot movement is completed; in an asynchronous movement, the robot program continues to run in parallel with execution. 3. How to move? In this work we mainly distinguish between point to point and linear movement. 4. Where should the robot move to? Here an axis position as well as a target frame can be transmitted and 5. Additional parameters such as abort conditions, speed and acceleration settings. It is important for programmed movements that the movement path is unpredictable and is specified by the robot controller. However, for the same trajectory (same velocity, same coordinates), motions are repeatable.

**Point to point:** A point to point movement describes a movement in the axis space of the robot. The axis angles of the target pose and the current pose are interpolated linearly. The robot therefore starts all joints at the same time and ends the movement of all involved joints at the same time.



**Linear movement:** In a linear movement, the motion planning is done in Cartesian space. This can be done from the TCS and thus in relation to the current tool position as well as in the world coordinate system. The calculation of the axis changes of the robot necessary for the linear movement are also determined by the internal control.

**Null space movement:** Due to the seventh axis and the associated degree of freedom, a so-called null space movement can be performed. In this case, both the position and the orientation of the tool in space are maintained. Only the joint position of the robot is changed. This null space motion is specified via the axis value of the third axis.

**Force estimation:** The KUKA LBR iiwa has an internal force estimation. This means it can specify a force estimate based on its torque values of the individual axes. This can be applied to any frames connected to the robot. For example the Tool Center Point (TCP).

**Impedance:** This force estimate allows it to implement compliance. This can be done using spring constants and can be related to both Cartesian axis space (Cartesian impedance) and joint axis space (joint impedance). The general concept of Cartesian impedance and the underlying robot developed by DLR are presented by [Albu-Schäffer und Hirzinger, 2002].

**Singularities:** For the freedom of movement of the robot it is important to pay attention to so-called singularities. These prevent a movement along one or more Cartesian axes as soon as two robot axes are colinearly aligned.

**Smart servo:** In addition to the conventional motion commands point-to-point (PTP) and linear (LIN), there is also the possibility to send cyclic position updates to the robot. The robot then dynamically changes the current motion control immediately and sets the transmitted value as the new target coordinate. In Sunrise OS, direct smart servo control can be used here (transmission rates up to 1 kHz), for axis control as well as a smart servo LIN motion for Cartesian coordinate transmission in the 50 Hz range.

**Break conditions:** To abort a motion, abort criteria can be defined. For example, the robot's internal force estimate can be used for a spatial force condition, which then monitors the spatially acting force on the previously transmitted point during the motion. Alternatively, the joint moments of the robot can be monitored. In addition to termination conditions, the conditions can also be used to initiate a motion.

**Atomic monitoring functions:** In addition to direct monitoring of motion commands, AMF can also be defined in the robot's safety controller, which, for example, monitor Cartesian velocity or torques and pause robot control if threshold values are exceeded. AMFs are also used for switching between manual guidance mode with foot switch and the normal application.

**human-robot-interaction (HRI):** In this work, HRI refers to interacting with the robot to transmit motion commands. That is, for example, haptic gestures are used to start a motion. Once the motion is started, however, it occurs without any further action on the operator side.

**Human Robot Collaboration (HRC):** In contrast, HRC refers to direct collaboration between robots and humans in solving a task. In this thesis, HRC describes the interaction of the robot between the patient and the robot. This means the definition includes not only pure collaboration, but also acting on humans.

### 2.1.5 Safe Human Robot Collaboration (HRC)

Safe human-robot interaction is a vast field with various concepts and techniques. Basic approaches used in this work are mainly inspired from [Lasota et al., 2017] and [Haddadin, 2014] and validated by the [ISO/TS 15066:2016, ].

Starting with the work of [Lasota et al., 2017], which considers four key aspects:

- **Safety through control:** This describes the safety aspects that are possible on the basis of the robot controller and, in addition to pre- and post-collision, also includes a consideration of the speeds that are applied and the safety areas that have been set up.
- **Safety through motion planning:** In simple terms, this concept describes the avoidance of collisions with people by avoiding them as widely as possible.
- **Safety through prediction:** This paradigm assumes that both the human action and the robot action are predictable. Thus, the robot can react to the human's movements and vice versa.
- **Safety through consideration of physiological facts:** This addresses the desired behaviour of the robot and the associated sense of security.

[Haddadin et al., 2017] provide basic methods for handling collisions with robots. They use an event pipeline for this purpose, which utilizes the context as well as available signals (e.g., axis values, force measurements). These are used in each of the 7 states of a collision presented by them. The pipeline starts in the pre collisions phase and ends in the post collision. In the beginning, the detection (phase 2), identifies the presence of a collision. This is followed in the isolation (phase 3) by the determination of the affected area (e.g. contact link). Additional parameters such as the direction of the force are then aggregated in the identification (phase 4) and evaluated in the classification (phase 5). This determines which parameters were associated with the collision (e.g. accidental, intentional). This classification then provides the basis for triggering a suitable reaction (phase 6).

The legal regulations are specified by [ISO/TS 15066:2016, ]. This describes general safety requirements and specifies the forces that are still allowed for various body segments. It should be noted, however, that this standard is primarily intended for industrial applications and that the limits specified here can certainly cause injuries (e.g. haematomas).

#### Force sensing and recognition

The determination of forces acting on the robot or its tool can be done in different ways. In this thesis, two approaches were used. First, the internal force estimation of the robot was used. This provides an estimated force value for any point connected to the robot, e.g. the TCP. These values are provided together with the measurement inaccuracy, which can be significantly increased at positions close to the singular, as well as, in the elongated state [Kuhlemann, ]. The exact implementation of the estimation is hidden, but can be done according to the methodology demonstrated in [Gautier und Jubien, 2014].

In particular, to determine the force acting on the tool, special force and torque sensors are used. For the factors acting on the sensor, such as its own weight and acceleration, various calibration methods have been created using mathematical approaches [Gámez García et al., 2004, Gong et al., 2013], up to methods of deep learning [Oh et al., 2017]. A completely automated process

is presented by Garcia [Gámez García et al., 2005]. In addition to existing force sensors based on the electromagnetic piezo effect, there are also methods that use optical wavelength [Chen et al., 2021].

### Collision Detection

For the above described necessary and possible collision detections [Haddadin et al., 2017] there are different approaches described in the literature. Besides the already shown solutions based on force sensors, there is also the possibility to use the axis values of the robot to detect collisions and to estimate the collision point [Popov et al., 2017]. For this purpose, newer approaches using neural networks [Sharkawy und Aspragathos, 2018] are also investigated. Additionally, a pre-collision detection based on camera data can be performed [Beyl et al., 2016]. However, it can be generally said that there is still no universal solution to these problems and it always requires an application-specific approach.

### 2.1.6 Medical Imaging Interaction Toolkit (MITK)

MITK is an open source medical imaging program developed at the German Cancer Research Center [Nolden et al., 2013], written in C++. It combines the two libraries VTK and ITK and contains various image processing tools but also interfaces for the integration of imaging hardware. It is divided into modules, which bundle e.g. filter operations or more abstract methods, and plugins, which provide a graphical representation for the interaction with the filter and methods implemented in the modules. The integration of existing functionality can be done either via micro services or through the direct integration of individual modules. The following basic functions required for a USgRT application are already available in Medical Imaging Interaction Toolkit (MITK):

- **Image guided Therapy (IGT):** MITK contains mechanisms for easy integration of IGT [Franz et al., 2012]. This also includes filter operations and graphical user interfaces for image registration and setup (connection of tracking device).
- **US Support:** Real time ultrasound support was realized by [März et al., 2014].
- **OpenIGTLink** The interface OpenIGTLink is used for communication and part of the openigtlink module [Klemm et al., 2017].

### 2.1.7 Preliminary work

Functionality for the application is based on own developments from [Seitz, 2018]. The existing application contains the following essential functionality for the USgRT:

- **Robot control:** Basic integration and connection of the robot in MITK based on OpenIGTLink according to [Tauscher et al., 2015].
- **Experimental Breathing and motion compensation (BaMC):** A simple experimental BaMC was implemented with control capabilities during compensation, but without verification of functionality or safety.
- **image processing:** A fusion of tracking and image information was realized by applying created filter operations. The spatially resolved images were then further used for the rendering of 3D ultrasound images.

## 2.2 Clinical scenario

USgRT is a broad subject area that encompasses many components, people, and techniques. As can be seen from the challenges (1.2), the main focus of this thesis is on safe control of the robot when having contact to the patient. This issue cannot be solved separately from other tasks (e.g. image processing, tumor identification, patient registration). In order to take a holistic approach, an experimental setup (2.2.1) and a potential clinical workflow (2.2.1) were designed.

### 2.2.1 Experimental Setup

The experimental setup reflects a simplified USgRT configuration. Figure 2.1 shows the corresponding setup including the spatial assembly. Core component is a lightweight robot (1) and its control unit (2) used together with the US probe (3e) mounted on the flange. The US probe mount further includes the force sensor (3b). The robot is mounted on a mobile stand (4). An Acuson, S 1000 was used as the US device (5). The US image stream was captured and transferred to the control computer via an Epiphan frame grabber (6). A conventional table was employed instead of the Linear Accelerator (LINAC) table as a support for the phantoms and volunteers (7) used. The position and orientation of the US probe is tracked by an NDI, Polaris Spectre (8) camera system. The force sensor (3b) is supplemented by the network box (9), which transmits the measured values. Devices 1-9 represent the treatment room setup. In addition to the treatment room setup, there are also the control components: control computer (11) and joystick (10). These form the necessary telemanipulation instruments for the control from the outside of the bunker. For the experiments in this thesis, however, they were not spatially separated. In detail, the following components were used:

- ① **Lightweight robot - KUKA, LBR Med 14 R820:** The robot used is the LBR Med, a lightweight robot from KUKA. It is specially optimized for HRI in the medical field. With its 7 axes, it allows not only translational and rotational manipulation of the tool, but also an alternative axis positioning with a constant tool position. Furthermore, an internal axis torque measurement enables a sensitive force estimation, which allows the robot to react to the user's touch.
- ② **Robot control computer - KUKA, Sunrise Cabinet Med:** The sunrise cabinet controls and pilots the robot motion. It is connected to the remote control computer (11) via Ethernet.
- ③ **Tool:** The US probe holder is composed as follows, starting from the view of the flange:
  - (a) *Mounting plate - DKFZ:* This in-house developed and 3D PLA printed mounting plate connects the robot flange and the force sensor.
  - (b) *Force sensor - Schunk, FTN-DELTA-IP65-10-NETB-0.2 SI-660-60:* The sensor part of the force sensor.
  - (c) *Rigid Body - DKFZ:* A rigid body for the mounting of the fiducials for optical tracking system with four passive NDI spheres.
  - (d) *US probe mounting shells - DKFZ:* Two complementary shells were designed and manufactured in-house for mounting. For this purpose, the US probe is placed in between and screwed into place. The inside of the shell is lined with silicone to prevent movement within the shell. Attachments for a rigid body are attached to both shells. The

shells themselves are additively manufactured in PLA and connected to the force sensor with screws. The US probe mount has an angle to the robot flange of about 60°.

- (e) *US probe - ACUSON, Curved array*: A commercial 2D US curved array for abdominal usage.
- ④ **Robot base- DKFZ**: The robot was mounted to a movable but fastenable metal pedestal.
  - ⑤ **US device - ACUSON, S1000**: The Acuson S1000 US device is a clinical US device with a typical B Mode.
  - ⑥ **Frame grabber - Epiphan, DVI2USB**: DVI2USB is a video recording device to digitalise a video input. The video of the US device can thereby used by the control computer. The US device is connected via HDMI and the control computer via USB
  - ⑦ **Phantom - DKFZ, Phantom and CIRCS, 057A**: For the tests, either the in-house developed phantom "Winfried" shown in Figure 2.1 or a triple modality phantom model 057A from CIRCS was used. CT images were taken of both phantoms. For registration with the optical tracking system, corresponding markers were attached.
  - ⑧ **Tracking device - Northern Digital Inc, Polaris Spectra**: A Polaris Spectra from NDI was used to track the US. The stereo camera system operates in the infra-red range and determines the spatial position by means of triangulation of the rigid body spheres in the two images. The system has a spatial accuracy of 0.132 mm [Elfring et al., 2010] and a sampling rate of either 20 Hz, 30 Hz or 60 Hz.
  - ⑨ **Schunk, FTN-DELTA-IP65-10-NETB-o.2 SI-660-60**: The built-in force sensor enables both translational forces and torques to be measured. Translational forces can be determined up to 660 N in x,y direction and 1980 N in z, torques up to 60 N m. The data is transmitted via this Net Box and a socket interface over Ethernet.
  - ⑩ **Logitech, Extreme 3D Pro**: A Logitech joystick was employed for spatial control of the US probe. This commercial device grants the user control of 3 axes simultaneously, as well as, the use of several buttons and a slider.
  - ⑪ **Control Computer**: The application can be controlled and the individual modalities addressed with the help of the control computer and the Graphical User Interface (GUI) located on it.

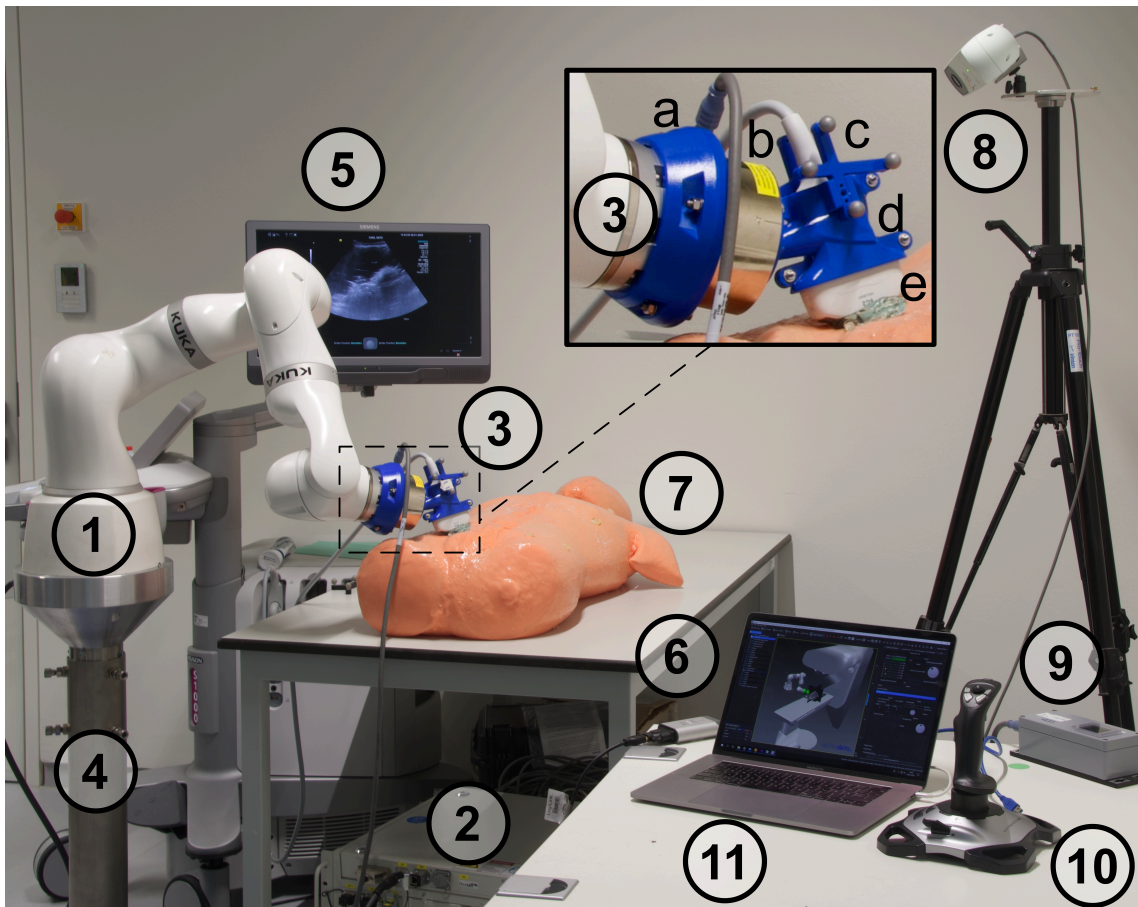


Figure 2.1: Experimental setup in the USgRT Lab at the DKFZ

### 2.2.2 Clinical Workflow

In addition to the hardware components shown and used in 2.2.1, USgRT also requires several human actors. These interact with the developed system at various points. Interaction takes place by software components (e.g. GUI), as well as, by haptic interaction (e.g. operating the joystick, guiding the robot by hand). For simplification, the following two actors were defined: The patient/proband presents a passive actor, who normally does not take direct control of the system. The robotic system reacts to the patient (i.e. respiratory movement) and adjusts for the BaMC. In addition, a reaction takes place in the event of a collision with the patient or if excessive force occurs. The second actor is the Medical Technical Assistant (MTA), henceforth referred to as "the user". The technician controls the system, sets up the devices, and instructs the patient. For a near clinical implementation of USgRT, a workflow consisting of four steps was created. A visualization of the workflow is given in Figure 2.2.

- **Setup:** The Setup includes all steps that are necessary prior to the actual application. The first step is to connect and set up the individual modalities. Afterwards, necessary calibration procedures can be carried out (e.g. spatial calibration of the tracking via a

predefined robot movement). During setup, the patient is positioned on the couch after these steps have been completed. For this reason, the robot is setup to an initial starting position.

- **Registration:** After the patient has been positioned, the planning images are registered with the current setup via the landmark-based tracking camera.
- **Positioning:** After the patient has been initially positioned, the US probe must be placed at a suitable location on the patient surface. More details on this step are covered in chapter 2.5.
- **Correction:** After positioning the US probe BaMC is performed directly. More details on this are given in section 2.4. Before the actual treatment, the alignment of the US probe can be adjusted in the correction step or additional scanning movements can be performed to find the desired image plane.
- **Treatment:** During treatment, motion compensation continues to be active, but the image plane is kept constant. The user can display the current event, as well as, the image plane including planning images.
- **End:** The US probe is moved away from the patient and the patient is discharged.

### 2.2.3 Coordination systems

A core component of the experimental setup is the developed US probe mount. It forms the link between the phantom, US, force sensor, and robot. The external design specifies a number of technical features, starting with the coordinate systems given by the geometry shown in figure 2.3. The TCS is defined for all experiments in the US probe tip. The Z-axis points in the direction of the US plane. The image plane of the US probe is thus spanned in the Y-Z plane. All CS have connections to this tool CS:

**Robot CS:** In the robot system, rotations are represented in relation to their respective axis as Euler angles  $a, b, c$  ( corresponding to a rotation matrix ZYX). With the given robot base (RB) to flange (RF) transformation  ${}_{RB}T^{RF}$  and the measured tool transformation  ${}_{RF}T^{TB}$ , the TCS can be determined by:  ${}_{RB}T^{TB} = {}_{RB}T^{RF} * {}_{RF}T^{TB}$ . Flange coordinates, as well as, tool coordinates can be requested via the robot controller.

**Optical tracking system:** According to the robot base to tool transformation, the optical to tool transformation is given by the optical base to rigid body transformation  ${}_{OB}T^{R_{Body}}$  and the rigid body to tool calibration  ${}_{R_{Body}}T^{TB}$ :  ${}_{OB}T^{TB} = {}_{OB}T^{R_{Body}} * {}_{R_{Body}}T^{TB}$ . The tool transformation  ${}_{OB}T^{TB}$  can be obtained directly from the optical tracking system.

**Force sensor CS:** The force sensor calibration with the necessary transformations will be presented in detail in 2.6.1. The force sensor to tool centre transformation is given by the previous determined robot flange to tool CS  ${}_{RB}T^{TB}$  and the transformation from the robot flange to force sensor Base  ${}_{RF}T^{FB}$ . In this case, this transformation is given by the offset introduced by the thickness of the force sensor and the adapter plate. Therefore, the force sensor transformation is given by:  ${}_{FB}T^{TB} = inv({}_{RB}T^{TB}) * {}_{RF}T^{FB}$

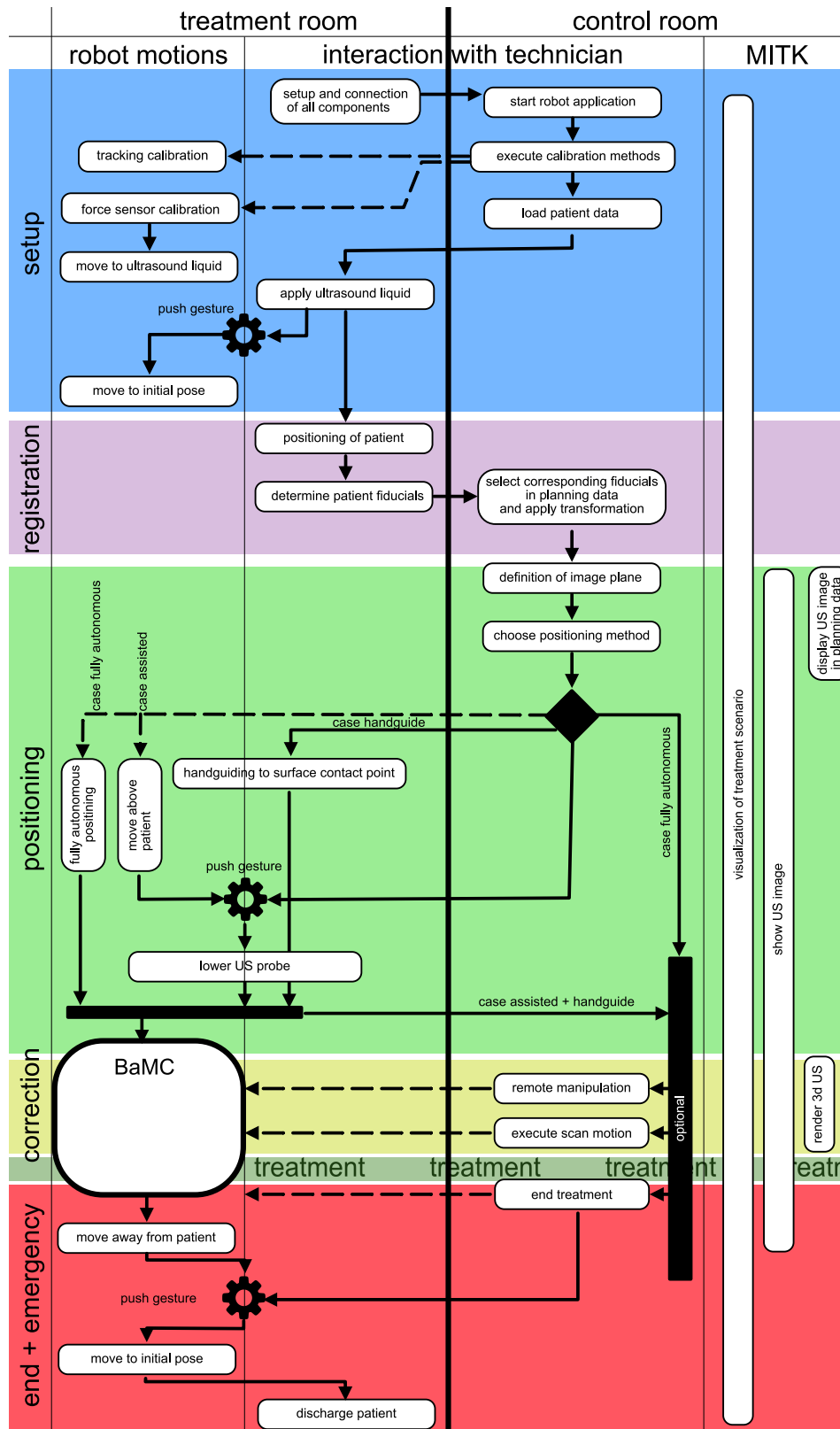


Figure 2.2: User interaction concept: The areas in the treatment room and from the control room are separated. In the treatment room, it is further divided into the sole robot movement, actions of the technician and collaborating areas (across both columns). In the control room, it is divided between interactions and information running in the background, both in MITK. Arrows indicated an interaction. If the centre line is crossed, the technician changes rooms. Except for dashed line. Here the control is done remotely.



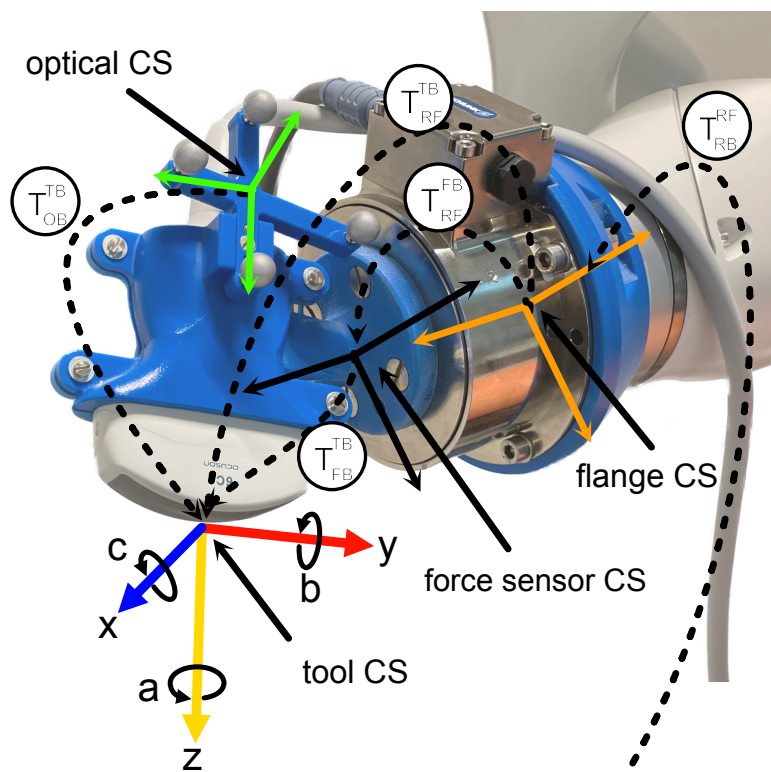


Figure 2.3: US probe mount and the different coordination systems CS.

## 2.3 Implementation

The basic framework of the implementation is based on the findings and created modules from [Seitz, 2018], presented in section 2.1.7. These were extended with missing components according to the workflow shown in (2.2.2) and existing functions and modules were modified. This includes, in particular, the aggregation of US device and the tracking camera, as well as, related image processing functions into a combined modality object (2.3.3). Further, the communication layer between MITK and robot os has been extended (2.3.2) and a force sensor has been included. The robot motion control, therefore, has been fundamentally changed (2.3.5).

Surface components have been regrouped according to the clinical workflow and enhanced with control options for autonomous positioning (2.3.4), setup controls as registration tools (2.3.4), and a virtual representation of the treatment scenario (2.3.4).

### 2.3.1 Architecture

As can be seen from the clinical workflow (2.2.2), the application is divided into two areas, one within the treatment room and the other in the control room. This division was also reflected in the software, which is why it was created as a distributed system. The central node is the control computer. All modalities (ultrasound, optical tracking, joystick and robot) converge at this point. The only exception is the force sensor, which is exclusively connected to the robot. The robot itself presents an independent subsystem, which receives commands from the control computer or via user and patient input. Motion control was directly implemented in the robot os (2.3.5) to minimize the risk in case of a broken control computer. The overall architecture is presented in 2.4. Within MITK existing functionalities and their corresponding widgets of the model layer were used to create a USgRT widget. For the USgRT extension a combined modality (2.3.3) object was developed. The developed widgets and functions presented in the overview 2.4 are described in detail in the corresponding subsections.

### 2.3.2 Integration of modalities into MITK

The existing US module [März et al., 2014] of the MITK was used to integrate and set up the US device in the application. The connection of the optical tracking system is done analogously using the IGT module [Franz et al., 2012]. Both modules were addressed via their micro services. For image fusion with tracking data, a Combined Modality class was developed according to [Franz et al., 2013]. Preliminary work on image processing from [Seitz, 2018] was bundled in this class. The initial setup of the two devices is designed into a setup window (2.3.4), which uses the existing widgets from the respective modules.

The integration of the robot is done analogously via the pre-developed robot module [Seitz, 2018] and via micro services. According to [Tauscher et al., 2015] Open IGTLink was used as message interface. The communication with the robot was kept simple. MITK sends command messages with parameters and receives status messages, containing robot limb angles and torque values, force on patient, and the current robot status.

### 2.3.3 Combined Modality

As previously illustrated in the integration, tracking, ultrasound, and the robot were bundled in the Combined Modality Object. This can be configured and initialized at the beginning of the

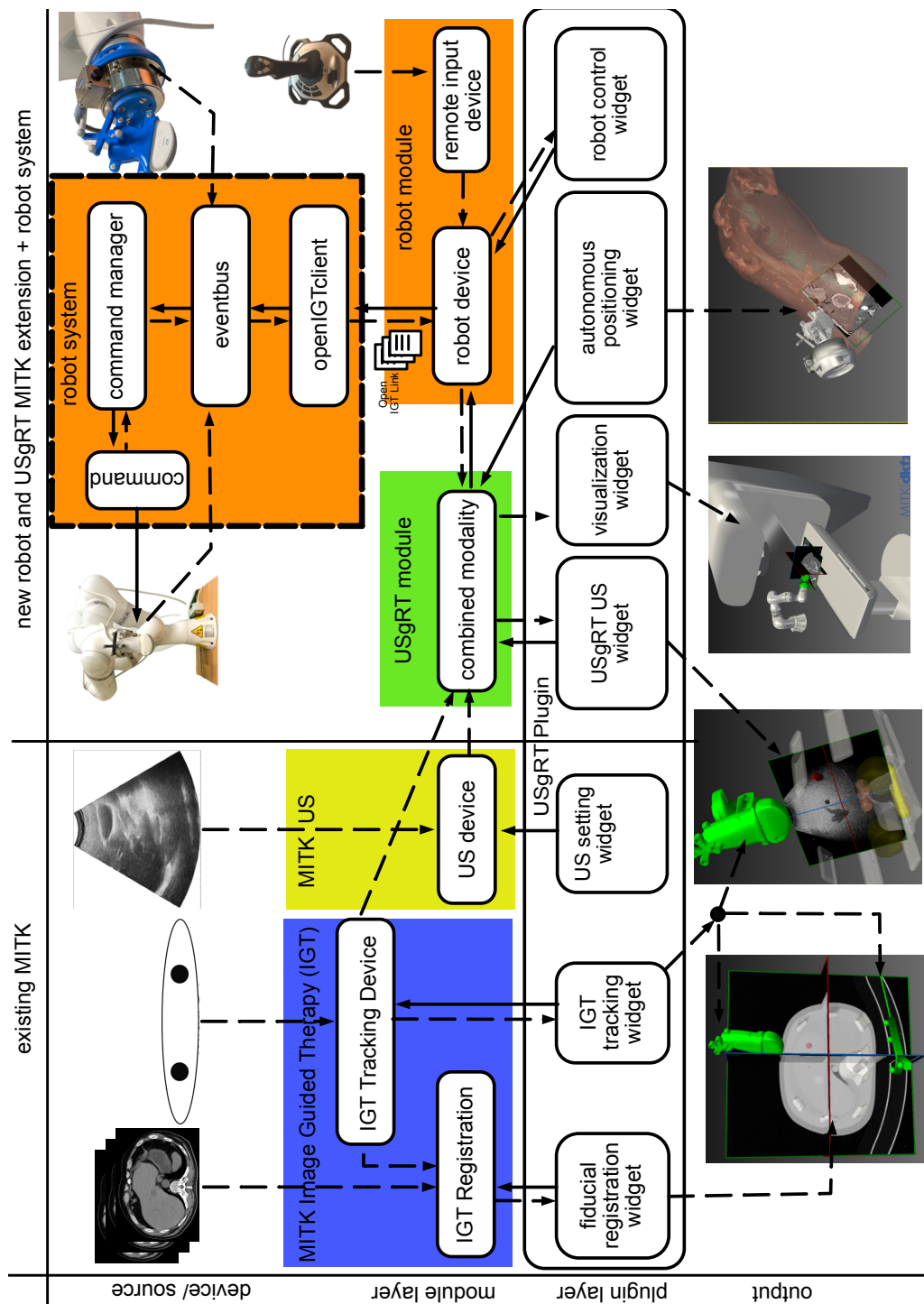


Figure 2.4: Implemented architecture: It is divided in a hardware layer, module layer and plugin layer and the output layer which is presented for the user. The robot system is independent of MITK and an system on its own and is connected to the face sensor. Arrows indicate control of one component over the other and dashed arrows indicate information flow. Smaller existed and developed widgets were bundled in the USgRT-plugin witch graphical aggregate them to represents the workflow.

application via the setup widget. After initialization, it provides access to the individual data of the modalities as an interface. An update of the object values is done in two ways. The image update of the ultrasound image is done by a filter pipeline. This connects in the Combined Modality Object, the ultrasound device as source, with the optical tracking system, or alternatively the robot. Corresponding filter operations were reused from [Seitz, 2018] accordingly. In addition, the class already includes methods for creating 3D ultrasound images based on 2D images (based on [Seitz, 2018]). The coordination between image acquisition and robot motion is also completed within this object.

The robot sensor values (axis position, torque values) are provided in terms of signals and slots. Corresponding subscribers (e.g. visualization widget and status widget) can subscribe to the Combined Modality Object. These values are then used by the visual representation widget and the status widget, for example.

### **2.3.4 Interaction with MITK**

According to the developed workflow 2.2.2, a user control was created. This allows the user to go through the individual steps. For each step, one or more graphical panels (widgets) have been created. For the initialization (step 1), a newly implemented initialize widget (2.3.4) connects the US, the robot, and the tracking device, based on the integration (2.3.2). Further, the patient data can be registered (step 2). For a better impression of the whole application, a visualization widget was created to represent all used modalities 2.3.4. Within an autonomous positioning widget (2.3.4), a target plane of the US probe can be defined (step 3) and one of the placement strategies can be selected and executed (step 4). After execution, BaMC motion (2.4) is started (step 5).

#### **Setup**

The first step of USgRT involves connecting the individual modalities. For this reason, a custom setup widget was created. It uses the existing widgets of the MITK presented in the integration (2.3.2). For initializing the combined modality object (2.3.3), both the ultrasound setup widget [März et al., 2014] and the IGT tracking widget [Franz et al., 2012] were included. The existing settings window [Seitz, 2018] was also used to fine tune the settings. This can be used, for instance, to define the ultrasound angle, ultrasound scan head depth, or image scaling factor. For test purposes, only individual components can also be connected. In this case, however, the functions of the other widgets are greyed out, if not usable with the selected modalities. Meanwhile, the registration and the differentiation of the rigidbodies can be aligned at the beginning in the setup widget, as well as, the transformation between robot world coordinate system and tracking coordinate system can be calculated. Afterwards, the integrated registration widget from the IGT tracking plugin [Franz et al., 2012] is used to register planning data with the current situation.

#### **Visual representation of treatment scenario**

A virtual three-dimensional representation of the treatment scenario was established using an existing limb model of the robot and a generic designed accelerator model [Goos, 2022]. The position of each link of the robot was set via combined transformation matrices and the robot sensor values. The virtual accelerator parts can be manipulated using sliders on the developed visualization widget or via an input stream. The spatial position is set accordingly. In addition, robot force and torque sensor values are used to indicate collisions by coloring affected axes

in red in the virtual representation. The virtual representation was registered with the planning data via the setup widget (2.3.4). The current US probe position and motions of the robot limbs are updated by the combined modality object (2.3.3).

### **Autonomous positioning widget**

An autonomous positioning widget was implemented in MITK, based on the idea presented by [Seidel, 2019], to set the US probe position. It uses the existing point set interaction method of MITK to set the position on the patient's surface by mouse. After determining the position, a 3D model of the US probe is transformed to this point. The orientation of the US probe model can be changed using sliders and buttons in the widget. The model is adjusted accordingly. For visual feedback, the resulting image plane of the planning image can be displayed as well. The transformation to the planned surface contact point can be manipulated by the point set interaction tool, if necessary. Planning is done in relation to the tracking camera coordination system and target coordinates are transformed into the robot coordination system before motion execution. Further details of the usage of this widget are presented in section 2.5.

### **Robot Control**

Based on [Seitz, 2018], two widgets were created to control the robot. One widget displays the actual state of the robot. Here, the current value of the axis positions, the force at the TCP and the currently executed command are displayed. The second widget contains control buttons for executing the basic movements required for the USgRT. These include setup movements for calibrating the force sensor, applying ultrasonic gel, and initializing the motion compensation (2.3.5). In addition to the control system developed in [Seitz, 2018], these buttons were designed to be case-sensitive. This means that, depending on the command currently executed or terminated on the robot, buttons are enabled or disabled accordingly. For testing purposes, an additional button was created to transmit commands directly (i. e. , for the tests performed and data collected). The control of the robot is based on the robot controller widget shown in [Seitz, 2018]. Improved usability was achieved by customizing the buttons after the robot motion has been executed.

### **Human Robot Interaction**

In addition to the graphical control via MITK, further direct user interaction concepts with the robot were implemented. This includes, for example, hand-guiding the robot by means of hand-guiding foot switches. For hand guidance, the methodology of KUKA was applied. Further, in the case of BaMC, as shown in [Seitz, 2018], a joystick can be used for precise reorientation and manipulation of the ultrasound head position. Gesture control as in [Berger et al., 2018] was implemented for autonomous positioning. For this, KUKA's own "trigger-when" condition was used. The condition is triggered from a force on the tool of 20N along the X-axis (2.3). In the event of an error, e. g. in the case of collisions, the interaction takes place by means of defined abort conditions, which are explained in detail in chapter (2.6).

### **2.3.5 Robot Motion**

Robot control (motion planning) is controlled in SunriseOS 2.1.4. Based on the implementation developed in [Seitz, 2018], different commands can be defined. These include several basic modules (for example, point-to-point movements) and are started and controlled by MITK using an

open IGT link message (2.3.2).

This basic implementation was maintained, but the underlying architecture was completely adapted and extended by an EventBus-based component. Thus, a separate bus was created for the force sensor, the message interface with MITK-internal system events, and robot values. The definition of newly created robot commands for the UsgRT is done via a generic interface. This requires a command to define the normal behaviour, as well as, actions to be taken in case of an error or an intentional abort of the motion command. Based on this interface, more complex motion commands, such as BaMC (for details see 2.4), or autonomous positioning (for detail see 2.5), were created. The motion commands can use one or more buses to control their behaviour. For instance, to manipulate the ultrasound probe position during motion compensation, the joystick values are transported to the corresponding position via the MITK bus.

The management of the sequence of individual motion commands is done by a main motion manager, which is conceptualized in such a way that only one robot command (e.g. motion compensation) can be executed at a time. Furthermore, this class also manages the follow-up commands, so that a seamless transition between movements can be realized. According to the defined clinical sequence, the corresponding transitions can be found (see Figure 2.5). These can merge into one another according to a state machine. For example, movement compensation is started after autonomous positioning. The transition of the individual movements into one another can be performed externally, such as by MITK or gesture control, as well as automatically via the main motion manager.

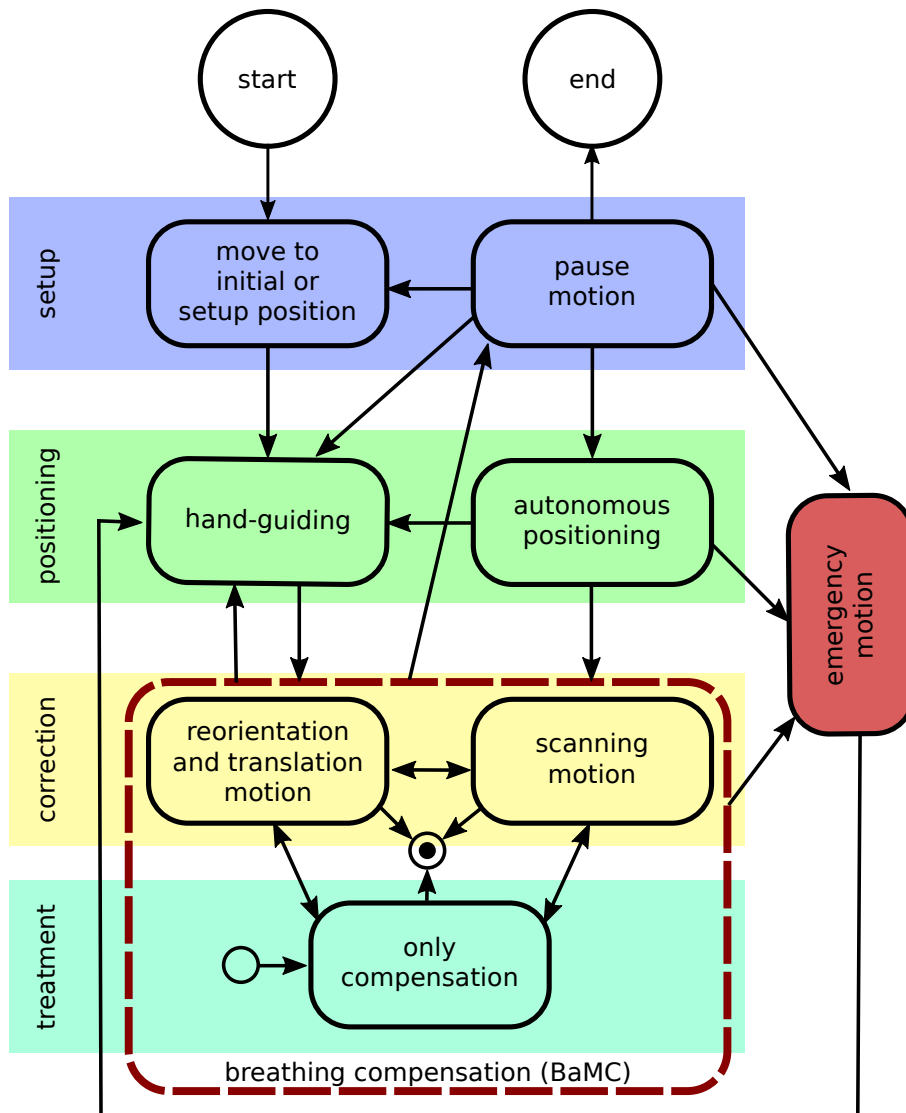


Figure 2.5: "Robot states are colored by their application. Arrows show possible transactions. BaMC is one general state with several sub- states (dashed red box)" [Seitz et al., 2020] Reproduced with permission from Springer Nature

## 2.4 Breathing and Motion Compensation

A stable contact of the US probe to the patient is essential for US imaging. It presents one key features of the USgRT application. Therefore, a complex breathing and motion compensation (BaMC) has been developed. (2.4.2).

### 2.4.1 Requirements

In 2.1.1 the contemporary definition and implementation of BaMC are described. In those papers, the main focus was put on a stable contact between patient surface and US probe. However, this definitions of BaMC in these studies were missing central requirements. Therefore, the following requirements for the BaMC were introduced for this thesis:

**stable contact:** The main requirement for BaMC is a continuous US image acquisition by means of a constant connection of the US probe to the patient's surface. This prevents reflections by air due to imperfect contact.

**breathing pattern independence:** BaMC should be independent of the respiratory motions of the patient from different breathing frequencies and amplitudes.

**US position independence:** US probe positions may vary according to the examined target structure. BaMC should, therefore, be independent of the defined US scanning position and the robot arms configuration (pose).

**deformation reduction:** In order to keep the error of inner organ deformation minimal [Virga et al., 2018] and to prevent patient inconveniences, contact forces should be less than 5 N. This was set as the desired average contact force. The upper limit of contact forces should be within 20 N.

**patient independence:** Patient tissue may vary, which is normally considered by the examiner. For adipose patient, more pressure is often needed to reach good image quality. Hence the contact pressure should also be adjustable for those cases.

**Constant image plane:** The image plane is given by the position and the orientation of the US probe. Translational motions along the z- axis of the US probe have no influence on the US image plane. Deviations along the other two axes do have an effect and should be minimized. The limits for translations (x,y) were set to  $\pm 1\text{mm}$  and rotations (Euler angle  $\alpha, \beta, \gamma$ )  $\pm 0.25^\circ$ , respectively

**controllable position:** During BaMC, it should be possible to change both the orientation and position of the US probe. This should be done by a generic interface that can be used e.g. for manual manipulation (joystick) or visual servoing motions (camera input).

**scanning motions:** In addition to the generic changeable position, performing specific preplanned scanning motions should be possible.

**zero motion:** In addition to the generic mutable position, there should be the capability to rearrange all axes during BaMC (only in case of 7+ Degrees of Freedom (DOF) robot system).

**universal usage without delay:** BaMC should be activated immediately after different preceding motions (e.g. handguiding, autonomous positioning)



**force control:** To ensure patient safety and reduce deformation the applied force of the probe should be monitored.

**interlock:** BaMC should be instantly interruptable immediately for other interactions. (E.g. handguiding, stop motions).

### 2.4.2 Implementation

According to the described architecture, the BaMC was implemented as a separate module in the robot controller. The aforementioned requirements were used as criteria for the motion. For the realization of BaMC, there are different approaches (see also 2.1.1) [Seitz, 2018, Ipsen et al., 2021]. As shown in [Seitz et al., 2020], the BaMC was implemented: The motion compensation was defined such that the image plane should be held and only a motion along the z-axis of the tool ( see picture 2.3) should take place. To achieve this, axis-specific compliance a cartesian impedance control of the robot module was used [Seitz, 2018]. This allows compliance to be defined by spring constants for one or more axes. The z-axis of the tool was set to fully compliant. For all other axes, the stiffness values were set to their respective maximum ( 5000 N/m). The coupling to the patient is achieved by an additional force application along the z-axis. According to the requirements (2.4.1), the contact pressure was set to 5 N by default.

A generic interface was created so that the position and orientation of the image plane can be changed. This allows the translation in X, Y direction of the tool, as well as, the rotation angle ( $\alpha, \beta, \gamma$ ) and the zero space angle  $r$  to be adjusted. All coordinates were defined relative to the actual ultrasound probe position. For this, the impedance control was coupled with a Smart Servo motion. This allows dynamic target input up to 50 Hz, which receives new coordinates using the interface created.

This interface was then used for different components of the application. For instance, for manual control of the transducer, values of the joystick were transmitted directly via MITK. Axis values of the joystick were converted directly into axis values of the ultrasound probe. Furthermore, the interface was used for scanning motions (2.4.3) and autonomous positioning (2.5).

During the BaMC, the ultrasound probe and thus the robot have permanent contact with the patient. Force monitoring was, therefore, set up as part of safe human-robot interaction in accordance with [ISO/TS 15066:2016, ]. The force monitoring was designed as a redundant system. The monitoring task used in [Seitz et al., 2020] directly uses the force estimation of the robot. This was validated by means of the force sensor (2.6.1). To enable a reaction in real time, a force condition was created, which checks the force at the TCP and is triggered at a threshold value. The threshold value was set to 20 N.

In case the threshold is exceeded, a two-stage safety movement was implemented according to [Seitz et al., 2020]. This moves the transducer along the z axis of the tool 10 cm away from the patient. From here, an axis-specific impedance control follows as a second step. Here, all axes are switched to be compliant, so that the robot holds its position but can be pushed away with little force.

In addition to aborting the BaMC, two other options were implemented to interrupt the motion compensation. As the first, regular method to halt the motion, the safety motion can also be triggered manually. As a second possibility, the manual guidance of the robot can be activated by means of a foot pedal. The transducer can be guided to new positions by hand. The BaMC starts again after manual guidance.

### 2.4.3 Volume scan

Scan movements of the transducer are primarily for diagnostic purposes only. By scanning an area, the tissue can be scanned autonomously and a 3-dimensional ultrasound volume can be reconstructed [Seitz et al., 2020]. This was performed according to [Seitz et al., 2020]: The motion trajectory of the scan was defined as passing through 2 to N frames. These frames define desired positions along the path. The path between the frames was linearly interpolated. A frame was designated as reached, when the distance to the current position  $(x,y)$  was below 0.5 mm and 0.5 degrees for rotation. A deviation of the frame along the z-axis (US probe plane) had no influence on the image plane and may be caused by the patient's breathing motion. A frame is therefore considered to pass regardless of the distance along the z-axis.

To create the motion paths, a start frame was defined for each trajectory. This reflects the current position of the transducer and forms the start and end point of the trajectory. In relation to this frame, child frames were created according to the desired trajectory. For example, a linear scan was set up, which has a displacement along the x-axis of 1.5 cm as the first child frame and then -1.5 cm along the x-axis as second frame, both relative to the start frame. In this case, a distance of 3 cm along the x-axis is scanned and passed through twice.

### 2.4.4 BaMC Tests

The BaMC was tested to prove the predefined requirements (2.4.1 according to [Seitz et al., 2020] on two healthy volunteers. Three independent probe positions were tested: (i) subcostal (below the ribs), (ii) next to the navel and (iii) axillary line (below the ribs). At each position, four different breathing patterns were simulated for approximately 30 s: (1) normal breathing, (2) deep inhale and exhale, (3) fast inhale and exhale and (4) breath hold. In addition to each breathing pattern, different probe motions were tested: (a) BaMC only, (b) BaMC + change probe orientation  $(\alpha, \beta, \gamma)$ , (c) BaMC + change probe position  $(x,y)$  and (d) BaMC + linear scanning motion (2.4.3).

During all tests, robot limb angle values, the current position, and the estimated force on the tool center point were recorded. The sampling rate was set to the updated interval of the smart Servo motion at 50 Hz.

In addition the clinical workflow (2.2.2) was simulated according to [Seitz et al., 2020] by aiming to observe a given target structure (gallbladder) and usage of the implemented methods.

## 2.5 Autonomous Positioning

### 2.5.1 Implementation

As shown in section 2.3.5 a self-implemented event pipeline was used for controlling the robot, based on the Kuka Sunrise OS. It connects incoming control commands, data from the force sensor or the robot data, and for the autonomous positioning additionally the optical tracking system. For the autonomous positioning an own command was designed, which uses point-to-point motion and the BaMC (2.4) together with the implemented safety methods (2.6) according to the following positioning steps (2.5.3).

### 2.5.2 Reference frames

In robotics, the tool spatial position, its orientation and, the redundancy angle configuration are summarized as a so-called frame (2.1.4). Robot motions are unpredictable and potentially dangerous for humans within the robot's range. To restrict the robot motion path, various known frames were defined in respect to the phantom and later used by the positioning strategies. A general start frame has been defined next to the patient table. For the autonomous strategies (AS, FA, see below) 30 default frames distributed around one side of the phantom at approximately 15 cm distance have been defined manually (see Figure 2.6). These frames demonstrate safe robot positions. It has been ensured that when approaching these frames from the start frame, the phantom is permanently out of the range of the robot. A central aspect of the positioning procedure is the defining of the spatial location of the US image plane. Therefore, the image plane is defined by the surface contact frame, which includes a spatial position and the orientation of the US probe. Both can be adjusted in the developed software (2.3.4). The surface contact frame can be chosen freely but should be on the phantom surface. Depending on the final surface contact frame, a second frame above the surface was calculated: This frame was set to be 10 cm in the negative z direction, above the surface contact frame (see Figure 2.6), and therefore, has the same orientation.

### 2.5.3 Positioning strategies

For various utilization scenarios of US application, five different positioning strategies have been introduced ranging from guiding the robot completely manually to completely autonomously.

- **Manual (M):** The US probe is positioned by hand from the starting frame to the surface contact frame. The robot reacts to external force and translates it into motion in real-time. Hand-guiding can be activated by a foot pedal. After placement, BaMC starts. If necessary, hand-guiding can be activated again by pressing the foot pedal.
- **Manual and joystick (MJ):** The position and orientation of the US probe can be adjusted remotely with a joystick after it was placed to the surface contact frame manually (M) [Seitz et al., 2020].

All the following methods include additional VS during BaMC. For VS tracking, data from the Polaris camera is used to identify planned surface contact frame and current position and orientation of the US probe. A basic proportional regulator (p-regulator) was used. It multiplies the difference of the actual surface contact frame and planned surface contact frame according to the optical tracking device by a constant and sets it as the new target for the robot. The robot

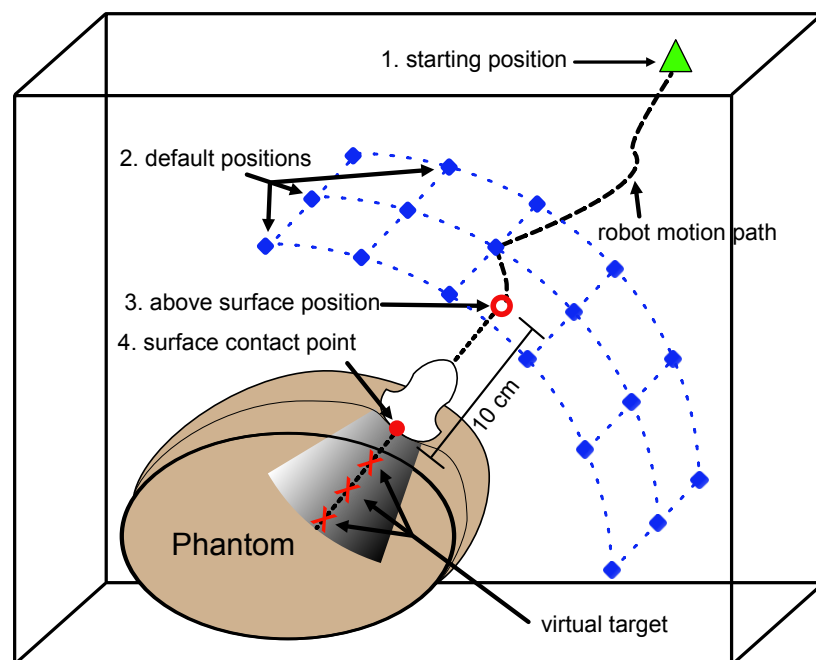


Figure 2.6: Setup related frames: A motion path is determined for the positioning of the US probe. Beginning with the starting position (1), the probe first moves to a known, defined default position (2), second, to a calculated position above (3), and third, to the defined surface contact point (4). Three virtual targets located at 3, 5, 7 cm depth are used to calculate the potential image plane-to-target distance for the various methods.

emits a signal when the target point is reached with 0.5 mm (x,y) accuracy, independent of its z distance, and 0.05 ° in orientation (Euler angles a, b, c). Those values specify the maximally accepted image plane deviation for autonomous methods.

- **Manual and visual servoing (MVS):** First, the US probe is positioned manually (M), afterwards the fine adjustment of the final position is done by the visual servoing (VS) mode during BaMC.

With the following methods, starting at the starting frame, first a suitable default frame and the above surface frame (2.6) are always approached one after the other. Both are reached PTP based and fully autonomously.

- **Assisted (AS):** With a physical push to the US probe along its x-axis, BaMC motion can be activated, and the US probe is lead down to the surface assisted by the user.
- **Fully Autonomous (FA):** There is no user interaction at all. US probe is moved towards patient to a pre-defined point on the surface autonomously by the robot. This is realized by a linear motion with a force constraint of 10 N (z-axis). If the surface contact frame is reached or the condition is triggered and BaMC starts immediately.

## 2.5.4 Experiments

Various tests were carried out to compare the positioning strategies, the repeatability of the position, and the safe execution of the corresponding motion. Across all experiments, robot sensor values, tracking data, and data from the force sensor were recorded. Virtual targets were defined to show the effects of an inadequately placed US probe. The distance of the actual image plane to the original one was then quantified by the distance of the image planes to the virtual target. These are located at 5, 7 or 10 cm depth and centered in the US image, depending on the desired surface contact frame (Figure 2.6).

### Comparison of different positioning strategies

The positioning strategies were tested and evaluated regarding their potential clinical application. For this, five surface contact points on the phantom were defined using the developed user interface. Three experienced users of the system navigated the robot to those positions and optimized the correlating planed and actual image plane by the different methods (3 persons x 5 positions x 4 methods (M, MJ, MVS)). For the same 5 positions also the autonomous methods were tested twice (5 positions x 2 x AS, 2 x FA). The 3D representation of the US probe and simulated target image plane in the planning data, displayed in the developed GUI, served as guidance. Elapsed time, motion path as well as forces were recorded. In accordance with the formula

$$R_{Diff} = R_{Planned} * R_{Actual}^{-1}(I)$$

(R= rotation matrix), the deviation of orientation resulted from the product of calculated and actual position. The total tilt angle is determined by the arccosines and trace (tr) of  $R_{Diff}(I)$ :

$$R_{Diff}\theta = \arccos\left(\frac{trT_{Diff} - 1}{2}\right)(II)$$

The translational deviation was calculated from the defined target point coordinate system (x, y, z)

### **Position independence, precision, accuracy**

For the autonomous positioning procedures AS, 60 test positions were approached twice. To test the method for position independence 25 out of the 60 positions were set with small translational and rotational variances longitudinal below navel according to a pelvis view [Gerlach et al., 2017a] and 35 were uniformly distributed in lateral direction (trans-abdominal US view). Another 60 randomly selected positions with a modified setup (different robot position in relation to phantom) were traversed. The desired US probe angle to phantom surface was set to be orthogonal but varied within  $\pm 30^\circ$ . The positions were defined via the developed define target plane widget (2.3.4) and control was carried out via the programmed user interface. Initially, the phantom was registered to the real scenario at the beginning via the user interface and the IGT-tracking plugin [Franz et al., 2012].

### **Safety**

In addition to the tests mentioned above, it was ensured that the safety mechanisms (2.6.3) work properly. To test exceptional situations, various limb parts of the robot and the tool (US probe) were blocked manually during motion. Through this, it was ascertained if the robot executed the desired pre-defined stop reaction. One abdominal and one pelvis US probe position were tested. For the two positions, 7 collisions of the tool, and 20 collisions distributed evenly over the limbs were assessed. In case of collisions with the tool, the time of contact between robot and phantom was assumed to be the time when the force sensor detects an additional force. The reaction time was then determined from the time of contact to the beginning of the stop reaction.

## 2.6 Safety

Force, applied to patient and especially at TCP (see section 2.2.3 Figure 2.3) plays a major role for safety. During BaMC and probe positioning, it describes the force applied on the patient. According to [ISO/TS 15066:2016, ], those forces need to be parametrized and limits must be set. For the autonomous positioning method, the maximum tolerated force on patient ( $F_P$ ) was set so 20 N according to [Seitz et al., 2020]. Since the robot's force estimation may be affected by its position [Kuhlemann, ], a redundant force sensor was installed 2.6.1. For this application, the limits for force and limb torque, as well as, application speed were chosen as lower than recommended in [ISO/TS 15066:2016, ] (threshold BaMC 20 N velocity autopoisoning 25 mm/sec). As recommended, a collision detection mechanism 2.6.3) is permanently active. The visualization of active forces via the implemented (2.3.4) builds one of the safety measurements.

### 2.6.1 Force Sensor

The force sensor was integrated into the existing robot application via the supplied socket interface (ATI) and passed on to the event pipeline. To calculate the contact total force  $F_P$  (see 2.3), the following forces acting on the sensor were considered [Richter et al., 2012, Karayiannidis et al., 2014, Gong et al., 2013]. The measured force sensor value  $F_S$  consist of the contact force  $F_P$ , the gravity of the tool  $F_G$ , and the force introduced due to acceleration ( $F_A$ ). As a result, the contact force can be calculated as:  $F_P = F_S - F_G - F_A$ . A calibration movement was implemented to determine the influence of gravity ( $F_G$ ). This tares the force sensor at the beginning and then rotates it around all axes of the tool coordinate system by 180 °. In detail the tare position has the following axis angles: A4 -90°, A5 90° all other axes 0°. The calibration movement itself is composed in detail of a rotation of axis A5 by -90° to 90°, then a rotation around axis A7 to 90°, then axis A6 to -90°, then 90° and then 0° and a rotation of axis A7 by -90° to 90°. To minimize the influence of acceleration on the weight measurement, the speed of the movement was set to 10% of the maximum robot speed.

The collected values were compared to the expected value based on the methods described by [Gong et al., 2013, Carlson, 2019]. After optimization of the parameters, the calculated values were subtracted from the sensor values. The influence of acceleration was examined in several tests (2.6.1). The influence of acceleration on force measurement was investigated in an experiment. Linear movements were carried out along the world coordinate axes at a distance of 60cm at different speeds. The speed was increased in each case stepwise (25mm/second increments) from 25mm/second up to 500mm/second.

This demonstrated that it only has an effect for accelerations occurring when the overall speed is above 25 mm/sec 3.4.1. As the used motions for the autonomous positioning are slower, this effect was not considered.

### 2.6.2 Collision types

[ISO/TS 15066:2016, ] basically distinguishes between two types of collisions: transient and quasi-static. In a transient collision, the user is free in space and can bounce off the corresponding robot component in the event of a collision. In a quasi-static contact, the operator is trapped in the comparative and subsequently cannot avoid the robot's motion. In addition, the collision point, duration, and motion were distinguished from each other.

Table 2.1: Collision points per robot limb.

axis segments	limb 1	limb 2	limb 3	limb 4	limb 5	limb 6	tool
collision points	A1_1	A2_1	A3_1	A4_1	A5_1	A6_1	Tool_1
	A1_2	A2_2	A3_2	A4_2	A5_2	A6_2	Tool_2
		A2_3	A3_3	A4_3		A6_3	Tool_3
		A2_4	A3_4	A4_4		A6_4	Tool_4
		A2_5		A4_5			Tool_5
collisionpoints/ axis	2	5	4	5	2	4	5
						total:	27

### Collision points

Collision points were defined both on the tool (US probe holder) and on the robot at which a collision is possible. For simplification, the surfaces of the individual axes were combined. Table 2.1 gives an overview of the chosen points per limb. On the tool itself, 5 collision points were identified (see Figure 2.7). The axes A7 to A5 were combined as the hand of the robot. Collision points on axis 7 were not identified because they correspond to collisions on the tool. On axis 6 there are 4 collision points, axis 5 has 2. axis 4 and axis 3 were summarized as arm. On axis 4 there are accordingly 5 collision points and at axis 3 there are 4 collision points. Collision points of the last two axes are assigned to the shoulder of the robot and here axis 2 has 5 collision points and axis 1 has 2 collision points.

### Duration

A collision can involve both an impulse and a permanent force. Therefore, the tests were divided into very short hits (contact time < 1s) and longer contacts (contact time >1s) with the hitting object.

### Motion

Depending on the movement taking place at the time of collision, different safety measures, as well as, detection mechanisms are necessary. Therefore, three types of movements were identified in the application. The first one is the respiratory motion compensation, the second, the standard setup movements that performs point-to-point movements, and the third, lowering movement for autonomous positioning.

### 2.6.3 Collision detection

A collision detection of the robot can be based on robot sensor values, as well as, external sensors. Accordingly, both the robot sensor values (force estimation as well as torques) and the external force sensor were used in this application. Three basic detection mechanisms were implemented.

1. **Spatial force condition:** Detection based on spatial force measurement by the robot force estimation on TCP.
2. **Torque force condition:** Detection based on robot external torque values.
3. **Force sensor:** Detection based on the measurements of the force sensor.



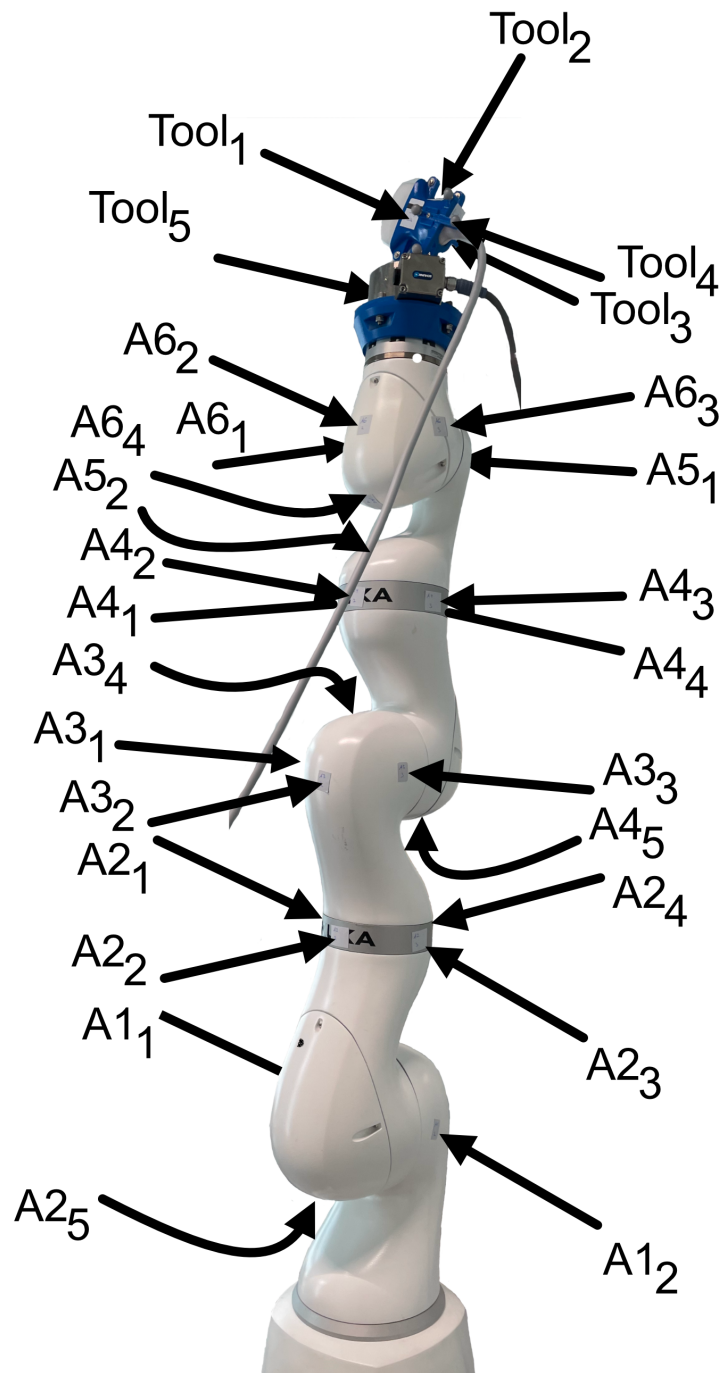


Figure 2.7: Spatial position of collision point for each limb segment.

Table 2.2: Collision detection mechanisms.

collision detection mechanism	detection mechanism		spatial force condition TCP	external torque condition	force sensor (FS)	
	threshold for motion	PTP		10N (TCP)	10 Nm	10N (FS)
		BaMC		20 N (TCP)	15 Nm all limb	20 N (FS)
		Positioning		10N (TCP)	15 Nm all limb	10N (FS)
SPATIAL		✓				
TORQUE		✓	✓			
FORCE_SENSOR		✓	✓	✓		

In a preliminary test, the effects of a collision on these sensor values were investigated. For this purpose, collisions were performed at the movements, collision points, collision duration defined above. Based on this procedure, threshold values were calculated at which a collision could be detected and which would result in a false positive rate as low as possible. Based on these data, the threshold value for the different motions was calculated. The limits for external forces and torques on limbs were set to 10 Nm and 10 N for collisions with the US probe during PTP motions. For BaMC, the thresholds were set to 15 Nm and 20 N on the TCP. For the lowering movement, the threshold values were set to 15 Nm and 10 N at the TCP. (see also Table 2.2).

The monitoring of these threshold values takes place in the Sunrise environment itself and was specified in each case as an abort condition. A corresponding triggering of these abort conditions emits the currently executed movement and is detected in real time by the robot system. The integration of the force sensor and the monitoring of the threshold values by means of the force sensor is done via the created interface (2.3.5).

The detection mechanisms have been aggregated into 3 final combined mechanisms: SPATIAL, TORQUE, FORCESENSOR. (2.2), using one or more mechanism.

To determine which of these final collision detection measures is sufficient, a test (2.6.5) was carried out.

## 2.6.4 Reactions

Various reactions were implemented depending on the interrupted movement executed during collision.

- **PtP-motions** (e. g., motion from start frame to default frame): A full stop was set.
- **Approaching the surface**: A position hold reaction was implemented. In doing so, the current position of the probe is softly maintained, i.e., the robot can be pushed manually out of the way.
- **BaMC**: The US probe is first moved away from the surface to release the patient. Then, the above-mentioned position hold method is used.

## 2.6.5 Validation tests

Several application-specific movements were performed to validate the collision detection, as well as, the reaction mechanisms.

Table 2.3: Test Positions for collisions during BaMC.

US prob positions and related axis angles	position on phantom	A1	A2	A3	A4	A5	A6	A7
	Axilliar_45	-27.68	68.77	-6.84	-86.53	7.93	-49.48	47.68
	Axilliar_90	-60.36	86.67	27.39	-82.84	-26.10	-63.03	57.91
	Navel	-7.73	67.21	1.43	-74.25	78.13	-52.05	-12.86
	Subcostal	-43.11	90.82	72.73	-53.90	31.27	-71.64	-85.71

1. 108 collisions during PTP motions: These included 4 PTP movements (start-position to ultrasound-fluid-apply-position (probe rotated upwards for an easy apply of ultrasound liquid), start to calibration position force sensor (2.6.1), and vice versa). For those collisions only the TORQUE detection mechanism was used. Each Collision point was hit with a short hit.
2. 3\*108 collisions during BaMC for each Detection mechanism Table 2.2: BaMC was applied at 4 different US probe positions (Navel, subcostal and axillary 45 degrees and axillary 90 degrees (see Table2.3)). During the movements, as well as, the different positions, a collision was generated at all of the collision points identified above. The collision point was manually pressed and the force was slowly increased in order to identify, if possible, the lower limit above which a collision is detected.



# 3

## Results

### Disclosures to this work:

Parts of this work ( section 3.2) have been published in:

**Peter Karl Seitz**, Beatrice Baumann, Wibke Johnen, Cord Lissek, Johana Seidel, Rolf Bendl. Development of a robot-assisted ultrasound-guided radiation therapy (USgRT) *Int J CARS* 15, 491–501, December 2020. doi: 10.1007/s11548-019-02104-y

### 3.1 Clinical workflow and user interaction

The tests performed demonstrate indirectly that the clinical workflow developed in 2.2.2 could be implemented. All four defined steps are possible. This indicates that from the setup, to the application to the patient, all necessary control concepts and interactions could be defined and implemented. In particular, the autonomous positioning demonstrated the successful interaction between graphical user interaction concepts, as well as, the direct interaction with the robot. In the handling of the robot, it was observed that the implemented safety measures were effective at all times. A detailed analysis of the security follows in section 3.4.

The linking or registration of planning images with the actual situation in the test setup was successfully demonstrated. This includes the precise representation of the robot in the treatment situation. Figure 3.1 demonstrates that the arrangement of the experimental setup (2.1) can be displayed virtually.

The direct interaction with the robot, such as in the applied gesture control, worked smoothly and was reliably recognized during the tests.

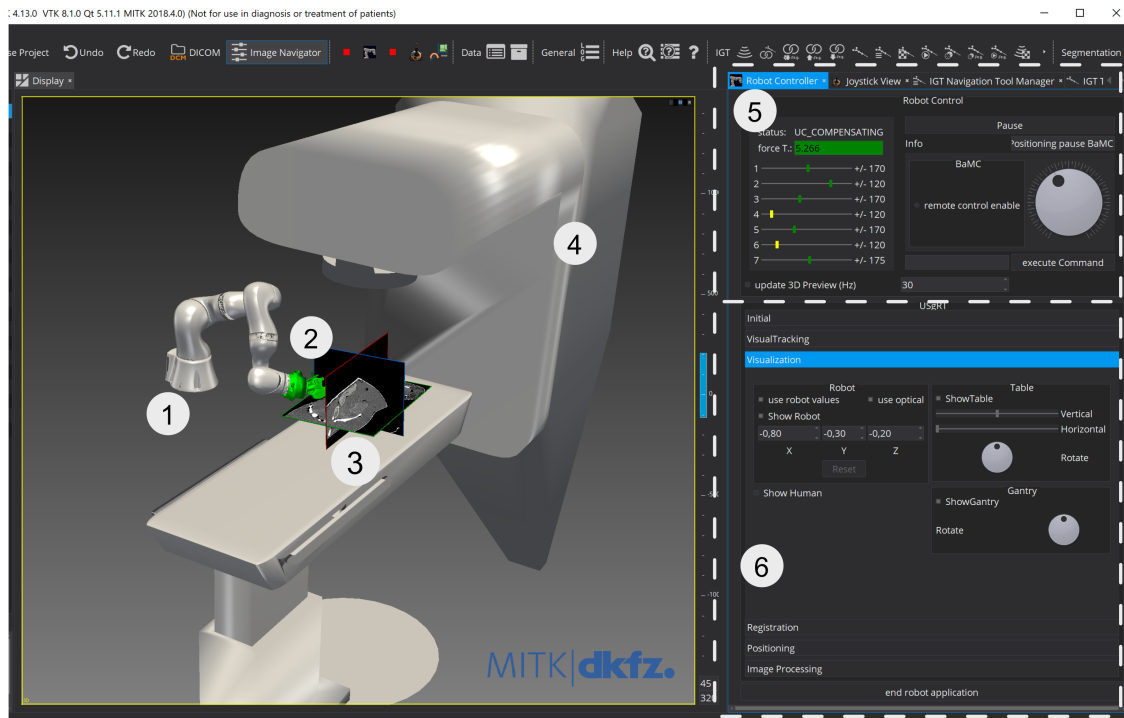


Figure 3.1: Visualization of the treatment scenario – 1) Robot model, 2) US probe and force sensor model (position based on optical tracking data), 3) Registered patient CT data, 4) Gantry, 5) Robot motion control widget, 6) USgRT workflow with visualization widget.

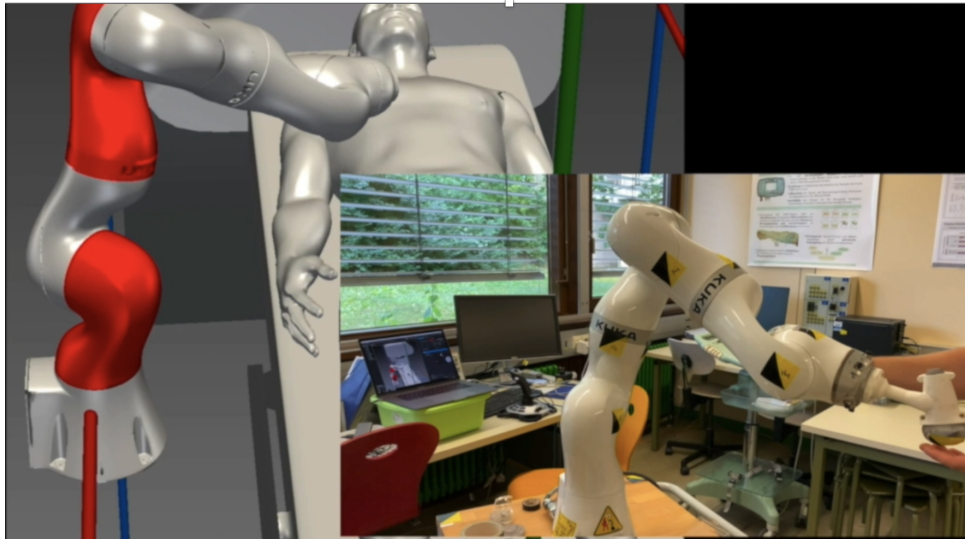


Figure 3.2: Simulation of a collision: Acting with the hand on axis 6 lead to higher torque on axis 2 and axis 4.

### 3.1.1 Visualization widget

The developed visualization widget (3.1) shows a virtual setup of the treatment scenario. The representation of the linear accelerator, robot and patient data is displayed and is updated based on the real situations. In case of a collision, the affected limbs of the robot are coloured red (3.2).

### 3.1.2 US probe positioning

Any US probe position with respect to planning data can be defined using the implemented user interaction in MITK. The developed software allows the selection of a target voxel within the planning data (e.g. CT) as surface contact point. The orientation of the probe can be adjusted in three axes. The virtually placed US probe indicates any collisions with the patient surface by visualizing the US Probe in the planning data (3.3).

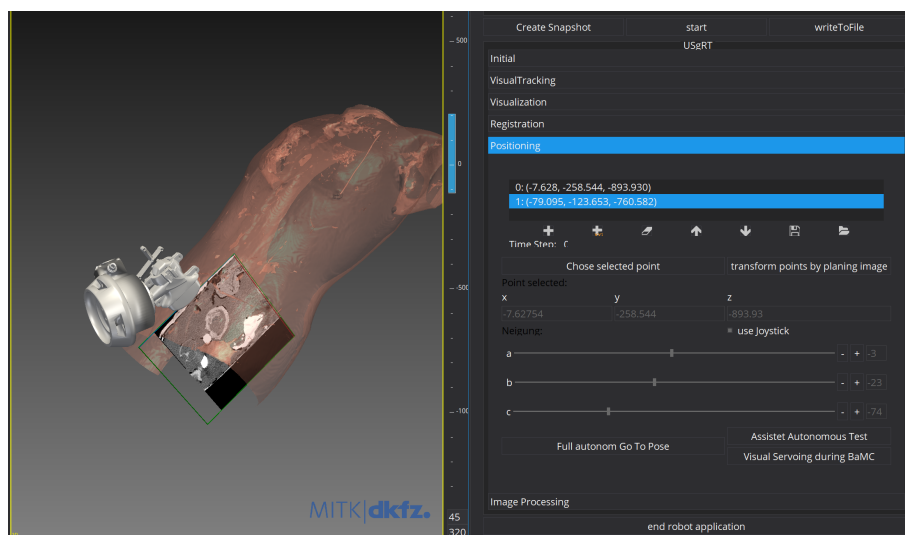


Figure 3.3: Left: 3D representation of planned US probe position and the corresponding image plane in relation to planning data. Right: Autonomous widget to manipulate the US position. 1. Translation, 2. Orientation, 3. Placement method

## 3.2 Breathing and Motion Compensation

The developed Breathing and motion compensation (BaMC) is the core component of ultrasound-guided radiotherapy. The tests performed in 2.4.4 could show that all requirements defined in 2.4.1 are fulfilled.

### 3.2.1 Stable contact and deformation less

As shown in [Seitz et al., 2020], a stable contact pressure with specification of 5 N can be maintained. The test with volunteers (2.4.4) confirms that the desired contact pressure along the

z-axis of the ultrasound probe is  $4.99 \text{ N} \pm 0.86 \text{ N}$  on average over all positions (i–iii see 2.4.4), breathing patterns (1–4), interaction types (a–d) and volunteers.

Figure 3.4 which shows force for each pattern for one volunteer, indicates a clear dependence of the applied force on the breathing pattern. This influence is especially visible on the main axis of motion  $z$ . The deviation increases with the breathing frequency, so that the greatest variance can be seen with hectic breathing. For the other axes of the ultrasound probe, a similar behaviour can be observed, which, however, seems to depend on the position of the probe. Thus, it appears that the force vector acting on the volunteer is position-dependent and varies from the orientation to  $F_z$ . Thus, for example, no forces occur along the  $x$ -axis in the axillary position, but they do in the other two positions. Nevertheless, the deviation along the  $x$ -axis with  $0.34 \text{ N} \pm 2.99$  and along the  $y$ -axis with  $0.54 \text{ N} \pm 2.08$  is comparably small. In addition, it can be seen that movements of the us probe (interaction type b-d) influence the lateral forces  $F_x, F_y$ . In particular, a force against the direction of travel becomes apparent during the scan movement (d). This behaviour was independent of the breathing pattern and the US probe position.

In consideration to the total force that is thereby exerted on the volunteer, this is  $5.41 \text{ N} \pm 1.03 \text{ N}$  for interaction type a. Across all trials (a-d, i-iii, 1-4, both volunteers, the total force is  $6.11 \text{ N} \pm 1.40 \text{ N}$ . Short-term peaks reached a force of up to 10 N, which, however, was not perceived by the volunteers, who rated the BaMC as comfortable. The internal threshold of 15 N were never triggered.

### 3.2.2 Steady image plane

As described in 2.4.2 a steady image plane is given by a motion path of the US probe only along the  $z$ -axis. All other axes should have only minimal deviation. As shown in [Seitz et al., 2020], the image plane is hold steady for all positions and breathing patterns. Figure 3.5 shows the path deviation for all axis and the orientation. Image plane deviation for BaMC only (a) is on average  $x: 0.1 \text{ mm}$ ,  $y: 0.1 \text{ mm}$ ,  $z: 2.87 \text{ mm}$ ,  $a: 0.02^\circ$ ,  $b: 0.02^\circ$ ,  $c: 0.04^\circ$ . "For scan movements, the deviation from the planned path should be minimal. For a linear scan (along  $x$  (Tool coordination system (TCS))), the image plane should be shifted in parallel (minimal angle changes ( $a, b, c$ ) and minimal deviation from the scan line ( $y$ )). The mean deviation therefore is:  $x: 8.12 \text{ mm}$ ,  $y: 2.16 \text{ mm}$ ,  $z: 5.58 \text{ mm}$ ,  $a: 0.05^\circ$ ,  $b: 0.13^\circ$   $c: 0.04^\circ$ . Details on path deviation are given in Fig. 3.5." [Seitz et al., 2020]

### 3.2.3 Mutable position and scanning motions

The US probe could be correctly reorientated and translated remotely using a joystick. The motion was smooth, and the required final positions were always reached. Furthermore, scanning motion can be performed linearly either by a pre-programmed robot motion or joystick-guided. Rotational or fan scans are limited due to motion thresholds of the robot axes. However, linear motion scans were more efficient and faster in acquiring large 3D volumes. Due to the stiffness of the rotation axes, the use of hand-guiding for probe placement is considered to be impractical. The developed semi-autonomous positioning offers a simpler and more precise placement method.



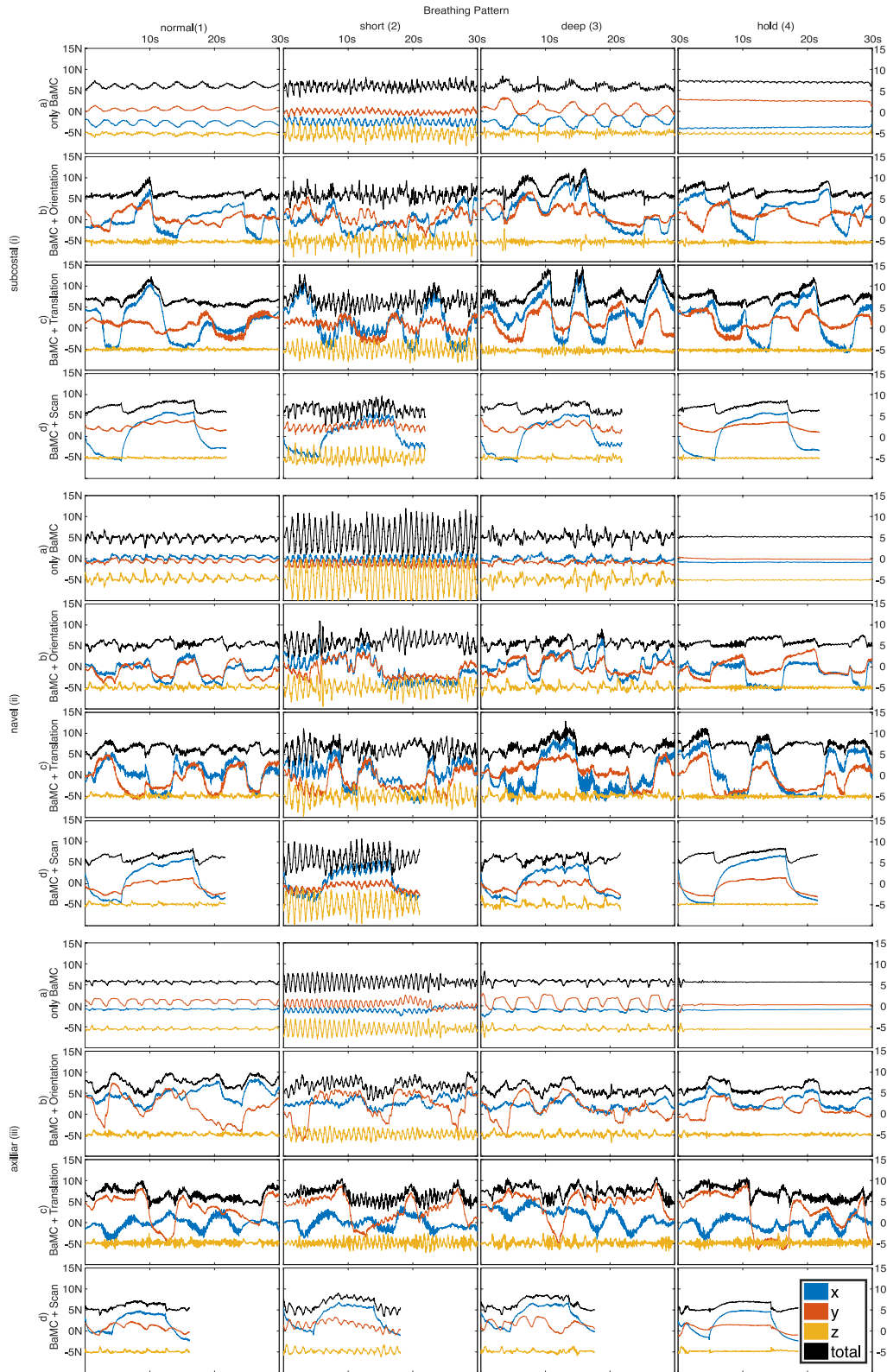


Figure 3.4: "Force on TCP per axis of TCS for one volunteer for test i-iii, a-d and 1-4" [Seitz et al., 2020]. Reproduced with permission from Springer Nature

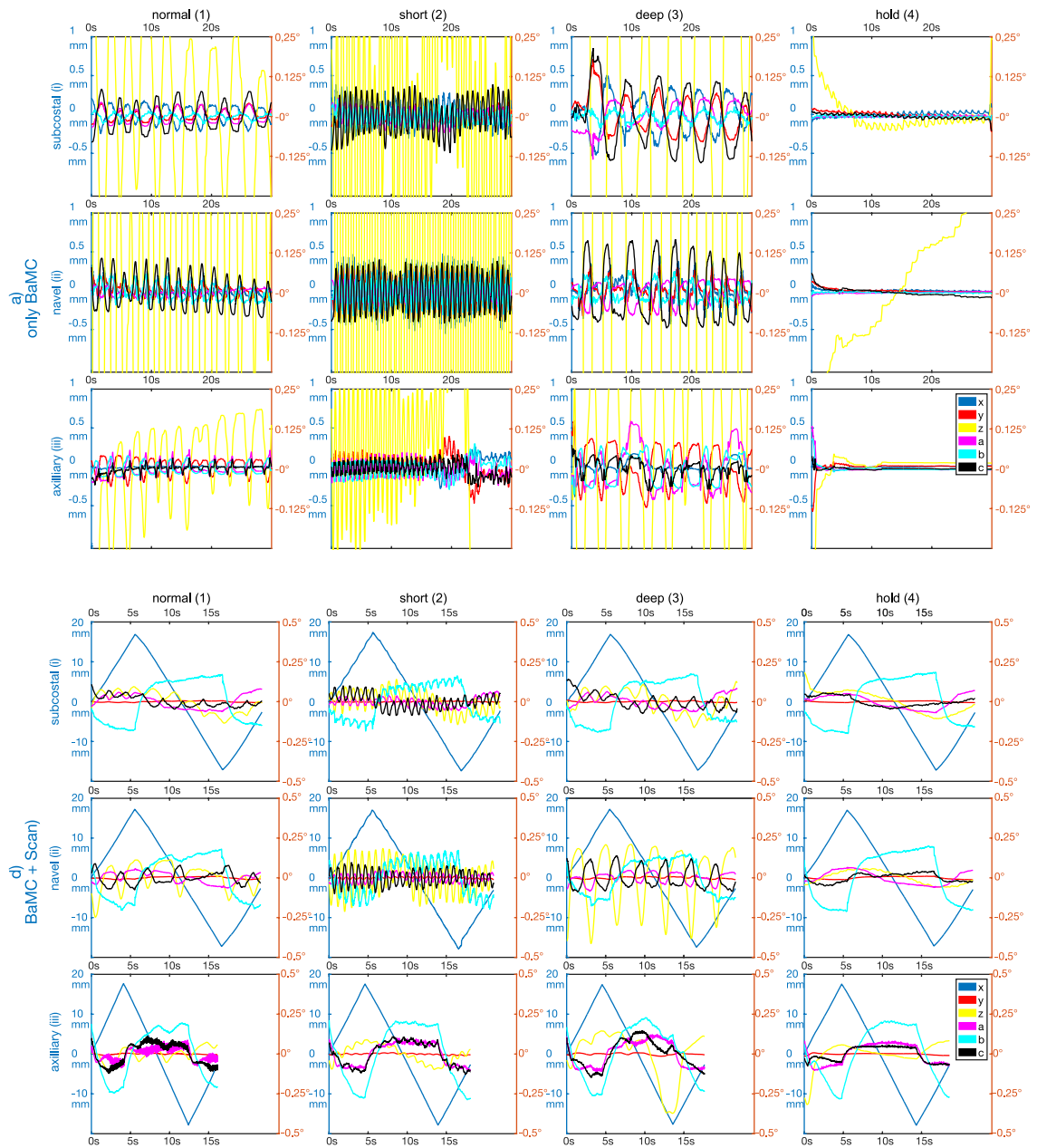


Figure 3.5: "Deviations of the image plane (TCS, xyz in mm, abc in °)"[Seitz et al., 2020]. Reproduced with permission from Springer Nature

### 3.3 Autonomous positioning

#### 3.3.1 Comparison between different positioning strategies

All methods allowed the US probe to be positioned on the surface of the phantom. The comparison of the test results shows that manual methods had a lower accuracy, a higher variation, and execution time compared to autonomous methods. An overview is given in 3.1. For the robot-guided motions VS, AS, FA, the precision at target point was less than 0.5 mm in x and y direction. Rotational deviations were 0.007 °, leading to an image plane distance of 0.93 mm at the potential virtual target points (2.5.2) at an image depth of 10 cm. The orientational deviations of manual guided strategies (M, J) were comparably high, with a maximum tilt of 0.26 °, causing an image plane distance of 30.5 mm in a depth of 10 cm. The distance between virtual target point and image plane is on average 0.26 mm for robot guided motions, 9.68 mm for manual strategies respectively. Execution time takes on average 3 times longer for manual methods (M, J), taking from 10.2 s for assisted strategy (TA) up to 116 s with the hand-guided strategy (M). The implemented manual touch-gesture worked very well for the assisted motions.

Table 3.1: Comparison between different positioning strategies (M, MJ, MVS, AS, FA) across all test scenarios. 1. horizontal Section: Comparison of reached and planned target surface contact position. 2. Section: Effect of positioning result on the distance of the image plane to a virtual target in the original planned image. 3. Section: execution time.

			placement strategy					
			manual (M)	manual + joystick (MJ)	manual + visual servoing (VS)	assisted (AS)	autonomous (FA)	
planned surface contact position compared to reached position (from the perspective of contact surface position)	distance X (mm)	Mean ± STD Min   Max	4.787 ± 4.922 0.499   14.508	3.750 ± 2.542 0.035   7.926	0.300 ± 0.096 0.176   0.440	0.202 ± 0.152 0.004   0.391	0.166 ± 0.108 0.043   0.429	
	distance Y (mm)	Mean ± STD Min   Max	5.558 ± 2.428 0.584   8.533	4.441 ± 1.937 1.661   7.267	0.218 ± 0.119 0.026   0.412	0.322 ± 0.117 0.128   0.485	0.179 ± 0.128 0.019   0.414	
	distance Z (mm)	Mean ± STD Min   Max	7.078 ± 3.898 0.316   13.087	6.569 ± 3.936 0.134   10.791	7.423 ± 4.349 0.162   10.827	9.609 ± 3.987 2.438   15.983	8.724 ± 4.094 2.097   12.960	
	rotational distance θ (°)	Mean ± STD Min   Max	0.140 ± 0.073 0.049   0.263	0.070 ± 0.039 0.020   0.168	0.004 ± 0.002 0.001   0.006	0.002 ± 0.001 0.001   0.004	0.003 ± 0.002 0.001   0.007	
virtual target positions z centimeters deep, middle planned US	z = 5cm	distance to image plane (mm)	Mean ± STD Min   Max	6.694 ± 6.977 0.249   22.517	6.021 ± 4.520 0.407   15.649	0.260 ± 0.186 0.060   0.638	0.219 ± 0.174 0.003   0.481	0.147 ± 0.131 0.004   0.383
		distance to image plane (mm)	Mean ± STD Min   Max	7.670 ± 8.179 0.150   25.720	7.003 ± 5.261 0.659   18.739	0.254 ± 0.238 0.016   0.743	0.233 ± 0.178 0.034   0.517	0.167 ± 0.121 0.033   0.364
	z = 7cm	distance to image plane (mm)	Mean ± STD Min   Max	9.680 ± 9.699 0.0002   30.526	8.475 ± 6.402 0.926   23.372	0.278 ± 0.303 0.012   0.900	0.255 ± 0.188 0.061   0.571	0.198 ± 0.120 0.018   0.383
		Duration (s)	Mean ± STD Min   Max	63.989 ± 32.056 16.878   116.773	74.615 ± 17.755 46.784   95.126	20.234 ± 1.620 16.915   22.539	11.770 ± 1.346 10.226   13.865	14.669 ± 0.722 13.460   15.549

#### 3.3.2 Precision and accuracy of the autonomous method

For the autonomous method (FA), over 60 evenly distributed positions were additionally achieved. A total of 70 autonomous positioning motions were successfully completed (2.5.4, which verifies the previous results from the comparison. Predefined and reached surface contact points were always within the specified limits (2.5.3). In detail, the accuracy was higher for most positions as shown in Figure 3.6. Five other positions could not be reached due to the

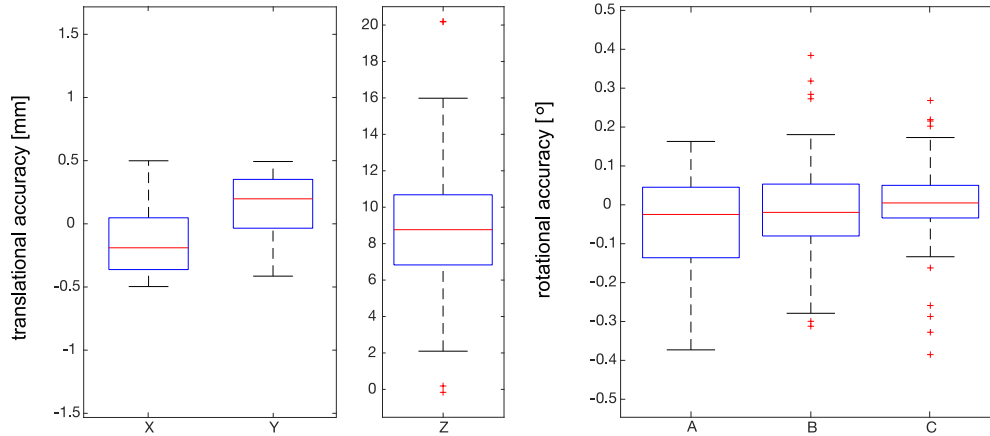


Figure 3.6: Distance between planned and achieved surface contact point coordinates ( $x,y,z$ ) for AS and FA– difference in mm and degree (euler angle A,B,C)

axis position of the robot and hardware limitations, highlighting the importance of a proper positioning of the robot in relation to the patient. In four other cases, the safety mechanism was triggered and the procedure was aborted. In these cases, the application immediately stopped the movement as intended.

### 3.3.3 Force acting on phantom

Figure 3.7 shows the patient force  $F_P$  and tool contact force  $F_z$  during robot guided positioning strategies for target points in the pelvis and abdominal region. During execution, a maximum  $F_P$  of 12.7 N was recorded and therefore the safety threshold of 20 N was never exceeded. The defined contact force  $F_z$  (Figure 1) of 5 N showed a maximum of 9.5 N during the positioning procedure.  $F_z$  shows a larger variation for the abdominal positions compared to the pelvis positions. Surface contact was established on average after 4.5 s and the force reached its maximum within 1 s. During BaMC + visual servoing the mean  $F_z$  force was 6.3 N and  $F_P$  7.9, respectively. During visual servoing the maximum  $F_P$  force was 12.17 N.

## 3.4 Safety

For safety, it was demonstrated that all measures required by [ISO/TS 15066:2016, ] have been implemented. The results of the integration of the force sensor into the existing system is presented in (3.4.1). The resulting collision detection allows a safe force-limited application on the phantom (3.4.3). For the other detection mechanisms, the implemented safety control was able to show that the selected reaction can reduce the force reliably and rapidly (3.4.4).

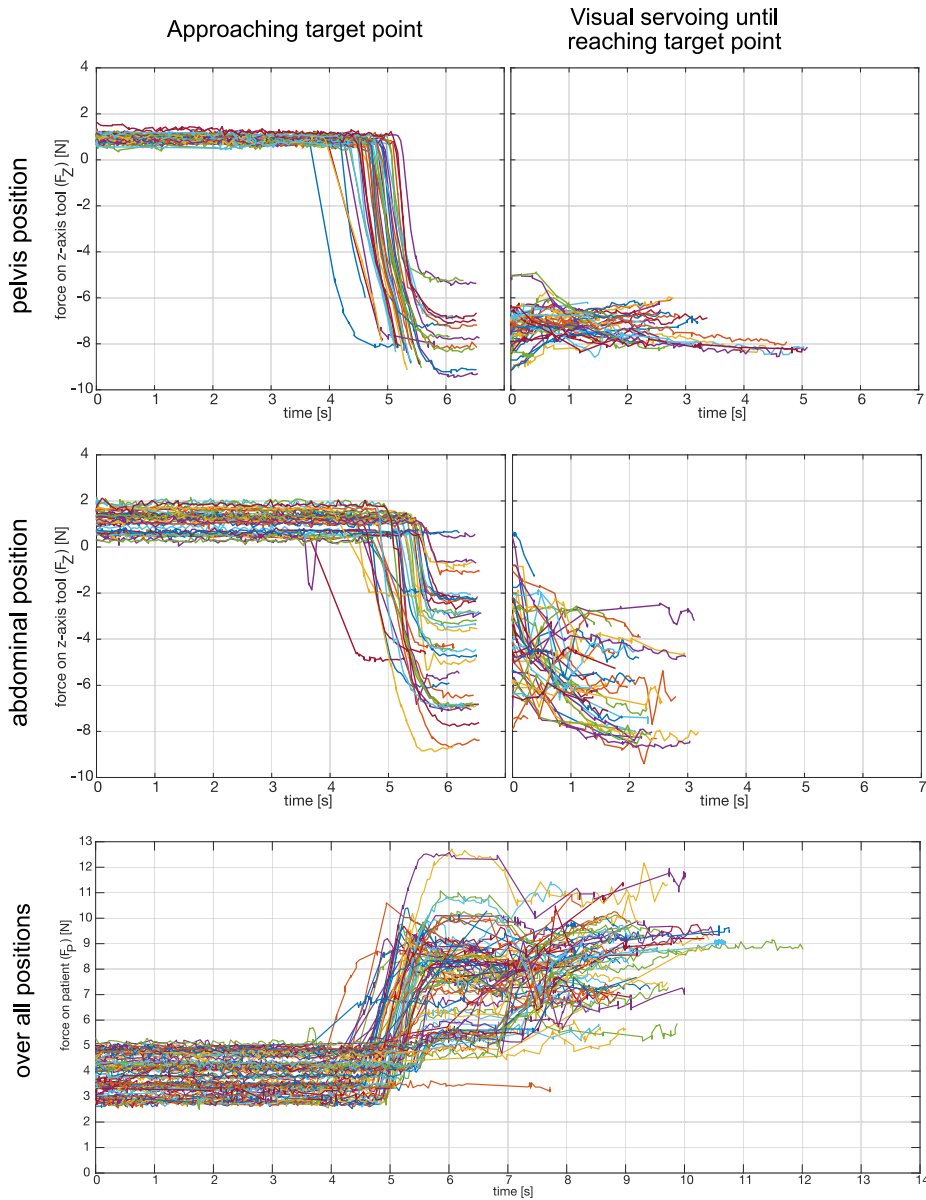


Figure 3.7: Acting forces during approach (FA). Top and middle panel show the force along the approach direction  $F_Z$  for the pelvis and abdominal regions, respectively. Left and right panels display the forces during approaching phase of the US probe placement and during the visual servoing, respectively. The transition between both panels corresponds to the time point when the US probe contacts the patient’s surface. The bottom panel shows the patient force  $F_P$  for both positions and both states (not separated into approaching and servoing phase).

### 3.4.1 Calibration force sensor

The integration of the force sensor via the selected methodology was successfully demonstrated. The calibration of the sensor provided values with an estimated accuracy of  $\pm 1.5$  N. This is derived from the calculated weight force. In Figure 3.9 the forces measured by the uncalibrated and the calibrated sensor are compared. A noise-independent residual force can also be recognized. This may be an effect caused by the freely hanging cable. However, since this effect is in the lower Newton range (below 1 N), it does not play a major role for the application.

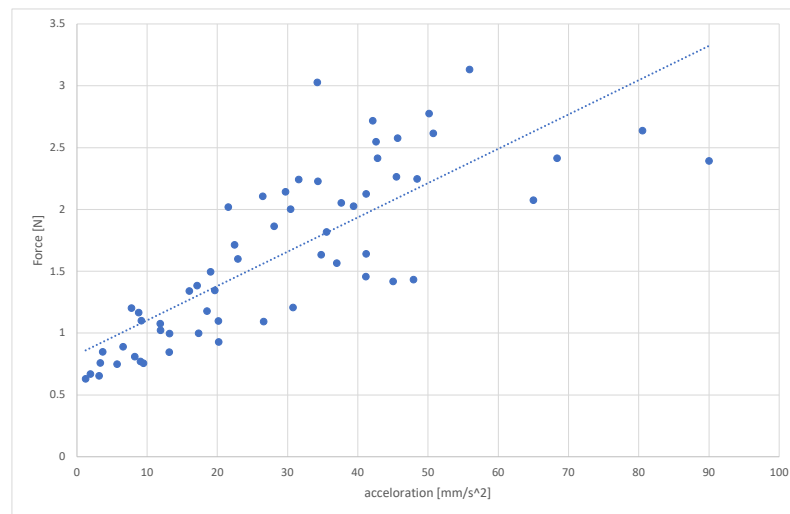


Figure 3.8: Acceleration effect on the force sensor

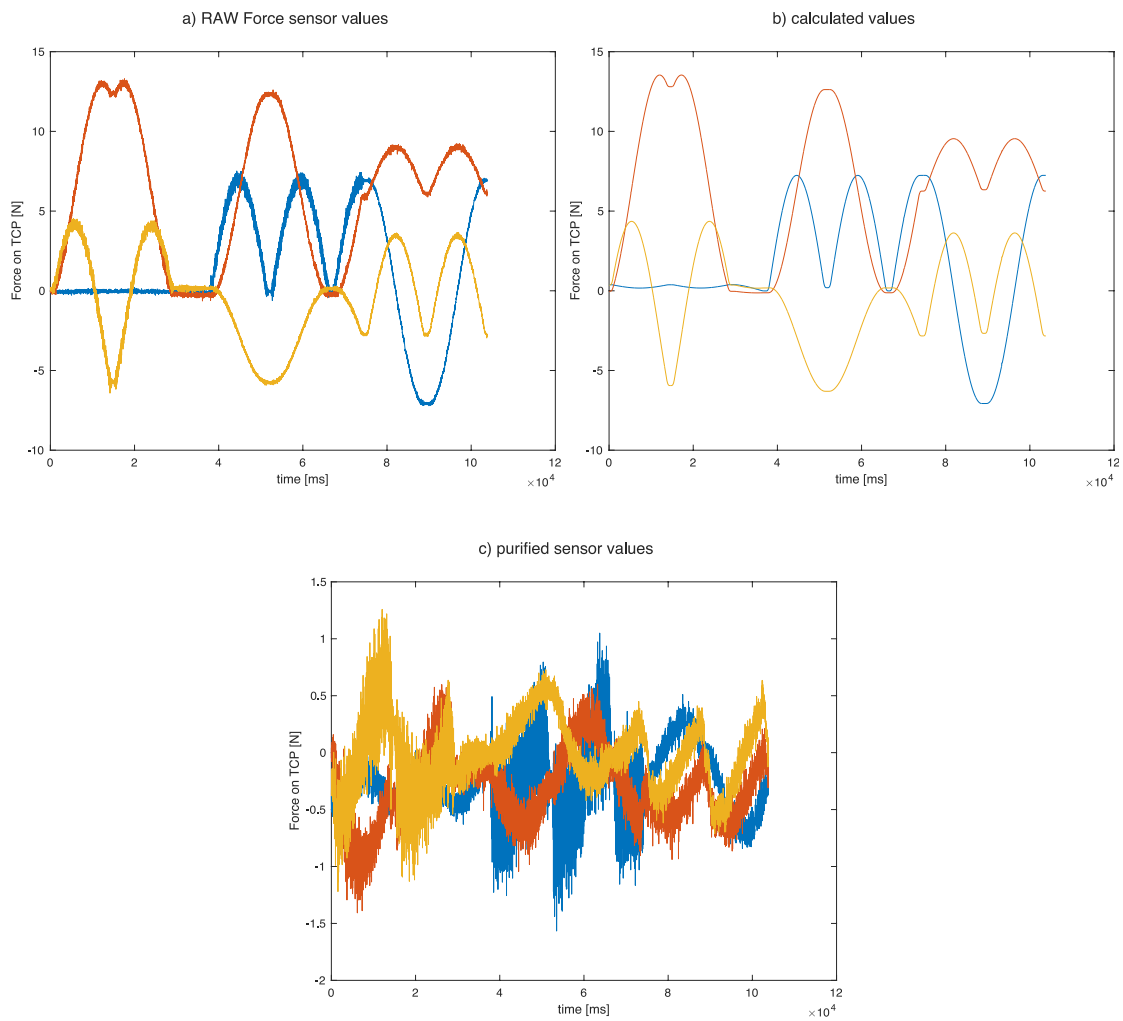


Figure 3.9: Force sensor calibration: a) Uncalibration force sensor values during calibration motion, b) calculated values after optimization, c) purified sensor force values.

The acceleration test was able to demonstrate a greater influence on the measured force. For example, from accelerations of  $60\text{mm}/\text{sec}^2$ , forces of an additional 2.5N are measured on average. For the motion compensation (typical  $16.5\text{mm}/\text{sec}^2$ ) the deviation remains at 1.3N, slightly above the weight-dependent force measurement from before. Overall, based on these facts, the force accuracy of the force sensor was estimated to be  $\pm 2$  N using the developed methodology.

### 3.4.2 Collision detection during setup motions

All 108 simulated collisions 2.6.5 (test 1) were detected, and the intended reaction was always executed. US probe collisions lead to a recorded force on the tool of 18 N and showed a reaction time of  $402 \pm 144$  ms. Limb contact caused external axis torques of up to 20 Nm.

### 3.4.3 Collision detection during BaMC

For the verification of collision detection during BaMC, a total of three different detection mechanisms (2.6.3) were tested at 27 collision points and four US probe positions each. This gives a total of 324 tested collisions. The results of the tests are summarized in figure 3.10 and figure 3.11. A table representation of these result can be found: Axilliar90: 8.2, Axilliar45: 8.1, Navel: 8.3, Subcostal: 8.4. During the tests, it became apparent that different US head positions and the resulting axis positions of the robot have different effects in the event of a collision. In general, the effects of a collision can be divided into three groups. First, an increase in force on the patient can be indirectly demonstrated based on an increase in force at the measured tool center point. Second, collisions can also result in a decrease in force and thus a loss of contact between ultrasound probe and patient surface. The third scenario is that a collision does not directly affect the force applied to the patient. An increase in force can usually be seen when the direction of collision is toward the patient or along the axis of the probe (group 1). In this case, this force is transmitted to the patient by the joint mechanics. Collision forces counter the BaMC direction often also cause the opposite reaction (group 2). Laterally acting forces can have both an increase and a decrease, as well as, no effect on the patient force  $F_P$ .

Since different US probe position results in different collision directions for each collision point a consequent correspondence between collision point and effect on  $F_P$  is not given, except for the collisions with the tool ( $T_1 - T_5$ ). It is, therefore, possible that a collision point results in both an increase for one US probe position and a reduction in another case. This behaviour occurs for all axis sections of the robot and can also result from collisions in the lower section ( $A_1$  or  $A_2$ ). Here, the subjective implication is that when a collision is generated, it requires a higher force at the collision point and is only slightly transmitted through the robot mechanics.

Collisions in front of the force sensor and along or against the US probe direction remain undetected. In this case, respiratory motion compensation continues in the direction of the patient and is amplified by the unnoticed acting force. As a result those collisions must be prevented by additional methods.

#### Detection based on BaMC conditions

When using the force-only monitoring at the tool center point by means of the robot's own force condition of 20N, 73 of the 108 executed collisions were identified. This resulted in 45 collisions that generated a force of more than 20N at the tool center point. Out of these, 7 remained undetected with a resulting maximum force of up to 113.1 N. On average, the undetected collisions over 20 N resulted in forces of  $41.69 \text{ N} \pm 24.76 \text{ N}$ . The axes involved in these collisions were from



axis 4 downwards to axis 1. Collisions above axis 4 were reliably detected with a maximum force of 48 N (average  $28.75 \text{ N} \pm 7 \text{ N}$ ).

In the case of the undetected collisions, the internal force estimation (2.1.4) of the robot was clearly too low. In these cases, the force sensor measured an average force of  $45.6 \text{ N} \pm 31.32 \text{ N}$  and a maximum force of 113.1 N. The values of the robot are clearly below 20 N on average at  $14.6 \text{ N} \pm 5.47 \text{ N}$ . An abort of the test was realized manually in these cases and occurring forces could have been higher than the measured value as a result.

Of 18 cases resulting in loss of coupling to the patient surface, 5 were detected. Contrary to the previous example, the detection of these cases was based on a force that was clearly too low. The force sensor showed an average of  $9.73 \text{ N} \pm 2.1 \text{ N}$  in these cases. The robot estimated the force to be  $20.41 \text{ N} \pm 1 \text{ N}$ , and thus triggered the collision detection and started the interlock movement accordingly.

Also for lateral hits that were below the 20 N threshold according to the force sensor, collision detection was triggered based on increased estimated force values. (mean  $24.98 \text{ N} \pm 6.79 \text{ N}$  vs  $12.8 \text{ N} \pm 3.43 \text{ N}$ )

#### **Detection based on BaMC conditions and additional robot values**

Additional force detection via the torque values was able to achieve a slight improvement in collision detection. In this case, 85 of the 108 collisions were detected. The maximum force is reduced to 70.71 N. In total, 43 of the 46 collisions with a value above 20 N were detected. On average, the collision intensity was  $36.44 \pm 15.23 \text{ N}$ . The undetected collisions with a value above 20 N were on average  $26.59 \text{ N} \pm 1.85 \text{ N}$  and on maximum at 30.73 N. Interestingly, the maximum force of 70.71 N was measured with a detected movement. It is noticeable that in this case, as with the previous detection mechanism, the force estimate of the robot is too low. Furthermore these cases occurred more frequently for the lower axes A1, A2 and A3.

In the case of collision with a decrease in contact pressure, 10 out of 18 cases could be detected. Thus twice as many as with the first mechanism.

#### **Detection based on BaMC conditions, additional robot and force sensor values**

With the help of the force sensor, the sensitivity of the collision detection could be further improved and it is possible to detect 96 of the 108 collisions performed. Among the non-detected collisions, four collisions were along the ultrasound direction and two times each were at the collision points  $A_{11}$ ,  $A_{12}$ ,  $A_{34}$  and  $A_{24}$ . The respective collisions at these points had no effect on the force at the Tool Center Point (TCP). Overall, the acting maximum force is reduced to 35.44 N. In this case, the maximum force was above 20 ms for 150 ms before the safety movement was performed. It should be emphasized that all collisions that lead to forces above 20 N to the patient were detected. The mean force is  $20.44 \text{ N} \pm 2.29 \text{ N}$ . This indicates that the reaction to the force is prompt and the safety movement is performed immediately after detection.

A reduction of the contact pressure and thus a lifting of the probe can be identified by the force sensor in 17 out of 18 cases. At this point, it should be noted that the selected threshold value of 2 N could certainly be set higher or lower. However, this would increase false positive detection rate of collisions during BamC.

Of the 96 collisions detected, 2 were detected based on the torque condition, 44 based on the internal force estimation, and 50 directly by the force sensor. Similar to the previous detection mechanisms, robot misestimation of the applied force resulted in collision detection for collision points that did not result in an increase in patient force.

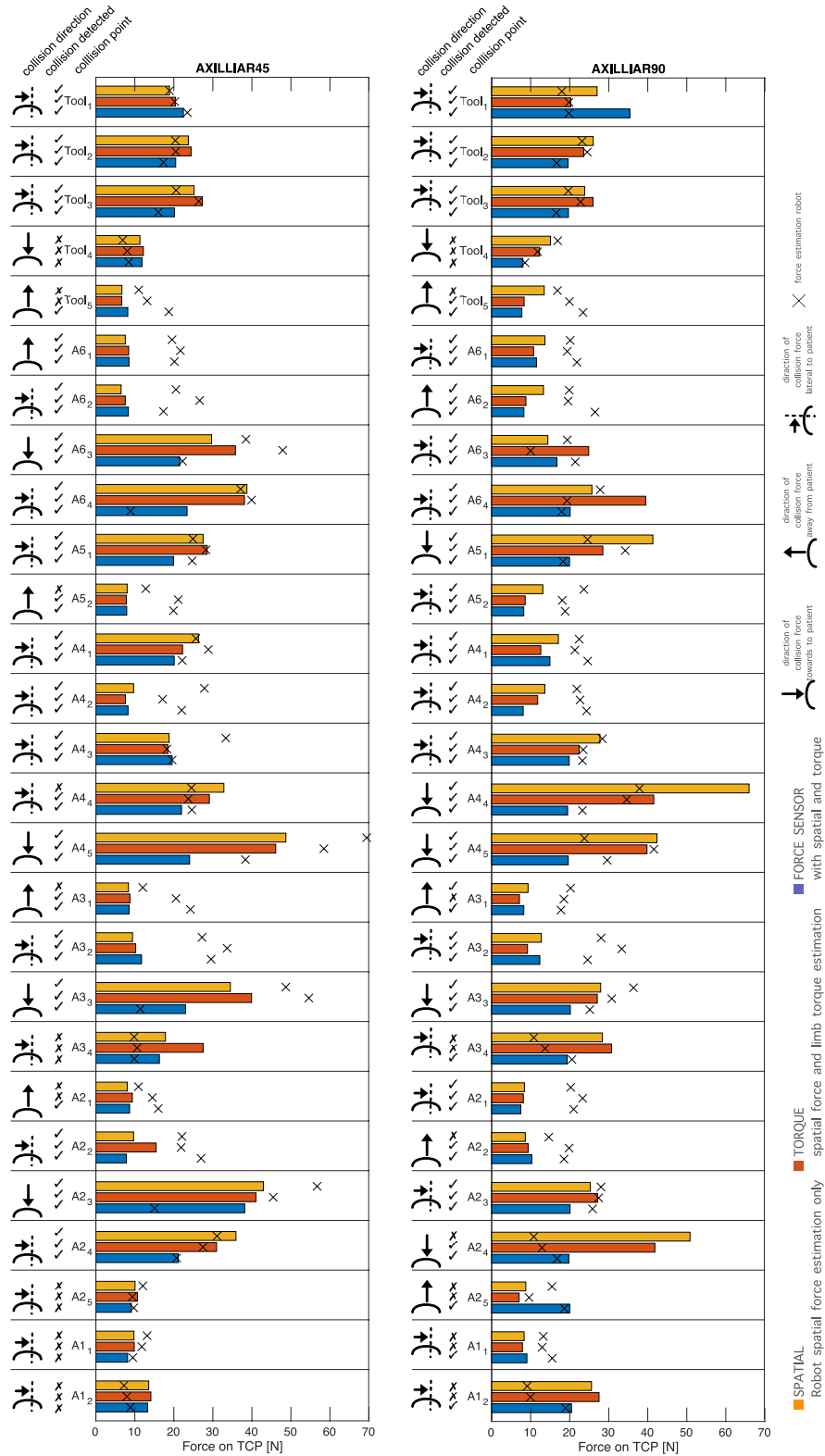


Figure 3.10: Maximum occurring measured forces (robot and force sensor), direction of collision force and if the collision was noticed, for each collisionpoint and detection mechanism during BaMC (Axilliar 45 and 90).

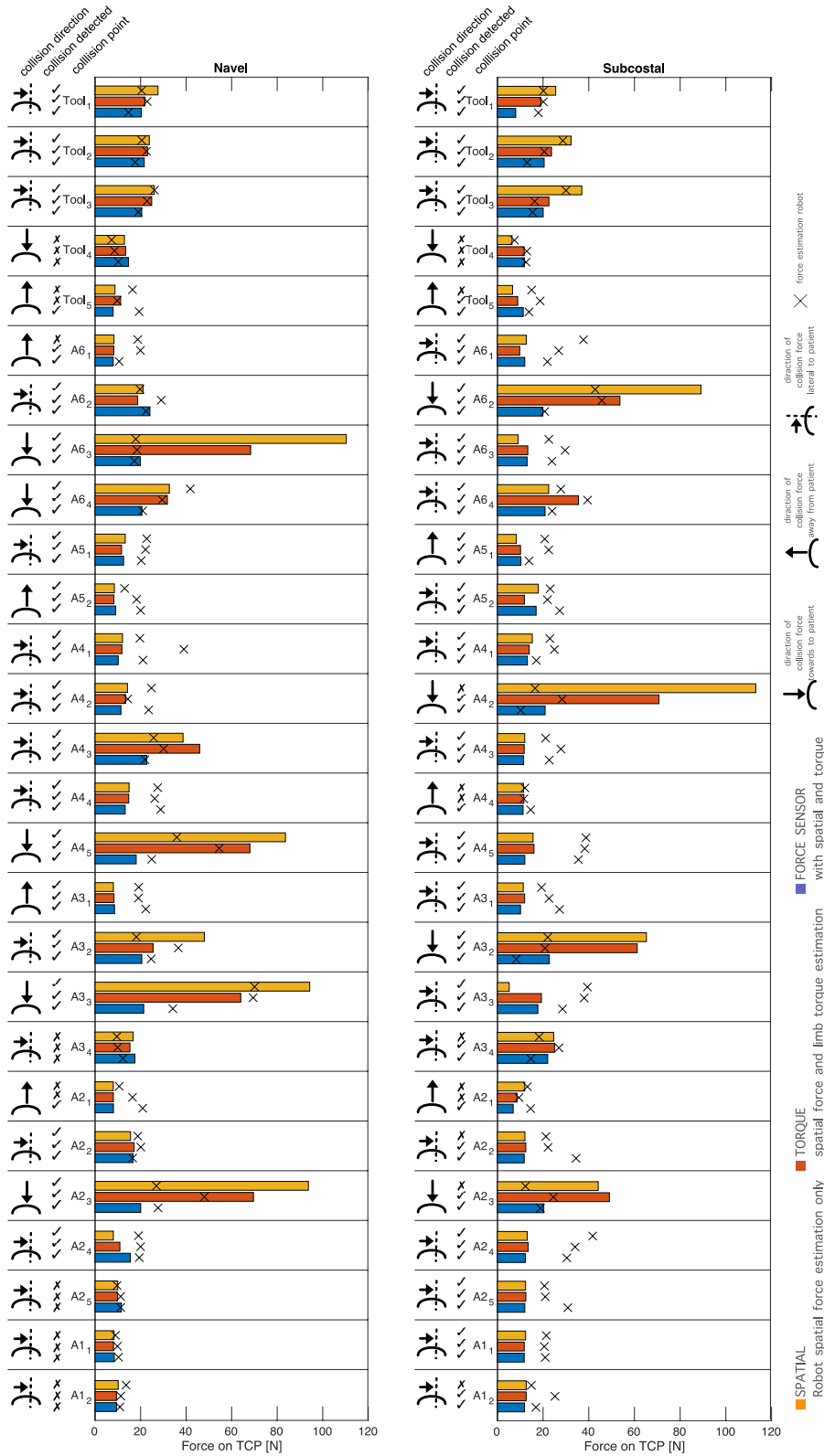


Figure 3.11: Maximum occurring measured forces (robot and force sensor), direction of collision force and if the collision was noticed, for each collisionpoint and detection mechanism during BaMC (Navel and Subcostal).

### Comparison of Detection Methods

The tests (2.6.5) were able to show that the robot sensor values are not sufficient to detect all collisions. The additional redundant force measurement by means of a force sensor could significantly improve the collision detection and drastically reduce the maximum acting force. Figure 3.12 shows a direct comparison of the different methods at one collision point. It can be shown by this example that the detection measures of the torque already is an improvement of the detection. However, torque detection still involves high forces (above 20 N). However, potentially dangerous force values (70.71 N maximum measured force) can already be detected with this method.

By adding the torque condition, unnoticed collisions with effects above 20 N of the first mechanism were detected. Interestingly, however, only two of the five collisions were triggered by the torque condition itself. Three were detected due to the first mechanism. It remained unclear, however, whether the reason has a control-related cause or if it occurred due to a slightly different force direction at the collision point. In the case of adding the force sensor, all undetected collisions of the first mechanism were detected directly based on the force sensor.

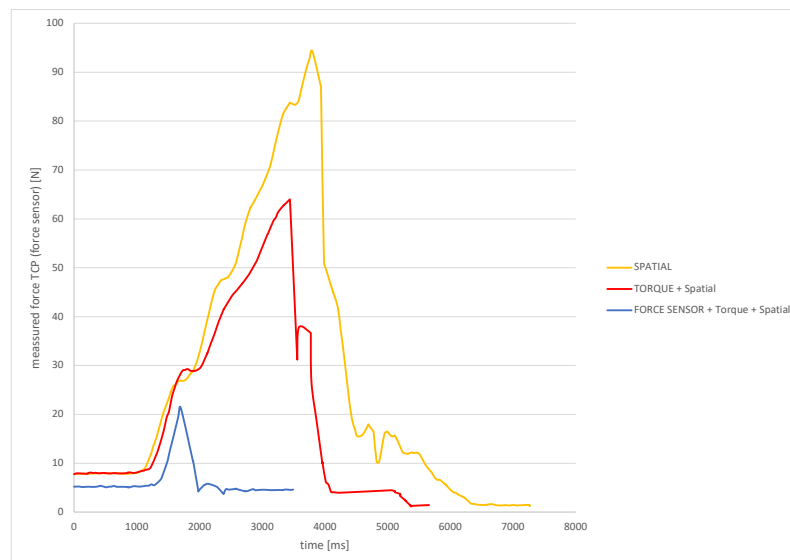


Figure 3.12: Comparison of the different detection methods for navel  $a_3$  collisions. This comparison shows the largest difference of the tested detection mechanism. The relation is proportional for the other collision points.

#### 3.4.4 Safety reactions

In the experiments (2.6.5), it could be shown that for each detected collision, the safety movement was performed as described in section 2.6.4. The desired effect of a reduction of the force sensor values could be shown in all tests, so that after the safety movement, the forces at the TCP were below 20N (see 3.13 ). This was supported by a direct execution of the safety movement without time delay. It is important to note that in case of collisions in the direction of the patient, the reaction of the system leads to the desired distance of the US Probe to the patient.

However, due to the implemented compliance at the end of the movement, the robot together with the tool could be moved towards the phantom surface again.

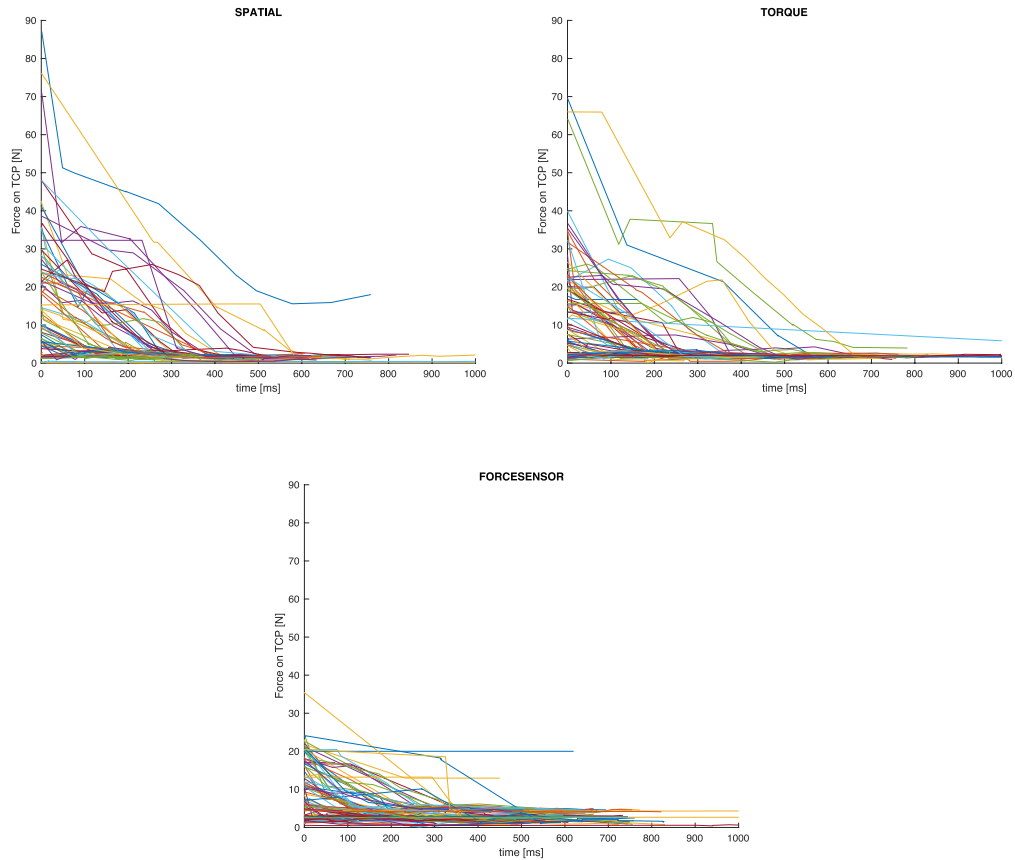


Figure 3.13: Absolute force on TCP after emergency motion separated for each collision detection mechanism (SPATIAL, TORQUE, FORCESENSOR), including each collision and US probe position, respectively. It can be seen that for all methods the emergency motion reduces the active force below 20 N within 600 ms.



# 4

## Discussion

### Disclosures to this work:

Parts of this work (section 4.3) have been published in:

**Peter Karl Seitz**, Beatrice Baumann, Wibke Johnen, Cord Lissek, Johana Seidel, Rolf Bendl. Development of a robot-assisted ultrasound-guided radiation therapy (USgRT) *Int J CARS* 15, 491–501, December 2020. doi: 10.1007/s11548-019-02104-y

This thesis has shown that all objectives defined in 1.3 are accomplished. First, the limitations for the obtained results, due to the experimental setup, are discussed in section 4.1. The integration of required components and the resulting user interaction (O1) are addressed in section 4.2 and for the clinical workflow developed positioning strategies are discussed in section 4.4 accordingly. Regarding objective O2, an universal Breathing and motion compensation (BaMC) was realised, fulfilling all defined requirements (2.4.1) and is considered in section (see 4.3). Finally, the developed safety measures (O3) are discussed in 4.5, followed by the conclusion 4.6.

### 4.1 Experimental setup

The main objective of this work is to develop a safe robotic application for Ultrasound guided radiation therapy (USgRT). Therefore, the laboratory setup poses a significant prerequisite for this work. The work is based on the following assumptions:

A USgRT application primarily uses Ultrasound (US) as an image guidance. However, it is not specified which image plane (US probe position and direction) is selected for this purpose. But the position of the US probe has a direct effect on the necessary robot pose, as this pose has to be selected in a way that BaMC can be physically accomplished. Therefore, first the geometry of

the US probe holder and second the mounting position of the robot are affecting the potential robot poses. For example, a more distant Tool Center Point (TCP) causes many axes of the robot to move outward when the tool is rotating. Reducing the distance, on the other hand reduces the required movement radii but may be impractical due to other reasons (e.g. distance to Linear Accelerator (LINAC)). For the second point of influence, the robot mounting position also depends on the distance to the phantom. A mounting that is too far away causes the robot to stretch out. This makes it difficult or even impossible to rotate the tool. Similarly, a position too close causes a potential lack of movement space and thus enables only limited movements of the robot. Furthermore, the resulting beam directions from the LINAC also depend on these two factors. Thus, the design of the tool and the mounting of the robot in space are of indirect but important relevance. The first simplification is therefore to restrict the US probe positions to the abdominal region. [Gerlach et al., 2017a] presented a possible setup that allowing for irradiation. The selected tool geometry and the position of the robot in space used in this thesis was therefore a result of this setup and are considered as feasible for abdominal use only.

The US probe used was a conventional 2D US probe. In addition to 2D US probes, 3D US probes are also available. Both approaches are discussed in the literature [Ipsen et al., 2016b, Seitz et al., 2020], as described (see also section 2.1.1), the following assumption was made: Due to the multidimensional US volume of a 3D US probe, the required rotations of the 2D US probe are reduced. It was therefore assumed that the robot pose and tool geometry are more dependent on the US probe position of a 2D than a 3D US probe. The demonstration of the safe use of a 2D US probe, therefore, allows also some conclusions on the safe use of a 3D US probe.

The model of the LINAC, including the patient table, was simplified: Since this work focuses on the safety of the robot in handling the patient, the gantry in the laboratory setup was omitted. As already shown by [Gerlach et al., 2017a], a robotic system can be used with an accelerator and allows multiple beam directions. With respect to safety, the handling of the gantry mainly includes the detection of collisions with the robot. For this, powerful interfaces with the commercial systems are required, which were not available at the time of this thesis. Therefore, the interface was already defined on the robot side.

For a better fixation of the phantoms, a fixed table was used instead of a patient couch. For a real setup, the assumption is that the robot could be fixed to the patient couch.

It was also assumed that, the control of the application would be in the bunker. Due to limited space, the experimental setup was not separated from the robot. It is assumed that the experimental setup can be separated between the irradiation room and the control room by means of appropriate hardware connections (i.e. cables).

## 4.2 User interaction

It was observed that the defined workflow (2.2.2) with the integrated components (2.3.2) and the implemented user interaction (2.3.4) depend on the fact that the objective O1 is fulfilled. The components are considered as suitable for the use of USgRT. First tests with the phantom were promising.



The separation into direct interaction with the robot (e.g. BaMC and hand guiding), next to the LINAC, and the remote control from the bunker (US probe position manipulation and autonomous positioning), was promising. For both cases the safety and an effective handling could be assured. Furthermore, in this context, the predefined setup movements, e.g. for calibration, allow for a time-efficient control of the robot and thus reduces the effort for the additional use of the US device during an existing application.

The registration with the planning images was point-based and suited for the experimental setup. It would have to be clarified to what extent this procedure can be used in this way or whether additional tattoos or markers on the patient's skin are required for registration. Due to the modular structure of the application, however, the registration can be easily exchanged, e.g. by a surface-based registration or by an image-guided registration with computer tomography (CT) or magnetic resonance tomography (MRT) [El-Baz et al., 2011]. In this regard, the developed scanning techniques offer the possibility for three-dimensional US acquisition.

The developed positioning widget improves the workflow of defining the planned US image plane as compared to previous used methods [Chen et al., 2021, Conti et al., 2014] by developing and implementing an intuitive user interface, as well as, a visual representation. Therefore, all voxels of the image may be selected as target point allowing for an unrestricted position definition. Potentially incorrect US probe positions and collisions of the robot arm with the patient can be identified already at the planning stage by means of the graphical display. An automatic pre-motion collision detection will be part of the future work.

The virtual representation widget visualizes the spatial configuration, and the acting forces of the individual components (gantry, robot) provides a visual feedback for the user comparable to [Tauscher et al., 2015].

The pre-existing implemented mechanisms for synchronization of the application between robot, US device, tracking device and Medical Imaging Interaction Toolkit (MITK) [Seitz et al., 2020] could already protect against misapplication for the first tests. These can be used as a basis for a real clinical application. In this case, the LINAC is considered as the decisive component that is still missing in the experimental setup. However, the previously developed interface offers an adequate measure to facilitate a later integration.

The chosen modular structure based on MITK also opens up additional areas of US guided diagnostics. Thus, the developed interfaces offer the possibility of telemanipulation with the US device even beyond radiotherapy applications. For example application for remote US acquisition [Akbari et al., 2021] are feasible with the current implementation. Further application such as US guided biopsies [Esteban et al., 2018] or screening of abdominal aortic aneurysms [Virga et al., 2016] can be realized with only small adjustments.

### **4.3 Breathing and Motion compensation**

An important component of USgRT meeting the key objective O2 is the BaMC to assure stable image quality over a longer time period during the treatment session. The performed experiments demonstrated that a stable contact pressure and stable imaging can be achieved for

a US probe held by a lightweight robot. Furthermore, it was shown that the US probe can be manipulated and realigned during motion compensation and under stable contact pressure on volunteers.

The universal implementation ensures the greatest possible flexibility, since all parameters of the motion compensation can be adjusted. This means that the contact pressure, the translation and orientation of the US probe, as well as, the zero-space motion can be adjusted. Apart from the contact pressure, all parameters can be controlled dynamically via an interface during BaMC.

The implementation of the BaMC fits seamlessly into the clinical workflow and can be used as a separate, self-contained component together with other robot movements, such as the autonomous positioning. There were no unintended breaks in the application, which could have potential dangerous side effect for the patient (e.g. due to a blocking situation). As a result all central requirements (2.4.1) are covered.

Analyzing the force acting during BaMC, the developed control demonstrates the desired behaviour. The defined contact pressure (force along the z axis of the tool) is maintained over all breathing patterns. However, the tests also showed that this contact pressure is subject to minimal fluctuations. These were particularly visible during fast, hectic breathing movements and correlate with the movement along the z axis. It can therefore be assumed that the latency of the internal robot control imposes some limitations. This effect, however, has no influence on clinical application, because it was not noticed by the volunteers and moreover did not influence the image acquisition. In this regard, even smaller peaks larger than 10 N remained unnoticed. Possibly, an increase of the contact pressure could achieve an improvement and reduce the oscillating behavior. However, the contact force was chosen sufficiently large to guarantee stable image acquisition. With this respect, the findings from [Virga et al., 2018] suggest that this value is also ideal for minimizing organ deformations caused by the contact pressure and the applied force was lower than in other studies (10 N prostate [Ipsen et al., 2021],  $34.5 \text{ N} \pm 1.2 \text{ N}$  liver [Lediju Bell et al., 2014]). If needed, the developed control system also allows setting higher contact pressure values.

However, it is important to note that the experiments showed that other forces may arise in addition to the contact pressure. These forces are independent of the test subject and can include various influencing factors. It is apparent that these forces are depend on body characteristics such as rib arches or on physical aspects (e.g. static friction due to insufficient US gel). However, there is no direct relevance for clinical application, since these forces are comparably low (<5 N). The total force was also far below the selected threshold value of 20 N. It should be noted in particular that according to [ISO/TS 15066:2016, ], significantly higher forces would be allowed in the context of Human Robot Collaboration (HRC).

Image plane compliance could be accurately maintained with the selected method and the accuracy showed to be within the submillimeter range for all breathing patterns, and US probe positions. Influence of the US probe during dose delivery [Wu et al., 2006] can be avoided by the additional null space movement or a radiolucent US probe, as presented by [Schlosser, 2016].

The scanning motion, which can be performed during BaMC, can be easily adapted and is universally applicable, especially in the abdominal region, where existing approaches often do not work ([Huang et al., 2019]). Compared to [Graumann et al., 2016], the scanning motion does not

require additional information (patient interface) or additional hardware [Chen et al., 2021]. Also network interference problems are covered due to the independence of the robot system and such problems are therefore solved in a different way than by the method presented in [Abbas et al., 2021].

## 4.4 Autonomous positioning

With the developed and tested autonomous (manual and visual servoing (MVS), assisted (AS), fully autonomous (FA)) positioning strategies, it is possible to reach a selected US image plane with submillimeter accuracy and precision. Since the chosen tolerances of 0.5 mm translational and 0.05 ° rotational movements for the MVS are within the accuracy of the tracking system (0.132 mm translation, 0.019 ° orientation) [Karayiannidis et al., 2014], the clinically achievable accuracy of the developed methods depends only on the accuracy of the initial registration of the patient and potential patient motion. Although registration and MVS is currently based on the optical tracking system, the chosen implementation allows adjustments and exchanges to the registration process, if required. However, alternative registration methods would need an additional calibration with the optical system for positioning.

Patient motion, such as breathing, is considered by the BaMC and the additional MVS allows for fast targeting within the spatial image plane. In future work, it is planned to improve the alignment by using US image information for the MVS.

Even though the different positioning strategies have a comparable accuracy, there is a clear preference which methods to use in a treatment situation. The robot guided strategies (MVS, AS, FA) have a clear advantage over manual methods (manual (M), manual and joystick (MJ)) regarding reproducibility, precision, and speed, since the faster the positioning method, the shorter the overall treatment time becomes. In this regard, the autonomous motion FA can be considered as the fastest method followed by the assisted method AS. FA would therefore be suitable for regular use as it is accurate, precise, and fast.

A major benefit of the robot guided methods is that no further knowledge of US probe positioning is needed. It independently and repeatably reaches a large number of predefined positions. The fact that all pelvis positions were reached, indicates that the defined robot position and tool geometry were suitable for this treatment site.

Nevertheless, the other strategies may also present advantages. With AS, the positioning of the US probe can be guided by a single person if necessary. This could possibly reduce discomfort for the patient experienced in FA positioning procedures. The strategies M and MJ are potentially associated with large deviations between planning images and the actual situation. For these cases, a new image plane can quickly be defined by the user.

In the future, the positioning procedures will be supplemented by image-guided methods. With the presented implementation, the calculated target position, which defines the US image plane, can be reliably translated into a robot movement.

## 4.5 Safety

Safety in USgRT involves several aspects and HRC requires customized solutions. In addition to the two main actors (Medical Technical Assistant (MTA) and the patient), the application includes several hardware components (US probe, robot, LINAC). It must be ensured for all involved humans that injuries are excluded or reduced to a permitted minimum. Also for the hardware components (LINAC and robot) collateral damage need to be prevented. With the developed application, the safe use of the robot for imaging of the patient could be demonstrated. Appropriate preparatory interfaces for an additional application within the LINAC were also created.

[ISO/TS 15066:2016, ] provides important standards on a safe design of HRC, however, these regulations are not sufficient for systems like the one developed for the purpose in this thesis. When considering the threshold values required in [ISO/TS 15066:2016, ] for collisions with humans, between 110 and 140  $N/cm^2$  would be allowed in the abdominal region. With a contact area of the US probe of approximately 2.25  $cm^2$ , this indicates that 220 N of contact force would be allowed for this application according to the standard. This threshold would allow an application without additional force sensor, as the results demonstrated for method TORQUE (2.6.3) that all collisions above 30 N could be detected. Nevertheless, the results of the experiments suggest to use a force sensor as this can significantly reduce the forces acting on the patient and reduce the reaction time.

Therefore, by implementing the standards, using additionally tightened threshold values and a force sensor, the safety for the present application could be ensured and the basis for the HRC was established. As required by this standard regulation, forces acting on the patient can now be monitored by means of the integrated force sensor and the forces in collisions were approximately an order of magnitude lower compared to the limits in the standard. The implementation can therefore be considered as safe. In addition, the short response times and implemented measures in the event of a collision suggest a safe operation, thereby increasing user acceptance.

For the normal procedure, the results of this thesis have demonstrated safe motion compensation, as well as, the safe autonomous positioning of the US probe. It has been shown that the forces are below the defined threshold values (<20 N) in the normal case. In the conducted safety experiment, it was demonstrated that the developed safety measures are effective and a safe HRC is possible also in extreme cases.

For point-to-point movements, sufficient stop criteria and thresholds were defined. It should be noted that this behavior applies primarily to the speeds applied. On the other hand, a higher speed here would not have offered any advantages and moreover would potentially violate requirements of existing regulations [ISO/TS 15066:2016, ].

For the undetected collisions during BaMC, the results indicate that they do not harm the patient because the force on the patient stays below 20 N at these positions. However, the tests would have to be repeated accordingly for other selected US probe positions and axis angles.

The present implementation shows a safety concept, that is embedded in the overall application. Thus, the clinical workflow can be continued, after unforeseen events (e.g. collision) are handled, since the implementation shows a reaction of the system in quasi real time. This significantly increases user-friendliness and subjectively also conveys an additional measure of safety by

itself, as pre-defined error handling measures automatically take place.

In the cases tested, collisions of a worker with the robot during BaMC were simulated in particular. However, the developed mechanisms also apply to collisions of the robot with the other components like the gantry. In this case, it should be noted that triggering the collision detection of the robot causes an interlock leading to a motion stop of the gantry. This ensures that the gantry does not indirectly transfer forces through the compliant robot on the patient. In addition suitable robot positions [Gerlach et al., 2017a], and treatment plan adoptions [Camps et al., 2018] should be applied to minimize potential collision with the LINAC. For this reason the investigated positions were adapted from [Gerlach et al., 2017a]. Furthermore, in addition to the technical measures already developed, it appears necessary to take further measures, such as a pre-collision detection (e.g. based on position information of the gantry and the robot). The developed software already provides the necessary interface for this and enables integrating the LINAC in the future. In addition to the technical measures, further organizational measures should be taken to prevent collisions, for example by appropriate training of personnel in handling the robot. This should include a demonstration of the introduced forces when operating the system in the wrong way and the resulting movements that are triggered by unforeseen events. For this purpose, the developed visualization of the robot, the colouring of exceeded joint values, and the displayed total force in MITK can be used. This interface can also be extended in the treatment room, for example, to show the user via LED light whether all values are within the permitted range.

Further pre-collision detection mechanism e.g. via time of flight cameras [Beyl et al., 2016] and collision point estimation as presented by [Popov et al., 2017], and recommended by [Haddadin et al., 2017] could improve the sensitivity and would result in collision point dependent reactions. However, the presented implementation is considered sufficient as a starting point for implementing an USgRT workflow. For the more advanced methods presented by [Popov et al., 2017, Beyl et al., 2016], it is currently unclear, whether they are applicable BaMC.

## 4.6 Conclusion

This thesis demonstrates a new approach for safe HRC during robot assisted USgRT. Several important solutions regarding HRC that could be used in USgRT or other medical robot assisted applications were presented. With the presented implementation, a seamless integration of different hardware and software components into a common platform was demonstrated.

The implemented BaMC offers an universal solution for a stable patient contact of the US probe. The developed positioning and scanning mechanisms were newly developed and offer innovative functionalities that were not available yet and which may serve as a basis for, medical robot-assisted applications. The integration of autonomous positioning into other motions simplifies the utilization, as well as, the clinical workflow.

In particular, robot guided positioning of the US probe demonstrated to be feasible with high accuracy and high precision over a wide range of surface contact points on a phantom.

Basic safety mechanisms as required by [ISO/TS 15066:2016, ] could be implemented and threshold values could even been tightened. Collisions were always detected and in these cases, the robot arm with the US probe automatically moves back to a safe position thereby limiting the forces to the patient to acceptable values. As a result of the low threshold values, a safe ap-

plication of the robotic system in patients is achieved, which increases user acceptance due to the selected low threshold values. Positioning and interlock scenarios were extensively tested and demonstrated to work properly. As an outlook, the results of the presented work serve as a basis for first clinical studies with volunteers for different US applications in diagnostics as well as therapy.

# 5 | Conclusion

This thesis shows that safe human-robot-interaction (HRI) and Human Robot Collaboration (HRC) is possible for Ultrasound (US) guided radiotherapy. Via the chosen methodology, all components (US, optical room monitoring and robot) could be linked and integrated and realized in a realistic clinical workflow.

US guided radiotherapy offers a complement and alternative to existing image-guided therapy approaches. The real-time capability of US and high soft tissue contrast allow target structures to be tracked and radiation delivery to be modulated. However, Ultrasound guided radiation therapy (USgRT) is not yet clinically established but is still under development, as reliable and safe methods of image acquisition are not yet available. In particular, the loss of contact of the US probe to the patient surface poses a problem for patient movements such as breathing.

For this purpose, a Breathing and motion compensation (BaMC) was developed in this work, which together with the safe control of a lightweight robot represents a new development for USgRT. The developed BaMC can be used to control the US probe with contact to the patient. The conducted experiments have confirmed that a steady contact with the patient surface and thus a continuous image acquisition can be ensured by the developed methodology. In addition, the image position in space can be accurately maintained in the submillimeter range.

The BaMC seamlessly integrates into a developed clinical workflow. The graphical user interfaces developed for this purpose, as well as direct haptic control with the robot, provide an easy interaction option for the clinical user. The developed autonomous positioning of the transducer represents a good example of the feasibility of the approach. With the help of the user interface, an acoustic plane can be defined and autonomously approached via the robot in a time-efficient and precise manner. The tests carried out show that this methodology is suitable for a wide range of transducer positions.

Safety in a human-robot interaction task is essential and requires individually customized concepts. In this work, adequate monitoring mechanisms could be found to ensure both patient

and staff safety. In collision tests it could be shown that the implemented detection measures work and that the robot moves into a safe parking position. The forces acting on the patient could thus be pushed well below the limits required by the standard.

This work has demonstrated the first important steps towards safe robot-assisted ultrasound imaging, which is not only applicable to USgRT. The developed interfaces provide the basis for further investigations in this field, especially in the area of image recognition, for example to determine the position of the target structure. With the proof of safety of the developed system, first study in human can now follow.



# 6

## Zusammenfassung

Diese Dissertation zeigt, dass eine sichere Mensch Roboter Interaktion für die ultraschallgeführte Strahlentherapie möglich ist. Über die gewählte Methodik konnten alle Komponenten (Ultraschall, optische Raumüberwachung und Roboter) miteinander verknüpft und in einem realistischen klinischen Arbeitsablauf integriert und realisiert werden.

Die ultraschallgeführte Strahlentherapie bietet eine Ergänzung und Alternative für existierende bildgestützte Therapieansätze. Durch die Echtzeitfähigkeit von Ultraschall und den hohen Weichteilkontrast lassen sich Zielstrukturen verfolgen und die Bestrahlung kann angepasst werden. Die USgRT ist jedoch klinisch noch nicht etabliert, sondern befindet sich noch in der Entwicklung, da verlässliche und sichere Methoden der Bildakquisition noch nicht zur Verfügung stehen. Insbesondere der Verlust des Kontakts der Ultraschallsonde zur Patientenoberfläche stellt bei Bewegungen des Patienten wie z.B. die Atmung ein Problem dar.

Zu diesem Zweck wurde in dieser Arbeit eine Atem- und Bewegungskompensation (BaMC) entwickelt, welche zusammen mit der sicheren Steuerung eines Leichtbauroboters eine Neuentwicklung für die USgRT darstellt. Mit Hilfe der entwickelten BaMC lässt sich der Schallkopf mit Kontakt zum Patienten steuern. Die durchgeführten Versuche haben bestätigt, dass ein stetiger Kontakt mit der Patientenoberfläche und damit eine durchgängige Bildakquisition durch die entwickelte Methodik sichergestellt werden kann. Außerdem kann die Bildposition im Raum im Submillimeterbereich genau gehalten werden.

Die BaMC fügt sich dabei nahtlos in einen entwickelten klinischen Arbeitsablauf ein. Die hierfür entwickelten grafischen Nutzerschnittstellen, sowie die direkte haptische Steuerung mit dem Roboter, bieten eine einfache Interaktionsmöglichkeit für den klinischen Anwender. Die entwickelte autonome Positionierung des Schallkopfes stellt ein gutes Beispiel für die Realisierbarkeit des Ansatzes dar. Mit Hilfe der Nutzeroberfläche lässt sich eine Schallebene definieren und autonom über den Roboter zeiteffizient und präzise anfahren. Die durchgeführten Versuche zeigen dabei, dass diese Methodik für eine Vielzahl an Schallkopfpositionen geeignet ist.

Die Sicherheit bei einer Mensch-Roboter-Interaktions-Aufgabe ist essenziell und es benötigt hierfür individuell abgestimmte Konzepte. In dieser Arbeit konnten adäquate Überwachungsmechanismen gefunden werden, um sowohl die Sicherheit des Patienten, als auch die der Mitarbeiter zu gewährleisten. In Kollisionsversuchen konnte gezeigt werden, dass die implementierten Maßnahmen zur Detektion funktionieren und, dass der Roboter in eine sichere Parkposition fährt. Die auf den Patienten einwirkenden Kräfte konnten so deutlich unter die von der Norm geforderten Grenzwerte gedrückt werden.

Mit dieser Arbeit konnten erste wichtige Schritte hin zu einer sicheren roboter-assistierten Ultraschallbildgebung gezeigt werden, welche nicht nur für die USgRT anwendbar ist. Die entwickelten Schnittstellen liefern die Grundlage für weitere Untersuchungen auf diesem Gebiet, insbesondere im Bereich der Bilderkennung, zum Beispiel zur Bestimmung der Position der Zielstruktur. Mit dem Nachweis der Sicherheit des entwickelten Systems, können nun erste Probandenstudien folgen.

# 7 | Bibliography

- [Aalamifar et al., 2016] Aalamifar, F., Cheng, A., Kim, Y., Hu, X., Zhang, H. K., Guo, X. und Boctor, E. M. **Robot-assisted automatic ultrasound calibration.** *International Journal of Computer Assisted Radiology and Surgery*, 11(10):1821–1829, oct 2016. ISSN 1861-6429. doi: 10.1007/s11548-015-1341-8. URL <https://doi.org/10.1007/s11548-015-1341-8>.
- [Abbas et al., 2021] Abbas, M., Al Issa, S. und Dwivedy, S. K. **Event-Triggered Adaptive Hybrid Position-Force Control for Robot-Assisted Ultrasonic Examination System.** *Journal of Intelligent and Robotic Systems: Theory and Applications*, 102(4), 2021. ISSN 15730409. doi: 10.1007/s10846-021-01428-9.
- [Akbari et al., 2021] Akbari, M., Carriere, J., Meyer, T., Sloboda, R., Husain, S., Usmani, N. und Tavakoli, M. **Robotic Ultrasound Scanning With Real-Time Image-Based Force Adjustment: Quick Response for Enabling Physical Distancing During the COVID-19 Pandemic.** *Frontiers in Robotics and AI*, 8(March), 2021. ISSN 22969144. doi: 10.3389/frobt.2021.645424.
- [Albu-Schäffer und Hirzinger, 2002] Albu-Schäffer, A. und Hirzinger, G. **Cartesian impedance control techniques for torque controlled light-weight robots.** *Proceedings - IEEE International Conference on Robotics and Automation*, 1 (May):657–663, 2002. ISSN 10504729. doi: 10.1109/ROBOT.2002.1013433.
- [Barnett und Morley, 2012] Barnett, E. und Morley, P. **Abdominal Echograohy: Ultrasound in the Diagnosis of Abdominal Conditions.** Butterworth & Co. (Publishers) Ltd., 2012.
- [Barr et al., 2013] Barr, R., Hindi, A. und peterson, c. **Artifacts in diagnostic ultrasound.** *Reports in Medical Imaging*, 6, 06 2013. doi: 10.2147/RMI.S33464.
- [Berger et al., 2018] Berger, J., Unger, M., Landgraf, L., Bieck, R., Neumuth, T. und Melzer, A. **Assessment of natural user interactions for robot-assisted interventions.** *Current Directions in Biomedical Engineering*, 4(1):165–168, 2018. ISSN 23645504. doi: 10.1515/cdbme-2018-0041.
- [Beyl et al., 2016] Beyl, T., Nicolai, P., Comparetti, M. D., Raczkowski, J., De Momi, E. und Wörn, H. **Time-of-flight-assisted Kinect camera-based people detection for intuitive human robot cooperation in the surgical operating room.** *International Journal of Computer Assisted Radiology and Surgery*, 11(7):1329–1345, 2016. ISSN 18616429. doi: 10.1007/s11548-015-1318-7.
- [Bø et al., 2015] Bø, L. E., Hofstad, E. F., Lindseth, F. und Hernes, T. A. **Versatile robotic probe calibration for position tracking in ultrasound imaging.** *Physics in Medicine and Biology*, 60(9):3499–3513, 2015. ISSN 13616560. doi: 10.1088/0031-9155/60/9/3499.
- [Boda-Heggemann et al., 2009] Boda-Heggemann, J., Mennemeyer, P., Wertz, H., Riesenacker, N., Küpper, B., Lohr, F. und Wenz, F. **Accuracy of Ultrasound-Based Image Guidance for Daily Positioning of the Upper Abdomen: An Online Comparison With Cone Beam CT.** *International Journal of Radiation Oncology Biology Physics*, 74(3):892–897, 2009. ISSN 03603016. doi: 10.1016/j.ijrobp.2009.01.061.

- [Camps et al., 2018] Camps, S. M., Fontanarosa, D., de With, P. H. N., Verhaegen, F. und Vanneste, B. G. L. **The Use of Ultrasound Imaging in the External Beam Radiotherapy Workflow of Prostate Cancer Patients.** *BioMed Research International*, 2018:16, 2018. URL <https://doi.org/10.1155/2018/7569590%25>] 7569590.
- [Carlson, 2019] Carlson, F. B. **On the calibration of force/torque sensors in robotics.** *arXiv*, Seiten 1–9, 2019.
- [Chandra et al., 2003] Chandra, A., Dong, L., Huang, E., Kuban, D. A., O’Neill, L., Rosen, I. und Pollack, A. **Experience of ultrasound-based daily prostate localization.** *International Journal of Radiation Oncology Biology Physics*, 56(2): 436–447, 2003. ISSN 03603016. doi: 10.1016/S0360-3016(02)04612-6.
- [Chen et al., 2021] Chen, S., Li, Z., Lin, Y., Wang, F. und Cao, Q. **Automatic ultrasound scanning robotic system with optical waveguide-based force measurement.** *International Journal of Computer Assisted Radiology and Surgery*, 16(6):1015–1025, 2021. ISSN 18616429. doi: 10.1007/s11548-021-02385-2. URL <https://doi.org/10.1007/s11548-021-02385-2>.
- [Conti et al., 2014] Conti, F., Park, J. und Khatib, O. **Interface Design and Control Strategies for a Robot Assisted Ultrasonic Examination System.** In Khatib, O., Kumar, V. und Sukhatme, G., Herausgeber, *Experimental Robotics: The 12th International Symposium on Experimental Robotics*, Seiten 97–113. Springer Berlin Heidelberg, Berlin, Heidelberg, 2014. ISBN 978-3-642-28572-1. doi: 10.1007/978-3-642-28572-1\_7. URL [https://doi.org/10.1007/978-3-642-28572-1\\_7](https://doi.org/10.1007/978-3-642-28572-1_7).
- [El-Baz et al., 2011] El-Baz, A., Acharya, U. R., Laine, A. und Suri, J. **Multi Modality State-of-the-Art Medical Image Segmentation and Registration Methodologies: Volume II.** 01 2011. ISBN 978-1-4419-8203-2. doi: 10.1007/978-1-4419-8204-9.
- [Elek et al., 2017] Elek, R., Nagy, T. D., Nagy, D. A., Takacs, B., Galambos, P., Rudas, I. und Haidegger, T. **Robotic platforms for ultrasound diagnostics and treatment.** *2017 IEEE International Conference on Systems, Man, and Cybernetics, SMC 2017*, 2017-Janua:1752–1757, 2017. doi: 10.1109/SMC.2017.8122869.
- [Elfring et al., 2010] Elfring, R., De La Fuente, M. und Radermacher, K. **Assessment of optical localizer accuracy for computer aided surgery systems.** *Computer Aided Surgery*, 15(1-3):1–12, 2010. ISSN 10929088. doi: 10.3109/10929081003647239.
- [Esteban et al., 2018] Esteban, J., Simson, W., Requena Witzig, S., Riemüller, A., Virga, S., Frisch, B., Zettinig, O., Sakara, D., Ryang, Y. M., Navab, N. und Hennersperger, C. **Robotic ultrasound-guided facet joint insertion.** *International Journal of Computer Assisted Radiology and Surgery*, 13(6):895–904, 2018. ISSN 18616429. doi: 10.1007/s11548-018-1759-x. URL <https://doi.org/10.1007/s11548-018-1759-x>.
- [Fontanarosa et al., 2015] Fontanarosa, D., Van Der Meer, S., Bamber, J., Harris, E., O’Shea, T. und Verhaegen, F. **Review of ultrasound image guidance in external beam radiotherapy: I. Treatment planning and inter-fraction motion management.** *Physics in Medicine and Biology*, 60(3):R77–R114, 2015. ISSN 13616560. doi: 10.1088/0031-9155/60/3/R77.
- [Franz et al., 2012] Franz, A. M., Seitel, A., Servatius, M., Zöllner, C., Gergel, I., Wegner, I., Neuhaus, J., Zelzer, S., Nolden, M., Gaa, J., Mercea, P., Yung, K., Sommer, C. M., Radeleff, B. A., Schlemmer, H.-P., Kauczor, H.-U., Meinzer, H.-P. und Maier-Hein, L. **Simplified development of image-guided therapy software with MITK-IGT.** *Medical Imaging 2012: Image-Guided Procedures, Robotic Interventions, and Modeling*, 8316(February 2012):83162], 2012. ISSN 16057422. doi: 10.1117/12.911421.
- [Franz et al., 2013] Franz, A., MÄÇrz, K., Seitel, A., Kenngott, H., Wagner, M., Preukschas, A., Meinzer, H.-P., Wolf, I. und Maier-Hein, L. **Combined Modality for Ultrasound Imaging and Electromagnetic Tracking.** *Biomedizinische Technik. Biomedical engineering*, 58, 2013.
- [Fuss et al., 2003] Fuss, M., Salter, B. J., Cavanaugh, S. X., Fuss, C., Sadeghi, A., Fuller, C. D., Ameduri, A., Hevezi, J. M., Herman, T. S. und Thomas, C. R. J. **Daily ultrasound-based image-guided targeting for radiotherapy of upper abdominal malignancies.** *International Journal of Radiation Oncology Biology Physics*, 59(4):1245–1256, 2003. doi: 10.1016/j.ijrobp.2003.12.030. URL <http://dx.doi.org/10.1016/j.ijrobp.2003.12.030>.
- [Gámez García et al., 2004] Gámez García, J., Robertsson, A., Gómez Ortega, J. und Johansson, R. **Sensor fusion of force and acceleration for robot force control.** *2004 IEEE/RSJ International Conference on Intelligent Robots and Systems (IROS)*, 3(Iros):3009–3014, 2004. doi: 10.1109/iros.2004.1389867.
- [Gámez García et al., 2005] Gámez García, J., Robertsson, A., Gómez Ortega, J. und Johansson, R. **Automatic calibration procedure for a robotic manipulator force observer.** *Proceedings - IEEE International Conference on Robotics and Automation*, 2005:2703–2708, 2005. ISSN 10504729. doi: 10.1109/ROBOT.2005.1570522.
- [Gautier und Jubien, 2014] Gautier, M. und Jubien, A. **Force calibration of KUKA LWR-like robots including embedded joint torque sensors and robot structure.** *IEEE International Conference on Intelligent Robots and Systems, (Iros)*: 416–421, 2014. ISSN 21530866. doi: 10.1109/IROS.2014.6942593.
- [Geng et al., 2020] Geng, C., Xie, Q., Chen, L., Li, A. und Qin, B. **Study and Analysis of a Remote Robot-assisted Ultrasound Imaging System.** *Proceedings of 2020 IEEE 4th Information Technology, Networking, Electronic and Automation Control Conference, ITNEC 2020, (Itnec)*:389–393, 2020. doi: 10.1109/ITNEC48623.2020.9084796.

- [Gerlach und Schlaefer, 2022] Gerlach, S. und Schlaefer, A. **Robotic Systems in Radiotherapy and Radiosurgery**. *Current Robotics Reports*, (0123456789), 2022. ISSN 2662-4087. doi: 10.1007/s43154-021-00072-3. URL <https://doi.org/10.1007/s43154-021-00072-3>.
- [Gerlach et al., 2017a] Gerlach, S., Kuhlemann, I., Ernst, F., Fürweger, C. und Schlaefer, A. **Impact of robotic ultrasound image guidance on plan quality in SBRT of the prostate**. *British Journal of Radiology*, 90(1078), 2017a. ISSN 00071285. doi: 10.1259/bjr.20160926.
- [Gerlach et al., 2017b] Gerlach, S., Kuhlemann, I., Jauer, P., Bruder, R., Ernst, F., Fürweger, C. und Schlaefer, A. **Robotic ultrasound-guided SBRT of the prostate: feasibility with respect to plan quality**. *International Journal of Computer Assisted Radiology and Surgery*, 12(1):149–159, jan 2017b. ISSN 1861-6429. doi: 10.1007/s11548-016-1455-7. URL <https://doi.org/10.1007/s11548-016-1455-7>.
- [Giuliani et al., 2020] Giuliani, M., Szcześniak-Stańczyk, D., Mirnig, N., Stollnberger, G., Szyszko, M., Stańczyk, B. und Tschelligi, M. **User-centred design and evaluation of a tele-operated echocardiography robot**. *Health and Technology*, 10(3):649–665, 2020. ISSN 21907196. doi: 10.1007/s12553-019-00399-0.
- [Gong et al., 2013] Gong, D., Jia, Y., Cheng, Y. und Xi, N. **On-line and simultaneous calibration of wrist-mounted Force/Torque sensor and tool Forces/Torques for manipulation**. *2013 IEEE International Conference on Robotics and Biomimetics, ROBOT 2013*, (December):619–624, 2013. doi: 10.1109/ROBOT.2013.6739528.
- [Goos, 2022] Goos, P. **Adaptive Visualisierung der Bestrahlungssituation anhand von Gerätedaten in MITK**, 2022.
- [Graumann et al., 2016] Graumann, C., Fuerst, B., Hengersperger, C., Bork, F. und Navab, N. **Robotic ultrasound trajectory planning for volume of interest coverage**. In *2016 IEEE International Conference on Robotics and Automation (ICRA)*, Seiten 736–741. John Hopkins University, Baltimore, may 2016. doi: 10.1109/ICRA.2016.7487201.
- [Grimwood et al., 2018] Grimwood, A., McNair, H. A., O’Shea, T. P., Gilroy, S., Thomas, K., Bamber, J. C., Tree, A. C. und Harris, E. J. **In Vivo Validation of Elekta’s Clarity Autoscan for Ultrasound-based Intrafraction Motion Estimation of the Prostate During Radiation Therapy**. *International Journal of Radiation Oncology Biology Physics*, 102(4):912–921, 2018. ISSN 1879355X. doi: 10.1016/j.ijrobp.2018.04.008. URL <https://doi.org/10.1016/j.ijrobp.2018.04.008>.
- [Haddadin et al., 2017] Haddadin, S., De Luca, A. und Albu-Schäffer, A. **Robot Collisions: A Survey on Detection, Isolation, and Identification**. *IEEE Transactions on Robotics*, 33(6):1292–1312, dec 2017. ISSN 1552-3098. doi: 10.1109/TRO.2017.2723903.
- [Haddadin, 2014] Haddadin, S. **Approaching Asimov’s 1st Law**. 2014. ISBN 9783642403071.
- [Harris et al., 2021] Harris, E., Fontanarosa, D., Camps, S. und Verhaegen, F., Herausgeber. **Modern Applications of 3D/4D Ultrasound Imaging in Radiotherapy**. 2053-2563. IOP Publishing, 2021. ISBN 978-0-7503-2552-3. doi: 10.1088/978-0-7503-2552-3. URL <https://dx.doi.org/10.1088/978-0-7503-2552-3>.
- [Hassani, 1976] Hassani, N. **Ultrasonography of the Abdomen**. Springer, 1976.
- [Hsu et al., 2005] Hsu, A., Miller, N. R., Evans, P. M., Bamber, J. C. und Webb, S. **Feasibility of using ultrasound for real-time tracking during radiotherapy**. *Medical Physics*, 32(6Part1):1500–1512, 2005. ISSN 2473-4209. doi: 10.1118/1.1915934. URL <http://dx.doi.org/10.1118/1.1915934>.
- [Huang und Zeng, 2017] Huang, Q. und Zeng, Z. **A Review on Real-Time 3D Ultrasound Imaging Technology**. *BioMed Research International*, 2017, 2017. ISSN 23146141. doi: 10.1155/2017/6027029.
- [Huang et al., 2019] Huang, Q., Lan, J. und Li, X. **Scanning for Three-Dimensional Imaging**. 15(2):1173–1182, 2019.
- [Ipsen et al., 2016a] Ipsen, S., Bruder, R., O’Brien, R., Keall, P. J., Schweikard, A. und Poulsen, P. R. **Online 4D ultrasound guidance for real-time motion compensation by MLC tracking**. *Medical Physics*, 43(10):5695–5704, 2016a. ISSN 00942405. doi: 10.1118/1.4962932. URL <http://dx.doi.org/10.1118/1.4962932>.
- [Ipsen et al., 2016b] Ipsen, S., Bruder, R., O’Brien, R., Keall, P. J., Schweikard, A. und Poulsen, P. R. **Online 4D ultrasound guidance for real-time motion compensation by MLC tracking**. *Medical Physics*, 43(10):5695–5704, 2016b. ISSN 00942405. doi: 10.1118/1.4962932. URL <http://dx.doi.org/10.1118/1.4962932>.
- [Ipsen et al., 2021] Ipsen, S., Wulff, D., Kuhlemann, I., Schweikard, A. und Ernst, F. **Towards automated ultrasound imaging - Robotic image acquisition in liver and prostate for long-term motion monitoring**. *Physics in Medicine and Biology*, 66(9), 2021. ISSN 13616560. doi: 10.1088/1361-6560/abf277.
- [ISO/TS 15066:2016, ] ISO/TS 15066:2016. **Roboter und Robotikgeräte – Kollaborierende Roboter**. Standard, Deutsches Institut für Normung e. V., 2016.
- [Jiang et al., 2020] Jiang, Z., Grimm, M., Zhou, M., Esteban, J., Simson, W., Zahnd, G. und Navab, N. **Automatic Normal Positioning of Robotic Ultrasound Probe Based only on Confidence Map Optimization and Force Measurement**. *IEEE Robotics and Automation Letters*, 5(2):1342–1349, 2020. ISSN 23773766. doi: 10.1109/LRA.2020.2967682.

- [Jürgen Debus, 2012] Jürgen Debus, Stefan Delorm, K.-V. J. **Sonografie**. Thieme, 3 edition, 2012.
- [Karayiannidis et al., 2014] Karayiannidis, Y., Smith, C., Vina, F. E. und Kragic, D. **Online contact point estimation for uncalibrated tool use**. *Proceedings - IEEE International Conference on Robotics and Automation*, Seiten 2488–2494, 2014. ISSN 10504729. doi: 10.1109/ICRA.2014.6907206.
- [Klemm et al., 2017] Klemm, M., Kirchner, T., Gröhl, J., Cheray, D., Nolden, M., Seitel, A., Hoppe, H., Maier-Hein, L. und Franz, A. M. **MITK-OpenIGTLink for combining open-source toolkits in real-time computer-assisted interventions**. *International Journal of Computer Assisted Radiology and Surgery*, 12(3):351–361, mar 2017. ISSN 1861-6429. doi: 10.1007/s11548-016-1488-y. URL <https://doi.org/10.1007/s11548-016-1488-y>.
- [Kuban et al., 2005] Kuban, D. A., Dong, L., Cheung, R., Strom, E. und Crevoisier, R. D. **Ultrasound-Based Localization**. *Seminars in Radiation Oncology*, 15(3):180–191, 2005. ISSN 1053-4296. doi: <https://doi.org/10.1016/j.semradonc.2005.01.009>. URL <http://www.sciencedirect.com/science/article/pii/S1053429605000111>.
- [Kuhlemann, ] Kuhlemann, I. **Masterarbeit Force and Image Adaptive Strategies for Robotised Placement of 4D Ultrasound Probes**.
- [Kuhlemann et al., 2015] Kuhlemann, I., Jauer, P., Schweikard, A. und Ernst, F. **Patient localization for robotized ultrasound-guided radiation therapy**. *Imaging and Computer Assistance in Radiation Therapy, ICART 2015, 18th International Conference on Medical Image Computing and Computer-Assisted Intervention - MICCAI'15*, Seiten 105–112, 2015.
- [Langen et al., ] Langen, K. M., Pouliot, J., Anezinos, C., Aubin, M., Gottschalk, A. R., Hsu, I.-C., Lowther, D., Liu, Y.-M., Shinohara, K., Verhey, L. J., Weinberg, V. und Roach M, I. I. I. **Evaluation of ultrasound-based prostate localization for image-guided radiotherapy**. *International Journal of Radiation Oncology Biology Physics*, 57(3):635–644. doi: 10.1016/S0360-3016(03)00633-3. URL [http://dx.doi.org/10.1016/S0360-3016\(03\)00633-3](http://dx.doi.org/10.1016/S0360-3016(03)00633-3).
- [Lasota et al., 2017] Lasota, P., Fong, T. und A. Shah, J. **A Survey of Methods for Safe Human-Robot Interaction**. *Foundations and Trends in Robotics*, 5:261–349, 2017. doi: 10.1561/23000000052.
- [Lediju Bell et al., 2014] Lediju Bell, M. A., Sen, H. T., Iordachita, I., Kazanzides, P. und Wong, J. **In vivo reproducibility of robotic probe placement for an integrated US-CT image-guided radiation therapy system**. *Medical Imaging 2014: Image-Guided Procedures, Robotic Interventions, and Modeling*, 9036:903611, 2014. ISSN 16057422. doi: 10.1117/12.2043681.
- [Martin. F. Fase, 2016] Martin. F. Fase, Tuathan P. O'Sheal, S. N. U. O. E. J. H. **First evaluation of the feasibility of MLC tracking using ultrasound motion estimation**. *Medical Physics*, (July), 2016. doi: 10.1118/1.4955440.
- [März et al., 2014] März, K., Franz, A. M., Seitel, A., Winterstein, A., Bendl, R., Zelzer, S., Nolden, M., Meinzer, H. P. und Maier-Hein, L. **MITK-US: real-time ultrasound support within MITK**. *International Journal of Computer Assisted Radiology and Surgery*, 9(3):411–420, 2014. doi: 10.1007/s11548-013-0962-z. URL <https://doi.org/10.1007/s11548-013-0962-z>.
- [Mason et al., 2017] Mason, S. A., O'Shea, T. P., White, I. M., Lalondrelle, S., Downey, K., Baker, M., Behrens, C. F., Bamber, J. C. und Harris, E. J. **Towards ultrasound-guided adaptive radiotherapy for cervical cancer: Evaluation of Elekta's semiautomated uterine segmentation method on 3D ultrasound images: Evaluation**. *Medical Physics*, 44(7):3630–3638, 2017. ISSN 00942405. doi: 10.1002/mp.12325.
- [McNair et al., 2006] McNair, H. A., Mangar, S. A., Coffey, J., Shoulders, B., Hansen, V. N., Norman, A., Staffurth, J., Sohaib, S. A., Warrington, A. P. und Dearnaley, D. P. **A comparison of CT- and ultrasound-based imaging to localize the prostate for external beam radiotherapy**. *International Journal of Radiation Oncology\*Biophysics*, 65(3):678–687, 2006. ISSN 0360-3016. doi: <https://doi.org/10.1016/j.ijrobp.2006.01.022>. URL <http://www.sciencedirect.com/science/article/pii/S0360301606001660>.
- [Moult et al., 2017] Moult, E. M., Lasso, A., Ungi, T., Pinter, C., Welch, M. und Fichtinger, G. **Improved Temporal Calibration of Tracked Ultrasound: An Open-Source Solution**. *Journal of Medical Robotics Research*, 02(04):1750008, 2017. doi: 10.1142/S2424905X17500088. URL <https://doi.org/10.1142/S2424905X17500088>.
- [Muratore und Galloway, 2001] Muratore, D. M. und Galloway, R. L. **Beam calibration without a phantom for creating a 3-d freehand ultrasound system**. *Ultrasound in Medicine and Biology*, 27(11):1557–1566, 2001. ISSN 03015629. doi: 10.1016/S0301-5629(01)00469-0.
- [Noble und Boukerroui, 2006] Noble, J. A. und Boukerroui, D. **Ultrasound image segmentation: A survey**. *IEEE Transactions on Medical Imaging*, 25(8):987–1010, 2006. ISSN 02780062. doi: 10.1109/TMI.2006.877092.
- [Nolden et al., 2013] Nolden, M., Zelzer, S., Seitel, A., Wald, D., Müller, M., Franz, A. M., Maleike, D., Fangerau, M., Baumhauer, M., Maier-Hein, L., Maier-Hein, K. H., Meinzer, H. P. und Wolf, I. **The Medical Imaging Interaction Toolkit: challenges and advances**. *International Journal of Computer Assisted Radiology and Surgery*, 8(4):607–620, jul 2013. ISSN 1861-6429. doi: 10.1007/s11548-013-0840-8. URL <https://doi.org/10.1007/s11548-013-0840-8>.

- [Oh et al., 2017] Oh, H. S., Kang, G., Kim, U., Seo, J. K., You, W. S. und Choi, H. R. **Force/torque sensor calibration method by using deep-learning**. *2017 14th International Conference on Ubiquitous Robots and Ambient Intelligence, URAI 2017*, (April 2019):777–782, 2017. doi: 10.1109/URAI.2017.7992824.
- [O’Shea et al., 2016] O’Shea, T., Bamber, J., Fontanarosa, D., Van Der Meer, S., Verhaegen, F. und Harris, E. **Review of ultrasound image guidance in external beam radiotherapy part II: Intra-fraction motion management and novel applications**. *Physics in Medicine and Biology*, 61(8):R90–R137, 2016. ISSN 13616560. doi: 10.1088/0031-9155/61/8/R90.
- [Pollet, 2012] Pollet, B. **Power Ultrasound in electrochemistry: From Versatile Laboratory Tool to Engineering Solution**. WILEY, 2012.
- [Popov et al., 2017] Popov, D., Klimchik, A. und Mavridis, N. **Collision detection, localization and classification for industrial robots with joint torque sensors**. *RO-MAN 2017 - 26th IEEE International Symposium on Robot and Human Interactive Communication*, 2017-Janua:838–843, 2017. doi: 10.1109/ROMAN.2017.8172400.
- [Priester et al., 2013] Priester, A. M., Natarajan, S. und Culjat, M. O. **Robotic ultrasound systems in medicine**. *IEEE Transactions on Ultrasonics, Ferroelectrics, and Frequency Control*, 60(3):507–523, mar 2013. ISSN 0885-3010. doi: 10.1109/TUFFC.2013.2593.
- [Richter et al., 2012] Richter, L., Bruder, R. und Schweikard, A. **Calibration of force/torque and acceleration for an independent safety layer in medical robotic systems**. *Cureus*, 2012. ISSN 2168-8184. doi: 10.7759/cureus.59.
- [Salcudean et al., 1999] Salcudean, S. E., Bell, G., Bachmann, S., Zhu, W. H., Abolmaesumi, P. und Lawrence, P. D. **Robot-Assisted Diagnostic Ultrasound – Design and Feasibility Experiments**. In Taylor, C. und Colchester, A., Herausgeber, *Medical Image Computing and Computer-Assisted Intervention – MICCAI’99: Second International Conference, Cambridge, UK, September 19-22, 1999. Proceedings*, Seiten 1062–1071. Springer Berlin Heidelberg, Berlin, Heidelberg, 1999. ISBN 978-3-540-48232-1. doi: doi:10.1007/10704282\_115. URL [http://dx.doi.org/10.1007/10704282\\_115](http://dx.doi.org/10.1007/10704282_115).
- [Schlosser, 2016] Schlosser, J. H. D. **Radiolucent 4D Ultrasound Imaging: System Design and Application to Radiotherapy Guidance**. *IEEE Transactions on Medical Imaging*, 35(10):2292–2300, oct 2016. ISSN 0278-0062. doi: 10.1109/TMI.2016.2559499.
- [Schlosser et al., 2010] Schlosser, J., Salisbury, K. und Hristov, D. **Telerobotic system concept for real-time soft-tissue imaging during radiotherapy beam delivery**. *Medical Physics*, 37(12):6357–6367, 2010. ISSN 2473-4209. doi: 10.1118/1.3515457. URL <http://dx.doi.org/10.1118/1.3515457>.
- [Schwahofer und Jäkel, 2018] Schwahofer, A. und Jäkel, O. **Planning target volume: Management of uncertainties, immobilization, image guided and adaptive radiation therapy**. *Radiologe*, 58(8):736–745, 2018. ISSN 0033832X. doi: 10.1007/s00117-018-0419-z.
- [Seidel, 2019] Seidel, J. **Konzeption und Entwicklung einer autonomen Positionierung für die Robotergestützte Bildgebung**, 2019.
- [Seitz, 2018] Seitz, P. K. **Konzeption und Entwicklung einer robotergestützten und ultraschallbasierten Lokalisationskontrolle**. Master thesis, 2018. URL <https://nbn-resolving.org/urn:nbn:de:bsz:840-opus4-1508>.
- [Seitz et al., ] Seitz, P. K., Sc, M., Seitz, P. K., Sc, M., Baumann, B. und Sc, M. **International Journal of Computer Assisted Radiology and Surgery Development of a robot assisted ultrasound guided radiation therapy ( USgRT ) To :**
- [Seitz et al., 2020] Seitz, P. K., Baumann, B., Johnen, W., Lissek, C., Seidel, J. und Bendl, R. **Development of a robot-assisted ultrasound-guided radiation therapy (USgRT)**. *International Journal of Computer Assisted Radiology and Surgery*, 15(3):491–501, 2020. ISSN 18616429. doi: 10.1007/s11548-019-02104-y. URL <https://doi.org/10.1007/s11548-019-02104-y>.
- [Sen et al., 2017] Sen, H. T., Lediju Bell, M. A., Zhang, Y., Ding, K., Boctor, E., Wong, J., Iordachita, I. und Kazanzides, P. **System Integration and in Vivo Testing of a Robot for Ultrasound Guidance and Monitoring during Radiotherapy**. *IEEE Transactions on Biomedical Engineering*, 64(7):1608–1618, 2017. ISSN 15582531. doi: 10.1109/TBME.2016.2612229.
- [Sharkawy und Aspragathos, 2018] Sharkawy, A. N. und Aspragathos, N. **Human-robot collision detection based on neural networks**. *International Journal of Mechanical Engineering and Robotics Research*, 7(2):150–157, 2018. ISSN 22780149. doi: 10.18178/ijmerr.7.2.150-157.
- [Sterzing et al., 2011] Sterzing, F., Engenhart-Cabillic, R., Flentje, M. und Debus, J. **Optionen der bildgestützten bestrahlung: Eine neue dimension in der radioonkologie**. *Deutsches Arzteblatt*, 108(16):274–280, 2011. ISSN 00121207. doi: 10.3238/arztebl.2011.0274.
- [Swerdlow et al., 2017] Swerdlow, D. R., Cleary, K., Wilson, E., Azizi-Koutenaeei, B. und Monfaredi, R. **Robotic Arm-Assisted Sonography: Review of Technical Developments and Potential Clinical Applications**. *American Journal of Roentgenology*, 208(4):733–738, 2017. doi: 10.2214/AJR.16.16780. URL <https://doi.org/10.2214/AJR.16.16780>.

- [Tauscher et al., 2015] Tauscher, S., Tokuda, J., Schreiber, G., Neff, T., Hata, N. und Ortmaier, T. **OpenIGTLink interface for state control and visualisation of a robot for image-guided therapy systems.** *International Journal of Computer Assisted Radiology and Surgery*, 10(3):285–292, 2015. ISSN 1861-6429. doi: 10.1007/s11548-014-1081-1. URL <http://dx.doi.org/10.1007/s11548-014-1081-1>.
- [Tutkun Şen et al., 2013] Tutkun Şen, H., Lediju Bell, M. A., Iordachita, I., Wong, J. und Kazanzides, P. **A Cooperatively Controlled Robot for Ultrasound Monitoring of Radiation Therapy.** *IEEE/RSJ International Conference on Intelligent Robots and Systems*, 2013:3071–3076, 2013. doi: 10.1109/IROS.2013.6696791. URL <http://www.ncbi.nlm.nih.gov/pmc/articles/PMC4727762/>.
- [Unger et al., 2021] Unger, M., Berger, J. und Melzer, A. **Robot-Assisted Image-Guided Interventions.** *Frontiers in Robotics and AI*, 8(July):1–7, 2021. ISSN 22969144. doi: 10.3389/frobt.2021.664622.
- [Verellen et al., 2008] Verellen, D., Ridder, M. D. und Storme, G. **A (short) history of image-guided radiotherapy.** *Radiation Therapy and Oncology*, 86(1):4–13, 2008. ISSN 0167-8140. doi: <https://doi.org/10.1016/j.radonc.2007.11.023>. URL <http://www.sciencedirect.com/science/article/pii/S016781400700624X>.
- [Virga et al., 2016] Virga, S., Zettinig, O., Esposito, M., Pfister, K., Frisch, B., Neff, T., Navab, N. und Hennersperger, C. **Automatic force-compliant robotic ultrasound screening of abdominal aortic aneurysms.** In *2016 IEEE/RSJ International Conference on Intelligent Robots and Systems (IROS)*, Seiten 508–513, 2016. doi: 10.1109/IROS.2016.7759101.
- [Virga et al., 2018] Virga, S., Göbl, R., Baust, M., Navab, N. und Hennersperger, C. **Use the force: deformation correction in robotic 3D ultrasound.** *International Journal of Computer Assisted Radiology and Surgery*, 13(5):619–627, may 2018. ISSN 1861-6429. doi: 10.1007/s11548-018-1716-8. URL <https://doi.org/10.1007/s11548-018-1716-8>.
- [von Haxthausen et al., 2021] von Haxthausen, F., Böttger, S., Wulff, D., Hagenah, J., García-Vázquez, V. und Ipsen, S. **Medical Robotics for Ultrasound Imaging: Current Systems and Future Trends.** *Current Robotics Reports*, 2(1):55–71, 2021. doi: 10.1007/s43154-020-00037-y.
- [Western et al., 2015] Western, C., Hristov, D. und Schlosser, J. **Ultrasound Imaging in Radiation Therapy: From Interfractional to Intrafractional Guidance.** *Cureus*, 7(6):e280, 2015. doi: 10.7759/cureus.280. URL <http://www.ncbi.nlm.nih.gov/pmc/articles/PMC4494460/>.
- [Wu et al., 2006] Wu, J., Dandekar, O., Nazareth, D., Lei, P., D’Souza, W. und Shekhar, R. **Effect of Ultrasound Probe on Dose Delivery During Real-time Ultrasound-Guided Tumor Tracking.** In *2006 International Conference of the IEEE Engineering in Medicine and Biology Society*, Seiten 3799–3802. University of Maryland, 2006. ISBN 1557-170X. doi: 10.1109/IEMBS.2006.260076.
- [Zhukov, 2022] Zhukov, B. **Development of an automatic ultrasound calibration workflow for ultrasound-guided and robot-assisted radiation therapy**, 2022.



# 8

## Own contribution

The aim of this chapter is to disclose the own contribution of each section of the thesis.

### 8.1 Implementation and validation

The software developed in this thesis, especially the motion compensation, the autonomous start-up and safety control has been programmed and tested by myself. This includes all tests performed as well as their evaluation.

The basis of the work used by me comes from my master thesis [Seitz, 2018], as well as from several bachelor and master theses supervised by me. Parts of these results are included in the current state of the application and marked at the appropriate place:

- **bachelor thesis [Goos, 2022]:** The designed 3D model of the linear accelerator was taken from this work.
- **Master thesis [Zhukov, 2022]:** The calibration of the optical tracking system was taken from this work.
- **Bachelor thesis [Seidel, 2019]:** The approach to the autonomous approach as well as partly the graphical user interfaces were taken over, but not the corresponding programming.

The development of the tools (US mount, robot mount and force sensor assembly) was done by Johnen Wibke, Fabian Dinkel based on my specifications.

### 8.2 Own publications

This section will list all papers that I was a part of and contributed to during my Ph.D. work. It is subdivided into First authorships peer reviewed journal publication, first authorships other (abstracts, or conference proceedings) and last outhorships other (abstracts, or conference proceedings).

## First authorships - peer reviewed journal publications

**Peter Seitz**, Beatrice Baumann, Wibke Johnen, Cord Lissek, Johanna Seidel, Rolf Bendl. Development of a robot-assisted ultrasound-guided radiation therapy (USgRT) *Int J CARS* 15, 491–501, Dezember 2019. doi: 10.1007/s11548-019-02104-y.

**Publication pending!** **Peter Seitz**, Christian P. Karger, Rolf Bendl, Andrea Schwahofer. Strategy for automatic ultrasound (US) probe positioning in robot-assisted ultrasound-guided radiation therapy *PMB*.

**Publication 1:** is based on the results of the chapters. My own share in this publication extends to ca.90 % The share on the remaining authors extends in equal parts. B. Baumann assisted in the execution of the experiments. W. Johnen took over the production of the used US head holder. C. Lissek as well as J. Seidel realized smaller used programmed functions (in the area of representation US picture as well as autonomous starting) in the MITK. R. Bendl took over the project management, as well as assistance with the writing of the work.

**Publication 2:** is based on the results of the chapters and should be submitted promptly. The share of the work is based on 95% support of the co-authors is significantly in the written part.

## First authorships - other

**Peter Seitz**, Andrea Schwahofer, Beatrice Baumann, Rolf Bendl. Entwicklung einer robotergestützten und ultraschallbasierten Lokalisationskontrolle für die Strahlentherapie *Poster DGMP 2019*

**Peter Seitz**, Development of a robot-assisted ultrasound-guided radiation therapy (USgRT) *Abstract volume Estro 2020*.

**Peter Seitz**, Andrea Schwahofer, P. Goos, R. Bendl. Detektion von Kollisionen und Entwicklung von Gegenmaßnahmen für eine sichere Anwendung der robotergestützten Ultraschall-diagnostik während der Bestrahlung *Abstract volume DGMP 2020*.

**Peter Seitz**, K. Loheswaran, J. Seidel, R. Bendl, A. Schwahofer. Autonomous robotic ultrasound probe positioning for ultrasound guided radiation therapy *Abstract volume ÖGMP, DGMP and SGSMP 2021*.

## Last authorships - other

Justus Kerber, Dieter Maier, Rolf Bendl, Andrea Schwahofer **Peter Seitz**. Ultraschallbasierte roboterassistierte Strahlentherapie – Räumliche Verfolgung von Zielstrukturen im Ultraschallbild mittels Bildverarbeitung und Visual Servoing *Abstract volume DGMP 2022*

# Appendix

Table 8.1: Collision detection for each detection method for Axilliar 45 US position.

US position	Collision point	robot SPATIAL force estimation				robot spatial force and TORQUE estimation				SPATIAL+ TORQUE + FORCE SENSOR			
		Detected by mechanism	Maximum force Sensor	robot estimated	robot measured	Detected by mechanism	Maximum force Sensor	robot estimated	robot measured	Detected by mechanism	Maximum force Sensor	robot estimated	robot measured
AXILLIAR45	Tool_1	SPATIAL	18.89	18.89	SPATIAL	20.39	20.39	20.25	FORCE_SENSOR	20.01	20.01	16.38	
AXILLIAR45	Tool_2	SPATIAL	23.73	20.39	SPATIAL	24.42	20.48	20.48	FORCE_SENSOR	20.00	20.00	20.91	
AXILLIAR45	Tool_3	SPATIAL	25.18	20.57	SPATIAL	27.31	26.35	26.35	FORCE_SENSOR	20.01	20.01	11.79	
AXILLIAR45	Tool_4	notDetected	11.32	6.89	notDetected	12.19	8.05	8.05	notDetected	11.85	11.85	8.43	
AXILLIAR45	Tool_5	notDetected	6.69	11.00	notDetected	6.65	13.16	13.16	SPATIAL	8.21	8.21	18.72	
AXILLIAR45	A6_1	SPATIAL	7.57	19.53	SPATIAL	8.42	21.68	21.68	SPATIAL	8.51	8.51	20.15	
AXILLIAR45	A6_2	SPATIAL	6.48	20.53	SPATIAL	7.56	26.61	26.61	SPATIAL	8.36	8.36	17.34	
AXILLIAR45	A6_3	SPATIAL	29.67	38.46	SPATIAL	35.79	47.89	47.89	FORCE_SENSOR	20.03	20.03	32.62	
AXILLIAR45	A6_4	SPATIAL	38.72	37.08	SPATIAL	38.10	39.92	39.92	FORCE_SENSOR	20.04	20.04	32.80	
AXILLIAR45	A5_1	SPATIAL	27.50	24.89	SPATIAL	28.52	28.25	28.25	FORCE_SENSOR	20.05	20.05	28.11	
AXILLIAR45	A5_2	notDetected	8.04	12.80	SPATIAL	7.83	21.13	21.13	SPATIAL	7.93	7.93	19.90	
AXILLIAR45	A4_1	SPATIAL	26.34	25.64	SPATIAL	22.24	28.82	28.82	FORCE_SENSOR	20.01	20.01	28.79	
AXILLIAR45	A4_2	SPATIAL	9.70	27.83	SPATIAL	7.61	17.11	17.11	SPATIAL	8.27	8.27	22.01	
AXILLIAR45	A4_3	SPATIAL	18.79	33.32	SPATIAL	18.46	18.23	18.23	FORCE_SENSOR	20.02	20.02	16.63	
AXILLIAR45	A4_4	notDetected	32.82	24.50	SPATIAL	29.10	23.71	23.71	FORCE_SENSOR	20.03	20.03	24.53	
AXILLIAR45	A4_5	SPATIAL	48.71	69.42	TORQUE	46.12	58.46	58.46	FORCE_SENSOR	20.06	20.06	42.44	
AXILLIAR45	A3_1	notDetected	8.37	12.06	SPATIAL	8.75	20.55	20.55	SPATIAL	8.54	8.54	24.24	
AXILLIAR45	A3_2	SPATIAL	9.41	27.23	SPATIAL	10.23	33.65	33.65	SPATIAL	11.73	11.73	29.54	
AXILLIAR45	A3_3	SPATIAL	34.49	48.69	SPATIAL	39.92	54.60	54.60	FORCE_SENSOR	20.03	20.03	39.44	
AXILLIAR45	A3_4	notDetected	17.86	9.81	notDetected	27.52	10.59	10.59	notDetected	16.30	16.30	9.86	
AXILLIAR45	A2_1	notDetected	8.06	10.92	notDetected	9.37	14.49	14.49	SPATIAL	8.67	8.67	16.00	
AXILLIAR45	A2_2	SPATIAL	9.69	22.07	SPATIAL	15.47	21.86	21.86	SPATIAL	7.84	7.84	26.97	
AXILLIAR45	A2_3	SPATIAL	42.96	56.71	TORQUE	41.03	45.46	45.46	FORCE_SENSOR	20.04	20.04	30.25	
AXILLIAR45	A2_4	SPATIAL	35.92	31.06	TORQUE	30.95	27.48	27.48	FORCE_SENSOR	20.00	20.00	16.78	
AXILLIAR45	A2_5	notDetected	10.05	12.05	notDetected	10.67	9.37	9.37	notDetected	9.11	9.11	9.72	
AXILLIAR45	A1_1	notDetected	9.77	13.14	notDetected	9.86	11.79	11.79	notDetected	8.16	8.16	9.47	

Table 8.2: Collision detection for each detection method for Axilliar 90 US position.

US position	Collision point	robot SPATIAL force estimation			robot spatial force and TORQUE estimation			SPATIAL+ TORQUE + FORCE SENSOR		
		Detected by mechanism	Maximum force Sensor	robot measured estimated	Detected by mechanism	Maximum force Sensor	robot measured estimated	Detected by mechanism	Maximum force Sensor	robot measured estimated
AXILLIAR90	Tool_1	SPATIAL	27.02	17.99	SPATIAL	20.28	19.83	SPATIAL	35.44	19.81
AXILLIAR90	Tool_2	SPATIAL	26.03	23.16	SPATIAL	23.59	24.49	FORCE_SENSOR	20.09	17.90
AXILLIAR90	Tool_3	SPATIAL	23.84	19.62	SPATIAL	25.99	22.79	FORCE_SENSOR	20.01	10.72
AXILLIAR90	Tool_4	notDetected	15.07	16.92	notDetected	12.28	11.78	notDetected	8.02	8.55
AXILLIAR90	Tool_5	notDetected	13.47	16.87	SPATIAL	8.32	19.92	SPATIAL	7.75	23.42
AXILLIAR90	A6_1	SPATIAL	13.66	20.12	SPATIAL	10.75	19.36	SPATIAL	11.51	21.85
AXILLIAR90	A6_2	SPATIAL	13.28	19.87	SPATIAL	8.78	19.59	SPATIAL	8.27	26.49
AXILLIAR90	A6_3	SPATIAL	14.39	19.38	SPATIAL	24.87	9.99	SPATIAL	16.74	21.43
AXILLIAR90	A6_4	SPATIAL	25.69	27.81	TORQUE	39.48	19.31	FORCE_SENSOR	20.00	33.00
AXILLIAR90	A5_1	SPATIAL	41.31	24.57	SPATIAL	28.49	34.23	FORCE_SENSOR	20.01	27.17
AXILLIAR90	A5_2	SPATIAL	13.12	23.63	SPATIAL	8.60	18.10	SPATIAL	8.23	18.83
AXILLIAR90	A4_1	SPATIAL	17.09	22.43	SPATIAL	12.59	21.33	SPATIAL	14.93	24.61
AXILLIAR90	A4_2	SPATIAL	13.63	21.82	SPATIAL	11.80	22.65	SPATIAL	8.09	24.31
AXILLIAR90	A4_3	SPATIAL	27.76	28.37	SPATIAL	22.41	23.45	FORCE_SENSOR	20.04	26.05
AXILLIAR90	A4_4	SPATIAL	65.98	37.87	SPATIAL	41.54	34.61	FORCE_SENSOR	20.03	28.64
AXILLIAR90	A4_5	SPATIAL	42.37	23.77	SPATIAL	39.80	41.57	FORCE_SENSOR	20.06	36.41
AXILLIAR90	A3_1	SPATIAL	9.33	20.22	notDetected	7.12	18.51	SPATIAL	8.24	17.76
AXILLIAR90	A3_2	SPATIAL	12.73	28.05	SPATIAL	9.19	33.33	SPATIAL	12.34	24.59
AXILLIAR90	A3_3	SPATIAL	27.94	36.35	SPATIAL	27.07	30.77	FORCE_SENSOR	20.09	34.52
AXILLIAR90	A3_4	notDetected	28.38	10.79	notDetected	30.73	13.67	FORCE_SENSOR	20.14	26.01
AXILLIAR90	A2_1	SPATIAL	8.40	20.26	SPATIAL	8.13	23.33	SPATIAL	7.48	21.00
AXILLIAR90	A2_2	notDetected	8.63	14.63	SPATIAL	9.35	19.83	SPATIAL	10.28	18.54
AXILLIAR90	A2_3	SPATIAL	25.29	28.02	SPATIAL	27.14	27.41	FORCE_SENSOR	20.03	24.01
AXILLIAR90	A2_4	notDetected	50.83	10.78	TORQUE	41.83	12.90	FORCE_SENSOR	20.02	21.05
AXILLIAR90	A2_5	notDetected	8.75	15.46	notDetected	7.03	9.58	FORCE_SENSOR	20.01	18.63
AXILLIAR90	A1_1	notDetected	8.32	13.24	notDetected	7.89	12.94	SPATIAL	9.04	15.51
AXILLIAR90	A1_2	notDetected	25.59	9.10	notDetected	27.52	9.95	FORCE_SENSOR	20.03	24.68

Table 8.3: Collision detection for each detection method for Navel US position.

US position	Collision point	robot SPATIAL force estimation			robot spatial force and TORQUE estimation			SPATIAL+ TORQUE + FORCE SENSOR		
		Detected by mechanism	Maximum force Sensor	robot measured estimated	Detected by mechanism	Maximum force Sensor	robot measured estimated	Detected by mechanism	Maximum force Sensor	robot measured estimated
Navel	Tool_1	SPATIAL	27.63	20.43	SPATIAL	21.87	22.88	FORCE_SENSOR	20.02	16.06
Navel	Tool_2	SPATIAL	23.82	20.50	SPATIAL	23.02	22.60	FORCE_SENSOR	20.00	19.36
Navel	Tool_3	SPATIAL	25.95	26.05	SPATIAL	24.88	22.83	FORCE_SENSOR	20.05	23.56
Navel	Tool_4	notDetected	12.89	7.26	notDetected	13.43	8.53	notDetected	14.63	10.19
Navel	Tool_5	notDetected	8.73	16.43	notDetected	11.20	9.71	SPATIAL	7.92	19.35
Navel	A6_1	notDetected	8.29	18.74	SPATIAL	8.25	19.91	SPATIAL	7.97	10.56
Navel	A6_2	SPATIAL	21.05	19.75	SPATIAL	18.71	29.04	SPATIAL	24.08	22.36
Navel	A6_3	SPATIAL	110.33	17.87	TORQUE	68.34	18.42	FORCE_SENSOR	20.01	29.29
Navel	A6_4	SPATIAL	32.62	41.83	SPATIAL	31.76	29.44	FORCE_SENSOR	20.01	30.78
Navel	A5_1	SPATIAL	13.26	22.68	SPATIAL	11.63	22.18	SPATIAL	12.51	20.27
Navel	A5_2	SPATIAL	8.46	12.98	SPATIAL	8.23	18.25	SPATIAL	9.04	20.00
Navel	A4_1	SPATIAL	12.05	19.69	SPATIAL	11.79	39.00	SPATIAL	10.16	21.05
Navel	A4_2	SPATIAL	14.23	24.74	SPATIAL	13.43	14.36	SPATIAL	11.35	23.52
Navel	A4_3	SPATIAL	38.65	25.72	SPATIAL	45.97	30.11	FORCE_SENSOR	20.05	32.96
Navel	A4_4	SPATIAL	14.94	27.48	SPATIAL	14.79	26.20	TORQUE	13.22	28.78
Navel	A4_5	SPATIAL	83.63	35.90	TORQUE	68.02	54.50	FORCE_SENSOR	20.01	30.33
Navel	A3_1	SPATIAL	8.04	19.15	SPATIAL	8.29	19.02	SPATIAL	8.55	22.27
Navel	A3_2	SPATIAL	48.04	18.14	TORQUE	25.49	36.56	FORCE_SENSOR	20.04	26.70
Navel	A3_3	SPATIAL	94.28	70.05	TORQUE	64.00	69.42	FORCE_SENSOR	20.00	52.93
Navel	A3_4	notDetected	16.72	9.57	notDetected	15.31	9.89	notDetected	17.49	12.24
Navel	A2_1	notDetected	8.00	10.60	notDetected	8.02	16.43	SPATIAL	8.06	20.93
Navel	A2_2	SPATIAL	15.57	18.74	TORQUE	17.15	20.08	TORQUE	16.68	16.51
Navel	A2_3	SPATIAL	93.68	26.93	TORQUE	69.58	47.99	FORCE_SENSOR	20.01	27.57
Navel	A2_4	SPATIAL	8.03	19.06	SPATIAL	10.89	19.98	SPATIAL	15.46	19.40
Navel	A2_5	notDetected	9.95	9.65	notDetected	9.90	11.22	notDetected	11.54	11.26
Navel	A1_1	notDetected	8.33	8.95	notDetected	8.09	9.81	notDetected	8.43	10.30
Navel	A1_2	notDetected	10.15	13.60	notDetected	9.40	11.30	notDetected	9.44	10.89

Table 8.4: Collision detection for each detection method for Subcostal US position.

US position	Collision point	robot SPATIAL force estimation			robot spatial force and TORQUE estimation			SPATIAL+ TORQUE + FORCE SENSOR		
		Detected by mechanism	Maximum force Sensor	robot measured estimated	Detected by mechanism	Maximum force Sensor	robot measured estimated	Detected by mechanism	Maximum force Sensor	robot measured estimated
Subcostal	Tool_1	SPATIAL	25.53	20.15	SPATIAL	19.10	20.12	FORCE_SENSOR	20.07	11.74
Subcostal	Tool_2	SPATIAL	32.25	28.66	SPATIAL	23.69	20.54	FORCE_SENSOR	20.02	16.89
Subcostal	Tool_3	SPATIAL	36.96	30.01	TORQUE	22.56	16.33	FORCE_SENSOR	20.01	21.57
Subcostal	Tool_4	notDetected	6.43	7.46	notDetected	11.73	12.87	notDetected	11.84	12.55
Subcostal	Tool_5	notDetected	6.65	15.00	SPATIAL	8.92	18.72	FORCE_SENSOR	11.34	13.84
Subcostal	A6_1	SPATIAL	12.70	37.68	SPATIAL	9.79	26.86	SPATIAL	12.00	21.91
Subcostal	A6_2	SPATIAL	89.12	42.79	SPATIAL	53.65	45.71	FORCE_SENSOR	20.14	26.76
Subcostal	A6_3	SPATIAL	9.07	22.53	SPATIAL	13.33	29.65	SPATIAL	13.01	23.86
Subcostal	A6_4	SPATIAL	22.47	27.76	TORQUE	35.47	39.47	FORCE_SENSOR	20.02	28.08
Subcostal	A5_1	SPATIAL	8.32	20.73	SPATIAL	10.14	22.47	FORCE_SENSOR	10.32	13.85
Subcostal	A5_2	SPATIAL	17.93	23.10	SPATIAL	11.83	21.91	SPATIAL	16.96	27.28
Subcostal	A4_1	SPATIAL	15.28	22.99	SPATIAL	13.93	24.96	SPATIAL	13.14	17.04
Subcostal	A4_2	notDetected	113.10	16.49	TORQUE	70.71	28.31	FORCE_SENSOR	20.00	33.37
Subcostal	A4_3	SPATIAL	11.98	21.13	SPATIAL	11.75	27.81	SPATIAL	11.50	22.70
Subcostal	A4_4	notDetected	11.45	12.06	notDetected	11.60	11.59	FORCE_SENSOR	11.26	14.57
Subcostal	A4_5	SPATIAL	15.62	38.79	SPATIAL	16.02	38.25	SPATIAL	12.03	35.46
Subcostal	A3_1	SPATIAL	11.34	19.32	SPATIAL	11.94	22.62	SPATIAL	10.13	27.23
Subcostal	A3_2	SPATIAL	65.24	22.07	SPATIAL	61.20	20.83	FORCE_SENSOR	20.07	26.48
Subcostal	A3_3	SPATIAL	5.19	39.40	SPATIAL	19.27	37.99	FORCE_SENSOR	20.03	32.81
Subcostal	A3_4	notDetected	24.65	18.25	SPATIAL	25.01	26.94	FORCE_SENSOR	20.01	22.70
Subcostal	A2_1	notDetected	11.98	13.13	notDetected	8.63	9.47	FORCE_SENSOR	6.92	14.55
Subcostal	A2_2	notDetected	12.07	21.25	SPATIAL	12.44	22.18	SPATIAL	11.75	34.45
Subcostal	A2_3	notDetected	44.14	12.28	SPATIAL	49.03	24.54	FORCE_SENSOR	20.18	18.16
Subcostal	A2_4	notDetected	13.07	41.71	SPATIAL	13.47	34.02	SPATIAL	12.26	30.41
Subcostal	A2_5	SPATIAL	12.35	20.60	SPATIAL	12.46	20.95	SPATIAL	12.01	30.83
Subcostal	A1_1	SPATIAL	12.37	21.42	SPATIAL	11.76	20.54	SPATIAL	11.76	20.95
Subcostal	A1_2	notDetected	12.64	14.87	SPATIAL	12.60	25.21	SPATIAL	11.88	16.88





# Lebenslauf

## Personalien

Name	Peter Karl Seitz
Geburtsdatum	14.06.1992
Geburtsort	Heilbronn
Staatsangehörigkeit	deutsch

## Schulischer Werdegang

2003 – 2009	Justinus Kerner Gymnasium, Weinsberg
2009–2012	Technisches Gymnasium GSOE, Öhringen

## Universitärer Werdegang

2012 – 2015	Ruprechts-Karls-Universität Heidelberg & Hochschule Heilbronn, Studium der Medizinischen Informatik Thema der Bachelorarbeit: “Konzeption und Entwicklung einer Applikation zur robotergestützten Ultraschallbildgebung”
24.09.2015	Abschluss: Bachelor of Science (B.Sc.)
2015 – 2018	Ruprechts-Karls-Universität Heidelberg & Hochschule Heilbronn, Studium der Medizinischen Informatik Thema der Masterarbeit: “Konzeption und Entwicklung einer robotergestützten und ultraschallbasierten Lokalisationskontrolle”
28.2.2018	Abschluss: Master of Science (M.Sc.)

## Beruflicher Werdegang

2015 – 2018	Akademischer Mitarbeiter, Hochschule Heilbronn, Fakultät Informatik
2018 – heute	Wissenschaftlicher Mitarbeiter, Hochschule Heilbronn, Fakultät Informatik
2018 – heute	Wissenschaftlicher Mitarbeiter, Deutsches Krebsforschungszentrum, Abt. Medizinische Physik in der Strahlentherapie



# Danksagung

Hiermit möchte ich mich bei allen bedanken die mich auf meinem Weg unterstützt und mir geholfen haben dort zu sein wo ich heute bin.

Mein erster Dank geht an meinen Doktorvater **Prof. Dr. Christian Karger**, der mich in den letzten dreieinhalb Jahren begleitet und den Einstieg in die Medizinische Physik erleichtert hat, sowie mir die wissenschaftliche Denkweise näher gebracht und meinen Schlusssprint erst ermöglicht hat.

Insbesondere möchte ich mich bei **Prof. Dr. Rolf Bendl** bedanken. Ohne Ihn hätte es dieses Projekt und damit diese Arbeit niemals gegeben. Er stand mir immer mit Rat und Tat zur Seite und begleitete und beeinflusste das Projekt maßgeblich. Auch hat er mich über die Jahre seit der Bachelorarbeit einiges gelehrt nicht nur für das Projekt, sondern auch für das Leben.

Meiner Kollegin **Dr. Andrea Schwahofer** möchte ich für die endlosen Hinweise und Korrekturen in allen Bereichen danken. Sie schärfte mein Blick für die wissenschaftliche Betrachtung der Dinge. Ich werde die konstruktiven Gespräche und kreative Ideensammlungen mit ihr vermissen.

Auch möchte ich meinen Bachelor und Masterstudenten, namentlich Cord Lissek, Axel Finsterle, Johanna Seidel, Kayanee Loheswaran, Philipp Goos, Justus Kerber, Bogdan Zhukov, Cara Hoffman, Lejla Cosic und Dominik Luhitle, danken.

Ein besonderer Dank gilt meiner Familie, die mir über das Studium den Rücken freigehalten haben und mich immer aufgebaut haben, wenn etwas nicht so lief wie es sollte. Insbesondere meiner Mutter, die immer die richtigen Worte zur Unterstützung fand.

Abschließend möchte ich noch meiner Frau für ihre aufopfernde Unterstützung und unser großartiges gemeinsames Leben danken. Ohne sie wäre diese Arbeit nicht möglich gewesen.



# Eidesstattliche Versicherung

1. Bei der eingereichten Dissertation zu dem Thema **Implementation of safe human robot collaboration for ultrasound guided radiation therapy** handelt es sich um meine eigenständig erbrachte Leistung.
2. Ich habe nur die angegebenen Quellen und Hilfsmittel benutzt und mich keiner unzulässigen Hilfe Dritter bedient. Insbesondere habe ich wörtlich oder sinngemäß aus anderen Werken übernommene Inhalte als solche kenntlich gemacht.
3. Die Arbeit oder Teile davon habe ich wie folgt an einer Hochschule des In- oder Auslands als Bestandteil einer Prüfungs- oder Qualifikationsleistung vorgelegt:

Titel der Arbeit: *Konzeption und Entwicklung einer robotergestützten und ultraschallbasierten Lokalisationskontrolle*

Hochschule und Jahr: *Universität Heidelberg 2018*

Art der Prüfungs- oder Qualifikationsleistung: *Masterarbeit*

4. Die Richtigkeit der vorstehenden Erklärungen bestätige ich.
5. Die Bedeutung der eidesstattlichen Versicherung und die strafrechtlichen Folgen einer unrichtigen oder unvollständigen eidesstattlichen Versicherung sind mir bekannt. Ich versichere an Eides statt, dass ich nach bestem Wissen die reine Wahrheit erkläre und nichts verschwiegen habe.

Eberstadt, 30.06.2022

---

Peter Karl Seitz